Chronic Two-photon Imaging of Neuronal Activity in Alzheimer's Disease Animal Models

---

Dissertation

zur
Erlangung der naturwissenschaftlichen Doktorwürde
(Dr. sc. nat.)

vorgelegt der

Mathematisch-naturwissenschaftlichen Fakultät
der
Universität Zürich

von

Annapoorna Bhat

aus Indien

Promotionskomitee

Prof. Dr. Roger M. Nitsch (Vorsitz, Leitung der Dissertation)
Prof. Dr. Fritjof Helmchen (Leitung der Dissertation)
Prof. Dr. Markus Rudin
Prof. Dr. Esther Stöckli

Zürich, 2012

“It is good to have an end to journey toward; but it is the journey that matters, in the end.”

— *Ernest Hemingway*

Table of Contents

1. Abbreviations

2PM	two-photon microscopy
AAV	Adeno-assosciated virus
AD	Alzheimer`s disease
ADL	activities of daily living
APOE	apolipoprotein E
APP	amyloid precursor protein
Aβ	amyloid-beta
BAPTA	1,2-bis(o-aminophenoxy)ethane-N,N,N',N'-tetraacetic acid
BBB	blood brain barrier
BOLD	blood oxygenation level-dependent
CAA	cerebral amyloid angiopathy
$CaCl_2$	calcium chloride
CAG	chicken β-actin
CFP	cyan fluorescent protein
CR	complement receptor
CSF	cerebrospinal fluid
CT	computed tomography
CX3CR1	fractalkine receptor
DMSO	dimethyl sulfoxide
DNA	deoxy nucleic acid
EAE	expreimental autoimmune encephalomyelitis
EEG	electro encephalogram
EOFAD	early onset familial Alzheimer`s disease
fMRI	functional magnetic resonance imaging
FRET	fluorescent resonant energy transfer
FTD	frontotemporal dementia
GABA	gamma amino butyric acid
GECI	genetically encoded calcium indicators
GFP	green fluorescent protein
GSK	glycogen synthase kinase
i.p.	intra peritoneal

i.v.	intra venous
IL	interleukin
IR	infra-red
ISI	intrinsic signal imaging
KCl	potassium chloride
LBD	Lewy body dementia
LOAD	late onset Alzheimer`s disease
LTD	long term depression
LTP	long term potentiation
MAPK	mitogen-activated protein kinase
MHC	major histocompatiblity complex
MHz	mega Hertz
MMSE	mini-mental state examination
MRI	magnetic resonance imaging
NA	numerical aperture
nAChR	nicotine acetyl choline receptor
NaCl	sodium chloride
NaOH	sodium hydroxide
NFT	neurofibrillary tangles
NMDAR	*N*-methyl-D-aspartate receptor
NRR	normal rat ringer
NSAID	non –steroidal anti-inflammatory drugs
OGB	Oregon green BAPTA-1
PBS	phosphate buffered saline
PCR	polymerase chain reaction
PET	positron emission tomography
PFA	paraformaldehyde
PHF	paired helical filaments
PiB	Pittsburg compound B
PPARγ	Peroxisome proliferator-activated receptor gamma
PSEN	presenelin
ROI	region of interest
RT	room temperature
s.c.	subcutaneous

SD	standard deviation
SR 101	sulforhodamine
SR	scavenger receptor
TBS	tris-buffered saline
TGF	transforming growth factor
TLR	Toll-like receptor
TNF	tumor necrosis factor
VPM	ventral posterior medical nucleus
YC	yellow cameleon
YFP	yellow fluorescent protein

2. Summary/Zusammenfassung

As life expectancy of humans is increasing all over the world, incidence of age-related diseases is increasing as well. One amongst them is Alzheimer's disease (AD), a multifactorial neurodegenerative disease, which is characterized by cognitive deficits, memory loss and personality changes. Histopathology of AD affected brains show abnormal accumulation and aggregation of the amyloid β (Aβ) peptide forming Aβ plaques and hyperphosphorylation of the neuronal tau protein resulting in the formation of neurofibrillary tangles, both of which are considered histopathological hallmarks of AD. Aβ, which can exist in various forms from soluble monomers to insoluble fibrils is presumed to be the main culprit in causing neuronal dysfunction.

The options for medical management of AD are very limited. There are only four FDA approved drugs available in the market, all of which are only palliative. Numerous molecular and drug targets have been identified over last decade thus making AD therapeutics an interesting field. The forerunner amongst various therapies is immunotherapy with anti-Aβ antibodies, which has been successful in animal models and currently undergoing large multi-center clinical trials.

The mechanism of neuronal dysfunction in AD yet remains to be completely understood. Technical and molecular advances such as two-photon microscopy (2PM) and genetically encoded calcium indicators are making it easier to answer these questions in an *in vivo* setting, more so in AD transgenic mice models. However, these approaches are technically very challenging. The first step towards chronic imaging was standardization of protocols. We used the standardization technique to look at morphological aspects of beta-amyloid plaque and microglia interaction in transgenic mice with GFP expressing microglia. Local application of anti-Aß antibodies was done and time-lapse imaging of microglia surrounding plaques was carried out to standardize operating and imaging protocols.

We then combined the techniques of chronic *in vivo* imaging, 2PM and genetically encoded calcium indicators to study sensory-evoked response of neurons in somatosensory cortex of living mice over a period of weeks in the context of pre-

plaque AD pathology. Furthermore, we passively immunized the mice with an in-house generated anti-Aβ antibody targeted against fibrillar Aβ to study neuronal responses before and after immunization. We were able to image the same population of cells over a period of time in wild type and AD transgenic mice. AD transgenic mice showed a trend towards having lower neuronal activity compared to wild type mice. Passive immunotherapy showed a promising trend towards improvement of some components of neuronal activity such as spontaneous response. Our results show that longitudinal imaging of neuronal ensembles in AD is now achievable and these chronic imaging protocols can be used to study therapeutics. This opens new opportunities in terms of studying AD pathophysiology starting from disease onset and follow the progression of neurodegeneration and monitor efficacy of treatment agents.

Overall, this dissertation was successful in establishing chronic imaging protocols and test them in pre-plaque AD mice, thus proving that chronic imaging of neuronal activity is possible in AD animal models.

Zusammenfassung

Mit der weltweit ansteigenden Lebenserwartung, steigt auch die Anzahl altersbedingter Erkrankungen. Die häufigste ist die Alzheimer Demenz (AD), eine multifaktorielle neurodegenerative Erkrankung, welche durch kognitive Defizite, Gedächtnisdefizite und Veränderungen der Persönlichkeit gekennzeichnet ist. Histopathologisch findet man in AD Hirnen eine abnormale Anhäufung und Aggregation des Aβ-Peptids, welches in Plaques akkumuliert, sowie eine Hyperphosphorylierung des neuronalen Tau Proteins, das zur Bildung neurofibrillärer Tangles führt. Beide gelten als sichere histopathologische postmortem Kriterien für AD.

Es wird vermutet, dass Aβ, welches in verschiedensten Spezies, von löslichen Monomeren bis hin zu unlöslichen Fibrillen existiert, die Ursache der Demenz und der neuronalen Dysfunktionen darstellt.

Die Möglichkeiten einer Therapie für AD sind kaum vorhanden. Es existieren nur vier FDA zugelassene Medikamente, die alle palliativ eingesetzt wirken. Es wurden zahlreiche molekulare Ansätze analysiert und mögliche Pharmakotherapien vorgeschlagen.

Der vielversprechendste Ansatz hier ist eine Immuntherapie mit anti- Aβ-gerichteten Antikörpern, die bereits Erfolge in AD-Tiermodellen gezeigt haben und im Moment grosse multizentrische klinische Studien durchlaufen.

Die Mechanismen hinter der neuronalen Dysfunktion in AD sind jedoch noch nicht vollständig aufgeklärt.

Moderne Technologien, wie die Zwei-Photonen-Mikroskopie (2PM), und genetisch codierte Kalzium Indikatoren erleichtern es, diese Fragen in einem in vivo transgenen Mausmodell näher zu erörtern. Diese Ansätze sind technisch aber sehr anspruchsvoll. Der erste Schritt bei der Etablierung der chronischen Bildgebung ist die Standardisierung von Methoden-Protokollen. Wir verwendeten diese Standardisierungstechnik, um morphologische Aspekte der Interaktion zwischen beta-amyloid Plaques und GFP-markierten Microglia in transgenen Mäusen zu analysieren. Es erfolgte eine lokale Applikation von anti- Aß-gerichteten Antikörpern, um durch eine Zeitraffer Bildgebung von Plaques, die von Microglia umgeben waren,

Aufnahmen machen zu können, denen standardisierte Protokolle zugrunde liegen.

Wir haben daraufhin die Techniken der Langzeit in vivo-Bildgebung, 2PM und genetisch kodierten Kalzium-Indikatoren miteinander kombiniert, um sensorisch ausgelöste Potentiale der Neuronen im somatosensorischen Kortex lebender Mäuse über einen Zeitraum von mehreren Wochen im Rahmen der Prä-Plaque-AD-Pathologie zu studieren. Darüber hinaus wurden die Mäuse mit einem selbst generierten anti-Aß-Antikörper, der gegen Aß-Fibrillen gerichtet ist, passiv immunisiert, um die Folgen für betroffene Neuronen vor und nach der Immunisierung untersuchen zu können. Der Vorteil der chronischen Bildgebung liegt darin, dass man die gleiche Population von Zellen über einen längeren Zeitraum hinweg aufnehmen kann. Transgene AD Mäusen zeigten im Vergleich zu Wildtyp-Mäusen die Tendenz zu verlangsamter neuronaler Aktivität. Die passive Immunisierung ist ein vielversprechender Ansatz zur Verbesserung der neuronalen Aktivität, so z.B. der Spontanaktivität der Neuronen. Unsere Ergebnisse zeigen, dass die Langzeit-Bildgebung neuronaler Netzwerke in AD darstellbar wird und dass die etablierten Protokolle verwendet werden können, um Therapeutika besser zu studieren. Dies eröffnet neue Möglichkeiten die AD Pathophysiologie zu erforschen, von Beginn der Krankheit bis hin zur Neurodegeneration und ermöglicht das Ueberwachen des Therapieerfolgs.

Abschliessend war diese Dissertation erfolgreich in der Etablierung von Langzeit-Bildgebungs- protokollen und der Erprobung dieser Protokolle in Prä-Plaque AD Mausmodellen, die nun dafür eingesetzt werden können, neuronale Aktivität in Tiermodellen zu manipulieren und darzustellen.

3. Introduction

3.1 Alzheimer's Disease

'Our memories define who we are' says psychologist Howard Eichenbaum. This couldn't have been more relevant in the case of Alzheimer's disease (AD) patients, who suffer from memory loss and cognitive deficits, which ultimately lead to personality changes. AD is the most common form of dementia and fourth in the list of leading causes of death in industrialized societies, preceded only by heart disease, cancer, and stroke (Carter, et al. 2010) and is on the rise in the developing countries too (World Alzheimer Report 2011).

3.1.1 Prevalence and risk factors

AD constitutes about 70% of all dementia cases (Castellani, et al. 2010). Incidence of AD increases with age, doubling every 5-10 years. For persons between ages 65 and 69, 70 and 74, 75 and 79, 80 and 84, and 85 and older the incidence of AD has been estimated to be 0.6%, 1.0%, 2.0%, 3.3%, and 8.4% respectively (Fratiglioni, et al. 1999, Small, et al. 1997). Prevalence also increases exponentially with age, rising from 3% among those 65-74 to almost 50% among those 85 or older (Hebert, et al. 1995). In 2010, there were 35.6 million cases of Alzheimer's disease in the world (Brookmeyer, et al. 2007). It is predicted that by the year 2050, the worldwide prevalence of Alzheimer's will grow fourfold, to 106.8 million with 1 in 85 persons living with AD (Brookmeyer, et al. 2007). The above data are in keeping in mind the projected demographic changes resulting from the 'baby boomer' generation reaching old age and the continued increase in life expectancy (Castellani, et al. 2010). The total estimated worldwide costs of dementia were US$604 billion in 2010. These costs account for around 1% of the world's gross domestic product, varying from 0.24% in low income countries, to 0.35% in low middle income countries, 0.50% in high middle income countries, and 1.24% in high income countries (World Alzheimer Report 2011).

Conventionally, AD is genetically divided into two forms (Bertram, et al. 2010): (1) familial cases with Mendelian inheritance of predominantly early-onset (<60 years, early-onset familial AD [EOFAD]), and (2) so-called 'sporadic cases' with less

apparent or no familial aggregation and usually of later onset age (≥60 years, late-onset AD [LOAD]). This traditional dichotomization is overly simplistic as there are cases of early-onset AD without evidence for Mendelian transmission while, conversely, LOAD is frequently observed with a strong familial clustering, sometimes resembling a Mendelian pattern. While EOFAD is caused by rare and highly penetrant mutations in three genes; amyloid precursor protein (APP) (Figure 3.1), Presenilin-1 (PSEN1) and Presenilin-2 (PSEN2), the genetics of LOAD is more complex. The current hypothesis is that susceptibility for LOAD is conferred by numerous genetic risk factors of relatively high frequency but low penetrance and therefore small effect size. While LOAD is also sometimes referred to as 'sporadic AD', it is important to emphasize that up to 60%–80% of this form of AD is genetically determined (Bertram, et al. 2010, Gatz, et al. 2006). Most of the APP mutations can be found in close proximity to or at the proteolytic cleavage sites at which APP is processed by its secretases (Figure 3.1). Notably, not all APP mutations lead to the same symptoms or do not even result in the EOFAD phenotype: for example, the E693Q Dutch mutation causes hereditary cerebral hemorrhage with amyloidosis (HCHWA-D) resulting in severe intracerebral bleedings and cerebral amyloid angiopathy (CAA) (Maat-Schieman, et al. 2005); the E693K mutation, however, causes exclusively CAA without AD-type dementia (Bugiani 2004), whereas the arctic mutation (E693G) shows a clear AD phenotype with both neuritic plaques and extensive CAA (Watson, et al. 1999).

Another line of evidence supporting the role of APP in AD pathology is the early plaque deposition and development of behavioral deficits and cognitive impairment typical of AD in people with Down's syndrome, which is caused by chronic over production of Aß resulting from triplication of chromosome 21 (Lemere, et al. 1996).

Another factor, which predisposes to AD, is the presence of apoliopoprotein E ε4 (*APOE* ε4) allele. As compared to individuals with no ε4 alleles, the increased risk for AD is 2- to 3- fold in people with one ε4 allele and about 12-fold in those with 2 ε4 alleles (Bertram and Tanzi 2009, Roses 1996). The *APOE* ε4 allele is also associated with an earlier age of AD onset (Meyer, et al. 1998, Raber, et al. 2004).

It is important to note that the ε2 allele of *APOE* is associated with a lower risk for AD (Corder, et al. 1993, Farrer, et al. 1997). However, it is difficult to define whether the *APOE* ε4 allele represents a gain of toxic function, a loss of neuroprotective function, or both (Kim, et al. 2009).

Still, environmental and epigenetic factors also make an important contribution in determining an individual's risk, although the precise nature and mechanisms underlying these non-genetic components remain largely undetermined, mainly because they are difficult to assess experimentally (Bertram and Tanzi 2009, Traynor and Singleton 2010).

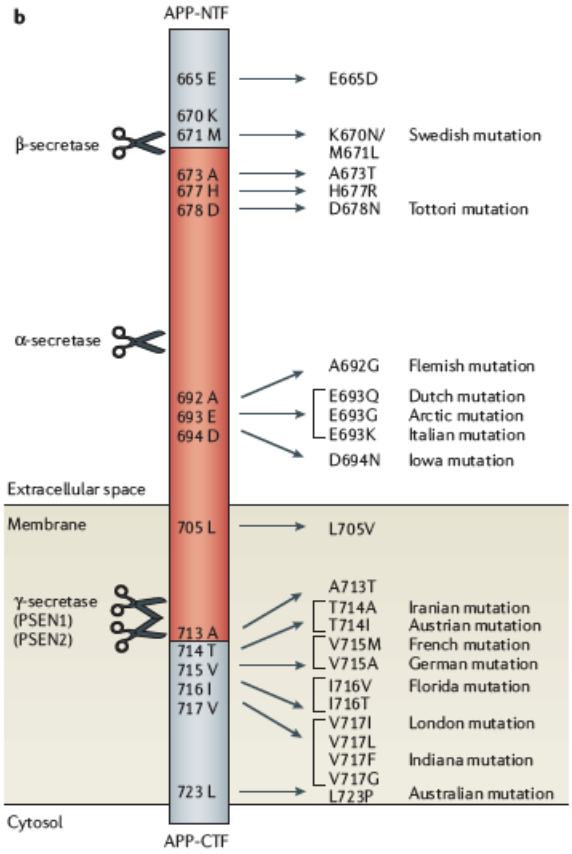

Figure 3.1: APP mutations in FAD. Part of the APP amino-sequence; mutations associated have been highlighted. The mutations are named after nationality or the location of the first family in which the specific mutation was demonstrated. It is important to note that most mutations are in the vicinity of secretase-cleaving sites, which influences APP processing. The Aβ sequence is indicated in red. (Image adapted from Van Dam 2006).

3.1.2 Clinical features

AD was first described as 'eigenartige Erkrankung der Hirnrinde' by Bavarian psychiatrist Alois Alzheimer in 1906 based on clinical findings and autopsy results of his 51-year-old patient Ms. August Deter. It was Emil Kraepelin who later named it as Alzheimer's disease (Alzheimer, et al. 1995).

The clinical disease stages are preceded by many years of prodromal AD, initially announced by mild cognitive impairment (MCI) that gradually progresses from subtle cognitive and memory problems such as word finding difficulty and decreased organization capacity to severe deficits such as inability to perform activities of daily living (ADLs), inevitably ending in severe dementia (Figure 3.2). The composite clinical picture at any stage is variable among AD patients, including cognitive and memory problems, and mild to severe changes in social behavior with mood swings and altered personality and character, including apathy, depression, irritability, agitation, psychosis and aggression (Blennow, et al. 2006).

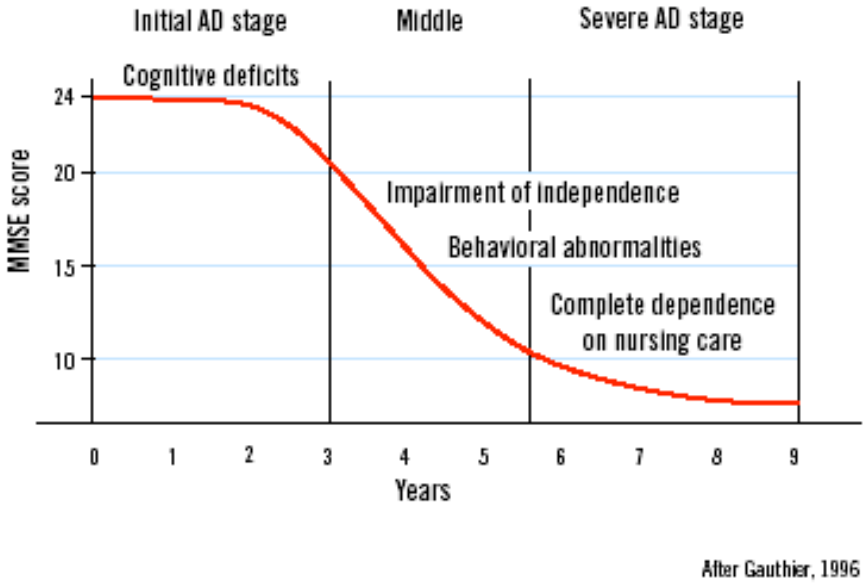

Figure 3.2: Clinical course of AD. The clinical features are insidious in onset and gradually progress over years. Adapted from Gauthier 1996 (image from EPG health media) Y-axis is MMSE score which is a neuropsychological test and highest score is 30.

The diagnosis of AD requires clinical evidence of memory loss and impairment of at least one other cognitive domain, with evidence of disturbance in social or occupational function. AD must be differentiated from other causes of dementia namely, vascular dementia, frontotemporal dementia (FTD), dementia with Lewy body (LBD), Parkinson's disease with dementia to name a few.

The major criteria for diagnosis of AD are defined by DSM-IV and National Institute of Neurological Disorders and Stroke-Alzheimer Disease and Related Disorders (NINCDS-ADRDA) (Dubois, et al. 2007, McKhann, et al. 1984) (Figure 3.3).

I. AD is characterized by progressive decline and ultimately loss of multiple cognitive functions, including both:
   Memory impairment—impaired ability to learn new information or to recall previously learned information and at least one of the following:
      Loss of word comprehension ability, for example, inability to respond to "Your daughter is on the phone." (aphasia);
      Loss of ability to perform complex tasks involving muscle coordination, for example, bathing or dressing (apraxia);
      Loss of ability to recognize and use familiar objects, for example, clothing (agnosia);
      Loss of ability to plan, organize, and execute normal activities, for example, going shopping

II. The problems in "I" represent a substantial decline from previous abilities, cause significant problems in everyday functioning, and begin slowly and gradually, becoming more severe.

III. The problems in "I" are not due to other conditions that cause progressive cognitive decline (eg, stroke, Parkinson's disease, Huntington's chorea, brain tumor, etc), and other conditions that cause dementia (eg, hypothyroidism, HIV infection, syphilis, and deficiencies in niacin, vitamin B12, and folic acid), not caused by delirium, and not caused by another mental illness, such as depression or schizophrenia.

Figure 3.3: NINCDS-ADRDA criteria for Alzheimer's disease. The table is adapted from Castellani et al. 2010

The medical history together with clinical, neurological and psychiatric examination serve as the basis in the diagnostic work-up. In very early cases, neuropsychological testing (such as mini-mental scale examination; MMSE) can help to obtain objective signs of memory disturbances (Blennow, et al. 2006). Neuroimaging (CT and MRI), plays an important part in the diagnosis of AD and the imaging usually shows diffuse or anteriorly predominant cortical and hippocampal atrophy. Positron emission tomography (PET) imaging of glucose metabolism and Aβ deposits by using Pittsburg compound B (PiB) and CSF biomarkers (Aβ 1-40 and 1-42, total and phospho tau) are also useful. Laboratory studies such as thyroid function tests and serum vitamin B12 are done to rule out secondary causes of dementia (Blennow, et al. 2006). A definitive diagnosis of AD can only be made by neuropathology, which is regarded as gold standard (McKhann, et al. 1984).

3.1.3 Neuropathology

Gross pathology

Classically, the brains of individuals with AD are atrophic with widened sulci, narrowed gyri and dilated ventricles (hydrocephalus ex vacuo) (Figure 3.4). The neurodegenerative process in AD probably initiates in the entorhinal cortex and the frontal cortex and disseminates to the hippocampus (Braak and Braak 1996) and other neocortical regions such as temporal, parietal and cingulate regions (Minoshima, et al. 1994). However, atrophy is mostly absent in the cerebellum and brain stem regions (Perl 2010).

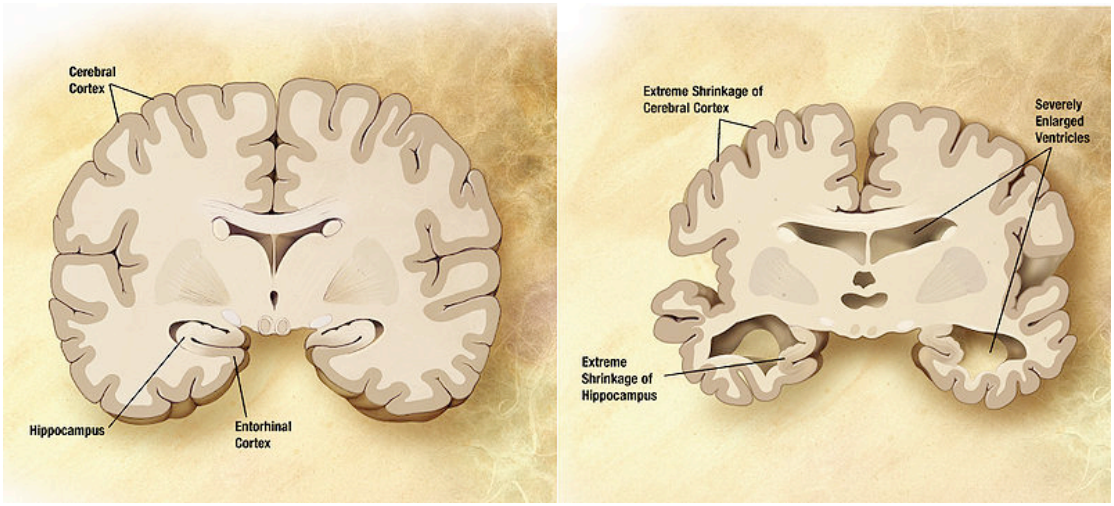

Figure 3.4: Comparison between brains of AD patient and healthy control *Left:* brain of a healthy control *Right:* brain of AD patient, showing generalized atrophy, ventricular dilation, widening of sulci and narrowed gyri. (Image from Alzheimer's Disease Education and Referral Center, a service of the National Institute on Aging).

Histopathology

The most common and distinctive 'hallmark' lesions present within the AD brain are the **senile plaques** and **neurofibrillary tangles (NFTs)**.

Senile plaques are complex, extracellular deposits composed primarily of amyloid-β, a 4 kDa β-pleated sheet structured peptide. The predominant beta-pleated sheet configuration of this protein confers its ability to bind the planar dye Congo red and produce birefringence when illuminated by polarized light; it thus conforms to the

physical definition of an amyloid (Perl 2010). The nosology of senile plaque has evolved over the years to include multiple plaque subtypes, including primitive, neuritic, compact, cored, cotton-wool and vascular (Castellani, et al. 2010). The neuritic plaque (Figure 3.5A) in particular has been touted to be the most pathogenically relevant and often highlighted as the plaque of significance. The neuritic plaques are thus called because of the dystrophic neurites, which surround them and show signs of neuroinflammation, such as activated microglia and astrogliosis. The vascular Aβ deposits, termed as cerebral amyloid angiopathy (CAA), affect medium and small-sized leptomenigeal and cortical arteries and arterioles and less frequently capillaries and veins (Rensink, et al. 2003). Microscopically, CAA consists of deposition of Aβ in the smooth muscle layer (tunica media) of the vessel wall. CAA leads to focal fragmentation of blood brain barrier and leakage.

NFTs are intraneuronal accumulation of hyperphosphorylated of microtubule-associated protein tau. NFTs are observed as abnormal fibrous inclusion bodies appearing as paired helical filaments (PHFs) within the neuronal cytoplasm in the brains of AD patients (Figure 3.5B). Most of these NFTs are found in the entorhinal cortex, amygdala, hippocampus and neocortex (Morrison and Hof 1997). Following neuronal death, NFTs remain extracellularly in the neuropil as ghost tangles.

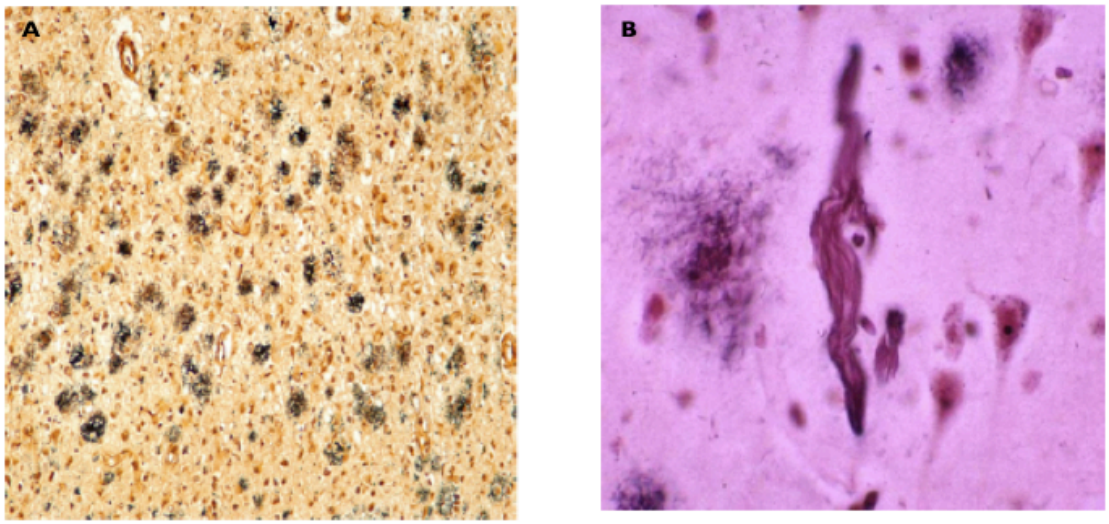

Figure 3.5: Plaque and NFT. (A) Senile plaque demonstrated by Bielshowsky silver impregnation **(B)** Neurofibrillary tangle as seen on Bielshowsky silver stain. Both images are adapted from Casetllani et al. 2010.

Apart from plaques and tangles, other histopatholigcal findings of the AD brain are neuronal and dendritic loss, neuropil threads, dystrophic neurites, granulovascular degenration and Hirano (Castellani, et al. 2010). The common refrain 'synapse loss is the most specific pathologic feature of AD' is now an accepted dogma, which is based on accumulating evidence associating synapse loss with soluble Aβ species (Castellani, et al. 2010). Even with the wealth of information available, the complete mechanism of neurodegenration is yet to understood.

3.1.4 Neuronal dysfunction in AD

There has been a paradigm shift over the last few years as to the mechanisms of neurodegeneration in AD. The original idea was that beta-amyloid plaque is the main neurotoxic species causing neuronal dysfunction, which was proposed by Hardy and Higgins in 1992 (Hardy and Higgins 1992). It is now known that Aβ can exist in diverse assembly states, including monomers, dimers, trimers, tetramers, dodecamers, high-order oligomers and protofibrils, as well as mature fibrils, which can form microscopically visible amyloid plaque in brain tissues (Glabe 2008). Much evidence suggests that Aβ oligomers are more potent than Aβ fibrils and amyloid deposits in eliciting abnormalities in synaptic functions and neural network activity (Cheng, et al. 2007, Cleary, et al. 2005, Klein, et al. 2001, Lesne, et al. 2006, Palop and Mucke 2010, Selkoe 2008, Shankar, et al. 2007, Shankar, et al. 2008, Tomiyama, et al. 2010, Walsh and Selkoe 2007). This has led to the revision of the original amyloid cascade hypothesis (Blennow, et al. 2006, Hardy and Selkoe 2002) (Figure 3.6).

Recent findings indicate that Aβ is part of an activity regulated mechanism that controls synaptic excitatory activation, in which Aβ induces presynaptic facilitation at low concentration and postsynaptic depression at high concentrations (Palop and Mucke 2010). Pathologically elevated Aβ may indirectly cause a partial block of NMDARs and shift the activation of NMDAR-dependent signaling cascades toward pathways involved in the induction of LTD and synaptic loss (Hsieh, et al. 2006, Kamenetz, et al. 2003, Shankar, et al. 2007).

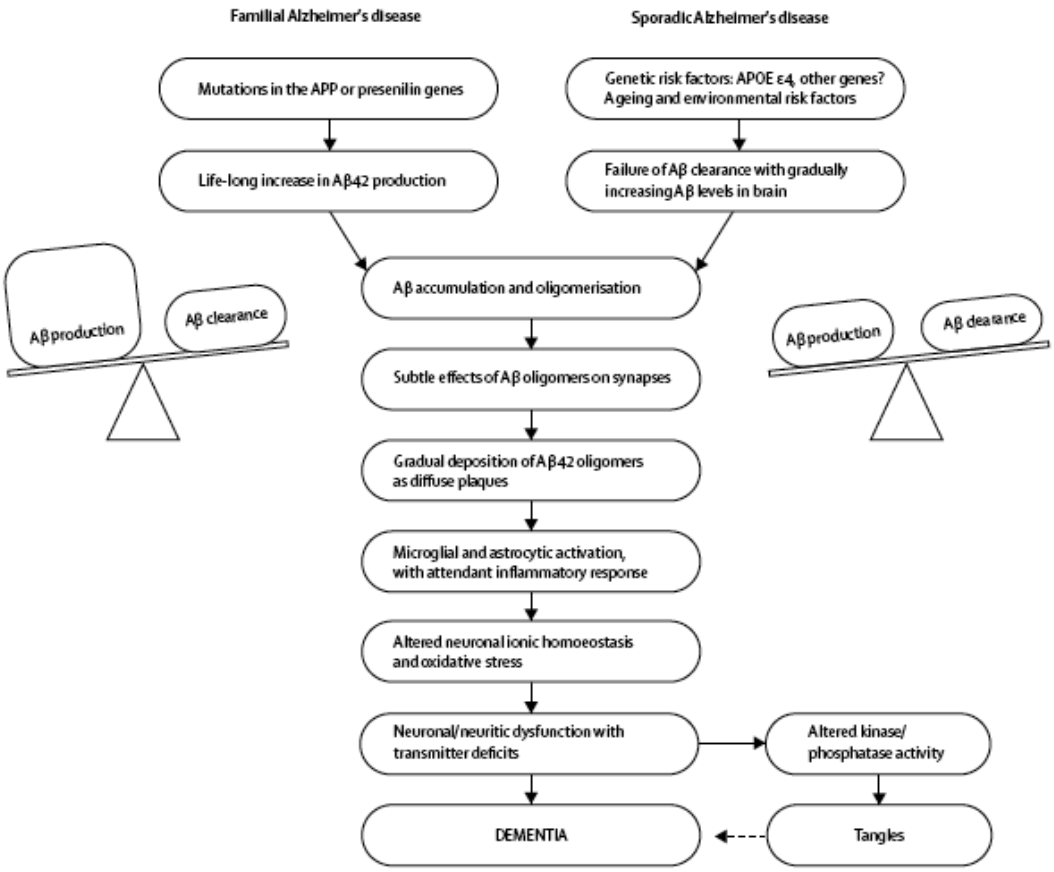

Figure 3.6: Revised amyloid cascade hypothesis. Sequential events in familial and sporadic AD that could ultimately lead to symptoms of dementia (adapted from Blennow, et al. 2006).

Although the mechanisms underlying Aβ-induced LTD have not yet been fully elucidated, they may involve receptor internalization (Hsieh, et al. 2006, Snyder, et al. 2005) or desensitization (Liu, et al. 2004) and subsequent collapse of dendritic spines (Hsieh, et al. 2006, Snyder, et al. 2005). Aβ-dependent effects on synaptic function may be mediated by activation of α7-nAChR (Snyder, et al. 2005), perisynaptic activation of NMDARs (Li, et al. 2009, Shankar, et al. 2007) and downstream effects on calcineurin–STEP–cofilin, p38 MAPK and GSK-3β signaling pathways (Li, et al. 2009, Shankar, et al. 2007, Tackenberg and Brandt 2009, Wang, et al. 2004)

Aβ also causes GABAergic dysfunction, which may contribute to the development of aberrant synchrony in neural networks and disruption of cognitive function (Palop and Mucke 2010). It is known that increased neuronal activity increases Aβ production and blocking neuronal activity has the opposite effect (Kamenetz, et al. 2003). Several recent reports in AD mouse models suggest that pathologically elevated Aβ

destabilizes neuronal activity at network levels (Palop and Mucke 2010). Defects in LTP are seen much before the appearance of plaques (Knobloch, et al. 2007a). *In vivo* calcium imaging of cortical circuits shows that APP/PS1 mice have a greater proportion of hyperactive and hypoactive neurons than nontransgenic controls (Busche, et al. 2008). Notably, these AD mouse models have reduced glutamatergic excitatory currents and synaptic loss, suggesting that high Aβ leads to aberrant patterns of neuronal activity by enhancing synchrony among the remaining glutamatergic synapses rather than by increasing excitatory synaptic activity *per se* (Palop and Mucke 2010). Emerging evidence also suggests that GABAergic dysfunction may be key in the pathogenesis of network dysfunction in AD. Important clues came from the demonstration of hyperactive and hypoactive neurons in cortical circuits of APP/PS1 mice, which point towards change of biophysics between excitatory and inhibitory neurons (Busche, et al. 2008, Grienberger, et al. 2012).

Different approaches which have been used to address the question of neuronal dysfunction in AD, ranging from non-invasive techniques such as electro-encephalogram (EEG) and fMRI in animals to invasive techniques such as extracellular recordings, calcium imaging in cells and slice cultures. Even though these techniques have provided a good understanding of the synaptic activity, not much is really known about the temporal alterations in neuronal activity and disease progression. Most recently Li et al. 2011 showed in cell culture model that soluble Aβ oligomers from three distinct sources (cultured cells, AD cortex, or synthetic peptide) inhibited LTP, and this was prevented by the selective NR2B inhibitors ifenprodil and Ro25-6981. Soluble Aβ enhanced NR2B-mediated NMDA currents and extrasynaptic responses. More *in vivo* studies addressing the issue of the relationship between Aβ-induced alterations at the level of circuits and networks are required.

3.1.5 Mouse models of AD

A number of transgenic mice have been created over the last two decades that overexpress APP and/or presenilin containing one or more mutations linked to familial AD. These mice recapitulate many key aspects of AD, including amyloid neuropathology, cerebral amyloid angiopathy, synaptic loss, dystrophic neurites, and reactive gliosis, as well as impairments in synaptic plasticity and learning and

memory. Such mouse models exhibit these characteristics to varying extents, and are widely used to investigate the roles of APP, Aβ, and amyloid pathology in the pathogenesis of AD. Although APP transgenic mice exhibit many of the key features of AD, neurofibrillary tangles are notably absent (Chin 2011).

Table 3.1 gives an overall summary of few widely used animal models in AD. However the following points should be kept in mind before choosing an animal model (Chin 2011).

1. None of the currently available transgenic lines fully recapitulate all aspects of AD, although several lines are able to recreate one or more of the major pathological hallmarks.
2. Different lines of transgenic mice exhibit varying ages of onset of impairment. This is an important consideration both for scientific and practical reasons. The animal model needs to be chosen according to the scientific questions. Early age of onset and fast disease progression may be useful for biochemical investigations but if behavioral training and therapeutics is involved, late onset and slow disease progressing line should be chosen (Chin 2011).
3. The background strains on which transgenic mice have been created are important to consider, particularly for behavioral analysis. Inbred mice often show less variability than outbred mice. Outbred mice have been used in many studies that have advanced our understanding of AD, but it is important to keep in mind that larger sample size may be required (Chin 2011).
4. Different inbred strains have different behavioral profiles, and some strains are ‘better learners’ than others or are more active than others etc (Chin 2011).

Finally, this repository of transgenic mice offers a wealth of opportunity to investigate the cellular mechanisms underlying AD, and the choice of mouse model for research should be guided by the specific questions to be answered.

In this dissertation, we used APPswe mice, which has slow growing AD pathology with initial plaques appearing around age of 8-10 months (Hsiao, et al. 1996).

Transgenic mouse	Transgene (mutation)[a]	Promoter	Strains	Amyloid plaques	NFTs	Neuron loss	Cognitive deficits
PDAPP	APP695, 751, 770 (APPInd)	PDGF-β	C57Bl/6 J, DBA/2, Swiss-Webster	6–9 months	No	No	Yes
Tg2576	APP695 (APPSwe)	Hamster PrP	C57Bl/6SJL, C57Bl/6	9 months	No	No	Yes
APP23	APP751 (APPSwe)	Mouse Thy-1	C57Bl/6, DBA/2	6 months (severe CAA also present)	No	14 months	Yes
J20[b]	APP695, 751, 770 (APPSwe, Ind)	PDGF-β	C57Bl/6	6 months	No	No	Yes
TgCRND8	APP695 (APPSwe, Ind)	Hamster PrP	C3H, C57Bl/6	3 months	No	No	Yes
mThy1-hAPP751	APP695 (APPSwe, Lon)	Mouse Thy-1	C57Bl/6, DBA/2	3–4 months	No	No	Yes
APPDutch	APP751 (APPDutch)	Mouse Thy-1	C57Bl/6 J	22 months (CAA only)	No	Not reported	Not reported
ARC6, ARC48	APP695, 751, 770 (APPSwe, Ind, Arc)	PDGF-β	C57Bl/6	3 months (6) 2 months (48)	No (6) No (48)	No (6) No (48)	No (6) Yes (48)
PSAPP	Tg2576 X PSEN1-M146L	Hamster PrP PDGF-β	C57Bl/6SJL, C57Bl/6 B6D2F1, Swiss-Webster	6 months	No	No	Yes
5XFAD	APP695 (Swe, Lon, Flo) PSEN1-M146L, L286V	Mouse Thy-1 Mouse Thy-1	C57Bl/6SJL	2 months	No	9 months	Yes

3.1.6 Therapeutic strategies

Despite decades of research, till today there is no cure for AD. The available treatments offer relatively small symptomatic benefit and largely remain palliative in nature. At the moment, there are only four FDA approved drugs in the market. Three of them (Donepezil, Galantamine and Rivastigmine) are **acetylcholinesterase inhibitors** and thus increase the cholinergic transmission in the brain. These drugs are used in mild to moderate disease. The fourth drug, **Memantine**, is a noncompetitive NMDA receptor antagonist and helps to reduce the neurotoxicity. Memantine is approved for treating the advanced stages of AD. Various new drug targets have been identified over the last decades. The categories include immunotherapy (Schenk, et al. 1999), Aβ aggregation inhibitors (Roberson and Mucke 2006), β and γ secretase inhibitors (Chang, et al. 2007, Roggo 2002, Siemers, et al. 2006), neurotropins (Tuszynski, et al. 2005), antioxidants (Jama, et al. 1996), statins (Fassbender, et al. 2001, Jick, et al. 2000), NSAIDs (Aisen, et al. 2003, Hirohata, et al. 2005, in t' Veld, et al. 2001), PPARγ agonists (Roberson and Mucke 2006) calcium channel blockers (Roberson and Mucke 2006), glycogen synthase kinase inhibitors (Roberson and Mucke 2006), phosphodiesterase inhibitors (Roberson and Mucke 2006), hormone replacement therapies (Casadesus, et al. 2007, Webber, et al. 2005) and Mediterranean diet (Scarmeas, et al. 2006) to name a few. Huge clinical trials are currently under way to prove the efficacy of these drugs.

Of all the new strategies mentioned above, immunotherapy has been the most promising with hundreds of reports over the last decade. In 1999, Schenk et al. reported the first evidence that active Aβ immunotherapy could reduce Aβ pathology *in vivo*. Ever since then, the AD community has been trying to validate the immunotherapy approach (DeMattos, et al. 2001, Hock, et al. 2003, Janus, et al. 2000, Morgan, et al. 2000, Spires-Jones, et al. 2009, Wilcock, et al. 2004a, Wilcock, et al. 2004b). Both active (injecting Aβ peptide) and passive (injecting anti-Aβ antibody) have been applied in various mice models and some of these have been tried in humans too. To mention one human trial, in 2000, a randomized placebo-controlled Phase IIa trial with vaccine AN1792 (synthetic form of Aβ 1-42 and surface-active saponin adjuvant QS-21) was initiated. However, the trial was stopped in 2002 after 6% of patients developed aseptic meningioencephalitis and leukoencephalopathy

(Bayer, et al. 2005, Gilman, et al. 2005). Even though this trial raised several questions about the safety of the vaccine, a cohort of the antibody responder patients did show cognitive improvement, reduced plaque load, increase in brain volume and serum titers of anti-Aβ antibodies (Fox, et al. 2005, Hock, et al. 2002, Nicoll, et al. 2003, St George-Hyslop and Morris 2008).

Several mechanisms could explain how antibodies directed at amyloid-β (Aβ) promote the clearance of this peptide *in vivo* (Lemere and Masliah 2010). When anti-Aβ antibodies form complexes with Aβ peptides, the Fc portion of the antibodies might bind the Fc receptor on microglia, inducing phagocytosis of these complexes (Bard, et al. 2000). This mechanism would require that anti-Aβ antibodies cross the blood–brain barrier (BBB) and bind Aβ within the CNS. Some evidence has been reported to support this mechanism; however, two studies have demonstrated that Fc mediated phagocytosis is not required for immunotherapy-induced Aβ clearance (Bacskai, et al. 2002, Das, et al. 2003). In an alternative mechanism, anti-Aβ antibodies in the blood might cause a shift in the concentration gradient of Aβ across the BBB, thus resulting in an increase in Aβ efflux from the brain to the periphery (DeMattos, et al. 2001, Lemere, et al. 2003). Aβ antibodies might bind and remove small Aβ aggregates, thereby neutralizing the effects of toxic Aβ species on synapses (Klyubin, et al. 2005). One study suggests that certain antibodies (for example, a midregion Aβ antibody, m266) sequester monomeric Aβ inside the brain, facilitating clearance of the peptide and preventing build up of toxic, aggregated forms of Aβ (Yamada, et al. 2009). Several of these proposed mechanisms are depicted in Figure 3.7.

These proposed mechanisms of Aβ clearance by immunotherapy are not mutually exclusive and might be disease stage-dependent. For example, a preventive vaccine administered before cerebral amyloid accumulation might not require that the antibodies cross the BBB to enhance Aβ clearance and maintain Aβ in its monomeric state. By contrast, a therapeutic vaccine (delivered once plaque deposition is well underway) would probably benefit from the transport of Aβ antibodies into the CNS to induce Aβ phagocytosis and neutralize local Aβ toxicity. Circulating anti-Aβ antibodies in the periphery might pull Aβ from brain to blood for clearance, thereby preventing further deposition (Lemere and Masliah 2010). More *in vivo* studies

looking at the plaque-antibody interactions are required dissect out the mechanism of action.

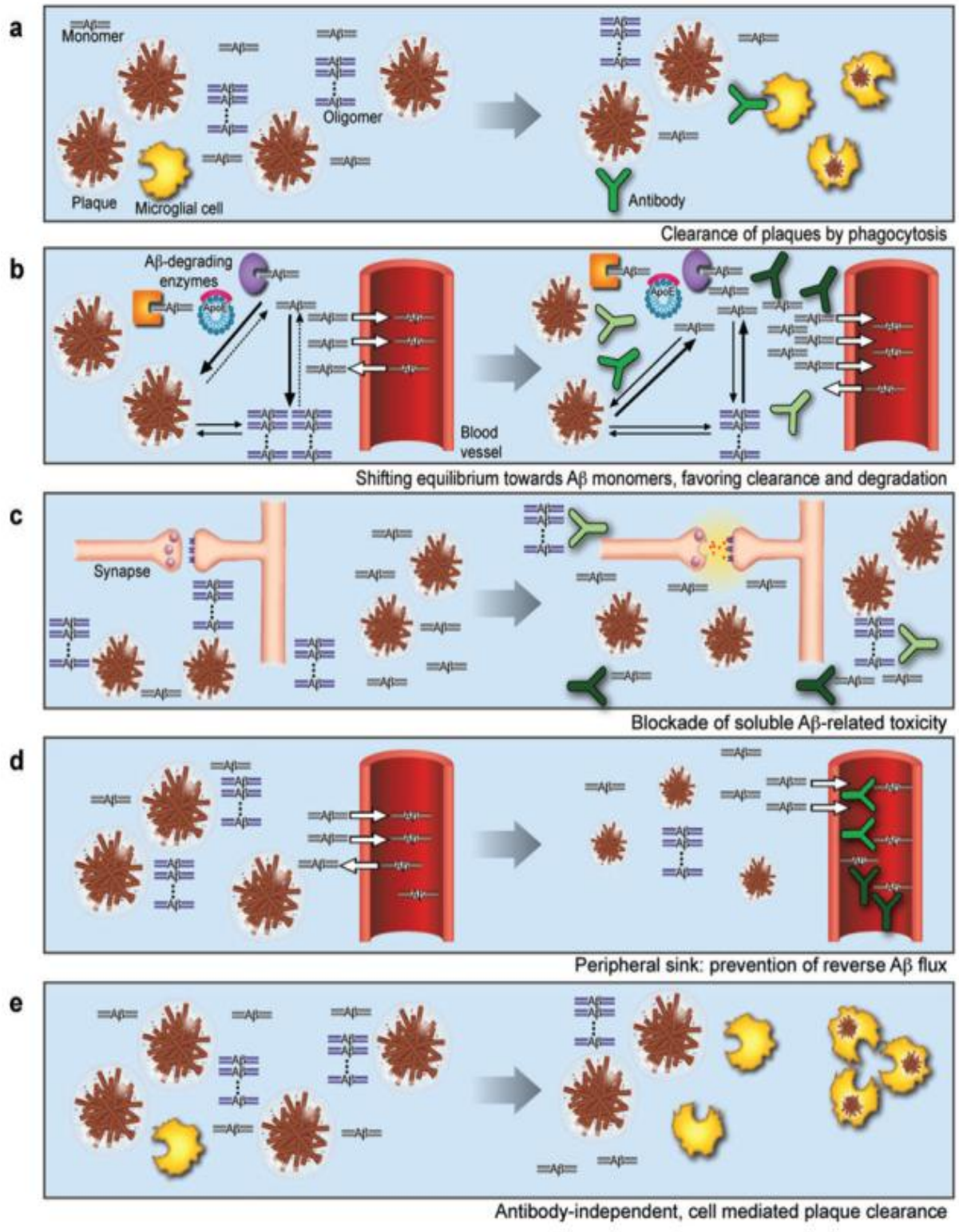

Figure 3.7: Proposed mechanism of action of immunotherapy. Image adapted from Brody and Holtzman 2008.

3.1.7 Microglia in AD

Microglia are brain-resident macrophages derived from myeloid cells in the periphery and comprise approximately 12% of cells in the brain (Block, et al. 2007). In the mature brain, microglia typically exist in a resting state characterized by ramified morphology and highly dynamic monitoring of the brain environment (Davalos, et al. 2005, Nimmerjahn, et al. 2005). Microglial overactivation is an early pathogenic event that precedes neuropil destruction in patients with AD (Cagnin, et al. 2001). Even before the development of symptoms, activated microglia cluster at the sites of aggregated Aβ and penetrate neuritic plaques (McGeer, et al. 1987, Veerhuis, et al. 1999).

Soluble and insoluble fibrillar Aβ can bind to a plethora of receptors expressed by microglia (Figure 3.8). At least *in vitro,* microglia are able to take up Aβ after direct or indirect binding to its respective receptors (Rogers and Lue 2001, Rogers, et al. 2002). Traditionally, focus of intensive research was the inflammatory and oxidative response of microglia stimulated by fibrillar Aβ. Upon stimulation with fibrillar Aβ, microglia can respond by secretion of neurotoxic and neuroprotective molecules. Among the most prominent factors considered to be neurotoxic in AD are cytokines (e.g., TNFα, IL-1, IL-6), chemokines, complement factors, prostanoids, and reactive oxygen species like superoxide and nitric oxide (Akiyama, et al. 2000). But microglia can also produce 'beneficial' cytokines such as IL-4, IL-10 and transforming growth factor – β (TGFβ), which may reduce neuroinflammation and thereby modulate disease progression (Tesseur, et al. 2006, Wyss-Coray 2006). One of such receptor, which controls microglial neurotoxicity, is fractalkine receptor (CX3CR1) (Cardona, et al. 2006). Knocking out of this receptor prevents neuronal loss indicating the critical role of CX3CR1 receptor in neuron-microglia communication (Fuhrmann, et al.). In CRND8 AD mouse model, deletion of CX3CR1 resulted in lower brain levels of Aβ 1-40 and Aβ 1-42 and CX3CR1 deficient microglia had greater phagocytic ability thus leading to greater amyloid content within microglial phagolysosomes (Liu, et al. 2010). Another study reported that ablation of microglia using thymidine kinase of herpes simplex virus in APP/PS1 mouse model did not alter either amyloid plaque formation, maintainence or amyloid associated neuritic dystrophy (Grathwohl, et al. 2009). Moreover, it is known that systemic application of anti-Aβ antibody

results in increased in both number of microglia and number of cellular processes per cell within 72 hours of application (Koenigsknecht-Talboo, et al. 2008). Thus, exact role of microglia in development of AD pathology and it's response after therapeutic treatments still need to be explored in greater detail.

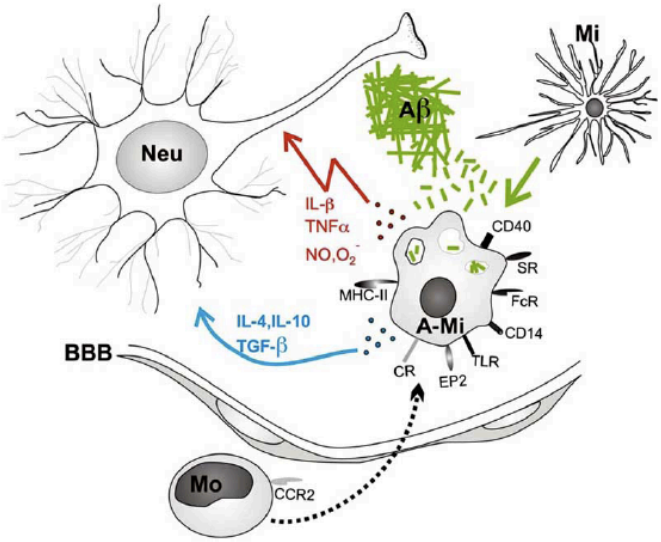

Figure 3.8: Plaque-microglia dynamics: Soluble Aβ (-), generated by neurons (Neu) is toxic to neurites and synapses. Soluble Aβ also seems to be sequestered from amyloid plaques. "Resting microglia" (Mi) become recruited to the amyloid plaques. Two populations could account for the increase in microglia: First, endogenous brain microglia migrate to the lesion and proliferate. Second, peripheral blood cells, e.g. Ly- 6ChiCCR2+monocytes (Mo), are recruited from the periphery and cross the blood-brain-barrier. Aβ can bind to a plethora of microglial receptors. Microglia become activated (A-Mi) and secrete neurotoxic and/or anti-inflammatory molecules. In addition, some microglia may have the ability to take up soluble or insoluble forms of Aβ. SR: Scavenger Receptor; TLR-Toll-like-receptor; CR-Complement receptor; MHC-II: major histocompatibility class II; BBB: blood brain barrier. Image adapted from Schlachetzki 2009.

The interplay between amyloid plaques and microglia is highly dynamic Bolmont, et al. 2008, showed in a transgenic AD mouse model, that the number of plaque associated microglia increased over time either via proliferation or infiltration. Microglial cells quickly migrated towards newly developed plaques and extend their processes towards the plaques. Microglia at the interface of the plaque were highly dynamic and showed membrane movement and process motility. Larger plaques were surrounded by larger microglia. The size of plaques corresponded over time to the volumes of the surrounding microglial cells. Interestingly, it seemed that there was a relationship between microglial cell volume and number; increase in the cell volume of microglia was accompanied with fewer cells in the vicinity of a plaque. It was

hypothesized to be a compensatory mechanism. A limited number of microglia in the vicinity of a plaque could respond with larger cell bodies to cover the plaque. The plaque size changed over time; the smaller plaques got bigger and the bigger plaques smaller (Bolmont, et al. 2008). The growing plaques had an initial smaller size with only little microglial coverage. The plaques that decreased in size over time had the highest number of microglial cells. This could imply that a sufficient number of microglia can prevent plaque growth by preventing the transformation of local soluble Aβ to insoluble fibrillar Aβ and by an uptake of the sequestered soluble Aβ. Furthermore, it points towards the potential of microglia to phagocytose and/or degrade Aβ extracellularly. Still, only scarce information is available about the role of microglia before, during and after plaque deposition occurs and how it modulates neuronal activity. There are few two-photon imaging studies that have addressed the question of microglia and neuronal interaction. Fuhrman el al showed that knocking out of CX3CR1 receptor prevents neuronal loss indicating the critical role of CX3CR1 receptor in neuron-microglia communication. We tried time-lapse imaging of GFP expressing microglia AD transgenic before and after topical antibody application as a means to understand plaque-microglia interactions.

3.2 *In Vivo* Two-photon Imaging in Neocortex

Scientists have always fancied visualization of live cells. Imaging with high resolution in the living animal while extracting quantitative information has become a reality now (Kerr and Denk 2008). The *in vivo* imaging spectra encompasses various modalities ranging from magnetic resonance imaging (MRI), functional MRI (fMRI), computed tomography (CT), positron emission tomography (PET) to optical imaging techniques such as optical coherence tomography and nonlinear optical imaging (two-photon microscopy). MRI, fMRI, CT and PET allow the imaging of the whole brain and offer very good temporal resolution, however, their spatial resolution of few millimeters is a limiting factor. Of all the currently available *in vivo* imaging techniques, two-photon laser scanning microscopy (2PM) is able to study both the structure and function of nervous system at high spatial resolution, resolving individual cells, which has been the main focus of this dissertation work.

3.2.1 *In vivo* two-photon microscopy

2PM emerged as a technique in 1990 (Denk, et al. 1990), although two-photon excitation has been predicted around 1930 (Göppert-Mayer 1931). In 2PM, fluorescent molecules are excited by the quasi-simultaneous absorption of two near-infrared photons (Figure 3.9A). Two-photon excitation has a quadratic dependence on excitation intensity and therefore produces excitation only in a small focal volume; negligible out-of-focus fluorescence is generated, causing intrinsic optical sectioning, reduced background and reduced photobleaching and photodamage outside the plane of focus. In practical terms, 2PM makes it possible to acquire high contrast images by using a wavelength that is less harmful to live cells. In particular the use of near-infrared light makes it possible to image deeper in the tissue, owing to less scatter of the incident light and the localized excitation makes 2PM less sensitive to light scattering because all photons can be correctly assigned to focal volume. Due to these special features, 2PM has become the method of choice for high-resolution, deep tissue, intravital microscopy (Helmchen and Denk 2005).

To improve the efficiency of two-photon excitation, ultrafast lasers emitting short pulses (<100 fs) of light at a rapid frequency (~100 MHz) are used. Using these

lasers, very large peak intensity can be achieved in a repeated pulse train to sustain fluorophore excitation exclusively at the focal plane where the density of the photon flux is sufficiently high. Typically, Titanium:Sapphire (Ti:Sapphire) lasers with average power of >1W and tunable wavelength in the range of 670-1,070 nm are used (Figure 3.9B).

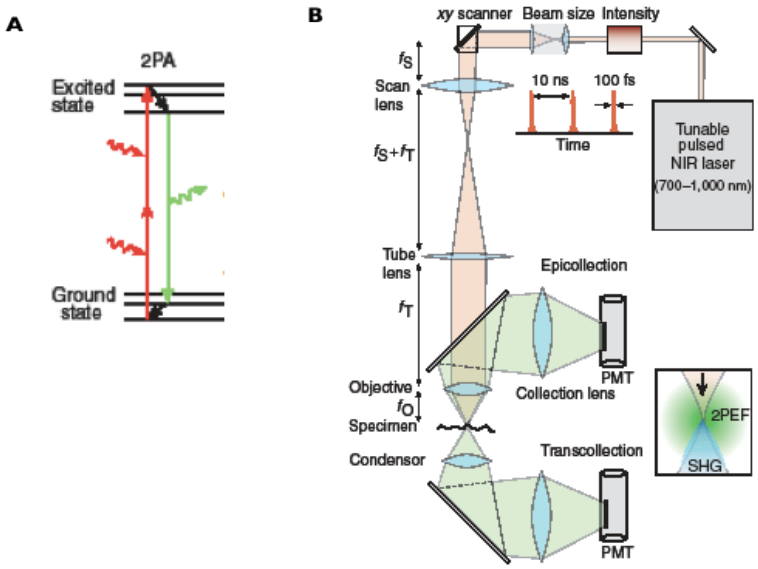

Figure 3.9: Principle of two-photon microscopy (A) Simplified Jablonski diagram showing two-photon excitation process. **(B)** Schematic of a two-photon microscope with epifluorescence and transfluorescene detection as used in this dissertation. Images adapted from Helmchen and Denk 2005.

A simple and efficient detection pathway is used in 2PM to capture as many of the potentially highly scattered signal photons as possible. In most systems a 'whole-area' epifluorescence detection scheme is used, with all the light that is collected by the objective also guided onto the detector (Figure 3.9B) (Helmchen and Denk 2005). For small or transparent specimens trans-fluorescence collection is used. However, in deep scattering specimens epicollection is the only practical mode that can be used (Helmchen and Denk 2005).

Ever since its discovery, 2PM has opened up new avenues in high-resolution imaging of intact tissues and living animals and is still an expanding field. Systems as diverse as immune system (Bousso and Robey 2004), renal system (Molitoris and Sandoval 2005), cardiovascular system (Rubart 2004), respiratory system (Nava, et al. 2010), skin (Laiho, et al. 2005) and nervous system (Helmchen and Denk 2002) have been examined in detail at depths of up to few hundred microns using 2PM, while leaving the tissue intact (Helmchen and Denk 2005). Observing the same cells over time is often more sensitive and more physiologic than trying to deduce how cells change from 'snapshots' of fixed tissue (Misgeld and Kerschensteiner 2006). Observation of the sequence of pathological events can establish their causative relationship and the pathology can be compared before and after therapeutic intervention. Nervous system is a highly dynamic organization of neurons and glial cells, where information exchange occurs in time scale of milliseconds. Thus, making it an optimum system for 2PM, which has been utilized to study neuronal activity (Busche, et al. 2008, Grienberger, et al. 2012), microglial dynamics (Nimmerjahn, et al. 2005) and astrocyte activity (Kuchibhotla, et al. 2009). Furthermore, 2PM is also a useful tool to study disease progression and has been used to study pathophysiology of different disease models (discussed in detail below). We have applied the principles of long term imaging for structural and functional imaging of nervous system in our project.

With the development of new *in vivo* fluorescence techniques, 2PM is currently widely used in all fields of neurobiology. With the development of various types of genetically modified mice and vital dyes, it is now possible to image almost all the cell types in the mammalian brain, such as dendrites, axons (Lee, et al. 2006, Portera-Cailliau, et al. 2005), microglial (Jung, et al. 2000), astrocytes (Nimmerjahn, et al. 2004) and oligodendrocytes (Fuss, et al. 2000, Nolte, et al. 2001). Congo red derived dyes such as Methoxy-X04 can be injected intraperitoneally and stain the beta-amlyoid plaques specifically (Klunk, et al. 2002). Viral labeling strategies also available and can be combined with transgenic mouse lines (Dittgen, et al. 2004). Intravenous injection of high molecular weight dextran allows labeling of neurovascular structures too (Bacskai, et al. 2002). Even cellular compartments can be labeled *in vivo* with fluorescent proteins by attaching them to membrane proteins or by using specific targeting sequences (De Giorgi, et al. 1999). Thus, almost all

cellular subtypes can be tagged, labeled and imaged. We have been able to label and image neurons, microglia, astrocytes, blood vessels and beta-amyloid plaques in this project.

As exciting as the field of two-photon microscopy is, it is important to understand the limitations of the technique. High-resolution optical imaging techniques are currently practically limited to within 500 μm (with most optimum preparations may be 800 μm) of the brain tissue. As a consequence, in the brain, these techniques are more suitable for the examination of grey matter diseases than white matter diseases, and favor studying pathology in the cortex (for example, Alzheimer's disease) over changes in deeper brain regions (for example, Parkinson's disease) (Misgeld and Kerschensteiner 2006). However, the anatomy is reversed in the spinal cord, where the axon tracts lie superficially and white matter pathology (such as axon trauma) is easier to study than grey matter pathology (such as motor neuron degeneration). Few other points have to be kept in mind, it is crucial that robust labeling exists for the cells that mediate a given disease and disease models with a well-defined trigger and time course are best suited for *in vivo* studies (Misgeld and Kerschensteiner 2006).

In vivo imaging has been used to study various nervous system dysfunction models---neurodegenerative diseases such as Alzheimer's disease (Bacskai, et al. 2002, Busche, et al. 2008), amyotrophic lateral sclerosis (ALS) (Schaefer, et al. 2005); spinal cord injury and trauma models (Kerschensteiner, et al. 2005); ischemia and stroke models (Zhang, et al. 2005a, Zhang, et al. 2005b); neuroinflammation models such as experimental autoimmune encephalomyelitis (EAE) (Kawakami, et al. 2005, Nitsch, et al. 2004). Below we will summarize the 2PM studies in field of AD (see 3.4).

3.2.2 Calcium indicators to study neuronal networks

Two-photon calcium imaging is currently the prevailing optical method for probing neuronal networks *in vivo* (Garaschuk, et al. 2006). The rational is that rises in cytosolic calcium can be used as an indirect measure of neuronal activity. When neurons fire action potentials, voltage gated calcium channels in the plasma membrane open up and lead to a rise in cytosolic calcium within few milliseconds (Garaschuk, et al. 2006). Detecting these changes with a fluorescent calcium indicator has been used to monitor activity of large numbers of neurons optically within the brain of living animals (Garaschuk, et al. 2006, Gobel and Helmchen 2007). The family of calcium indicators can be broadly divided into **synthetic calcium indicators** and **genetically encoded calcium indicators.**

The field of synthetic calcium indicators was revolutionized with the discovery of BAPTA and in particular Oregon Green BAPTA-1 (OGB), a fluorescent polycarboxylate compound with strongly improved fluorescence properties (Tsien 1981, Tsien 1989). The acetoxymethyl esters (AM esters) of these compounds can be noninvasively loaded into living cells (Tsien 1989, Tsien 1992). Because of their properties such as high sensitivity for calcium, fast binding and dissociation kinetics, fairly linear response properties, pH-resistance and photostability, over the last two decades AM dyes have been extensively used to study activity of neuronal populations. Unfortunately, there are several drawbacks of using synthetic calcium dyes in intact brain tissue. To name a few; compartmentalization of the dye to cellular organelles or leaking out of cells during long recording periods, diffuse and indiscriminate labeling of neuronal architecture, short duration (4-6 hours) of staining after loading and chronic imaging is impractical (Mank and Griesbeck 2008).

A breakthrough in the area of *in vivo* calcium imaging was achieved in 1997 with the development of genetically encoded calcium indicators (GECIs) based on green fluorescent protein (Miyawaki, et al. 1997). The term ‘genetically encoded’ refers to the fact that the sensors are solely composed of amino acids with no addition of any synthetic compound or cofactor that would be difficult to apply into a living brain. Thus, these sensors are encoded by a stretch of DNA that can be manipulated, mutated by recombinant DNA technology. When the DNA coding for the sensor is

delivered into a cell, the sensor is formed within the cell *in situ*. Combined with the use of cell-type specific promoters, cellular targeting sequences and transgenic technology, GECIs offer a noninvasive means to implant an indicator deeply within a living tissue (Mank and Griesbeck 2008).

During the last decade, several classes of fluorescent protein calcium sensors utilizing different mechanisms of activation have been designed (Figure 3.10). Most of these use calmodulin as the transducer protein and only recently calcium sensors using other calcium-sensitive proteins have been explored (Heim and Griesbeck 2004, Mank, et al. 2006). It was subsequently observed that some of the calmodulin-based sensors undergo specific interactions with other proteins in the neuronal cytoplasm, which render the sensor partially calcium insensitive (Hasan, et al. 2004, Palmer, et al. 2004). Thus, a new generation of probes with mutations in calmodulin interaction sites were designed, which has led to further improvements of performance (Heim and Griesbeck 2004, Palmer, et al. 2004). FRET-based sensors employing troponin C as calcium binding moiety are also promising (Mank, et al. 2008).

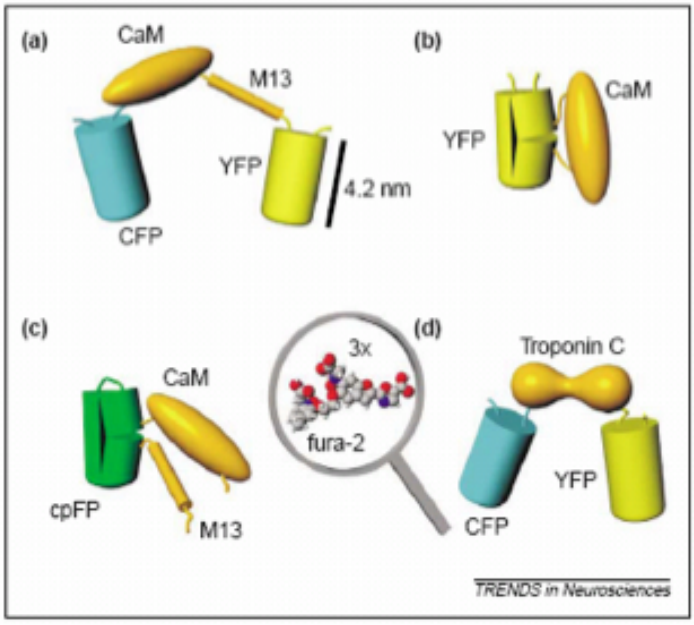

Figure 3.10: Genetically encoded calcium indicators. Four well explored designs **(a)** Yellow cameleon, **(b)** Camgaroo, **(c)** G-CaMP/Pericam, **(d)** TN-L15. Fluorescent reporter proteins are cyan (CFP), yellow (YFP) and green (GFP) fluorescent proteins. Calmodulin, the calmodulin binding polypeptide M13 (M13) or troponin C are sandwiched between a CFP-YFP FRET pair (a,d), inserted in YFP (b) or attached to a circularly permuted fluorescent protein (cpFP). Also shown is the 3x magnified molecular structure of the non-protein calcium indicator, Fura-2, for comparison. Image adapted from Knopfel 2006.

The first generation of 'yellow cameleons' (YC) were called so because of their color change from bluish to yellowish on excitation and extension of M13 into and out of the mouth of calmodulin like a large tongue (Miyawaki, et al. 1997). YC3.60 (Figure 3.11), the indicator that was used in this dissertation work was generated using circular permuted Venus 173 variant (cpVenus173) as a YFP FRET partner of CFP and showed efficient FRET responses with a large dynamic range in cuvette and cultured HeLa cells (Nagai, et al. 2004). However, functional characterization of YC3.60 had remained incomplete until now. It was recently shown that YC3.60 under human synapsin promoter (delivered using AAV2 vector) reported both spontaneous and whisker evoked neuronal activity with high sensitivity and dynamic range (Lutcke, et al. 2010). Calcium measurements were performed from individual apical dendrites of cortical neurons as well as from population of neurons using two-photon microscopy. It was also demonstrated that YC3.60 calcium signals in rodent barrel cortex could be read out in a bulk fashion (Lutcke, et al. 2010). With the development of gene delivery with the use of recombinant viral vectors using lentivirus and adeno-associated virus (Dittgen, et al. 2004, Wallace, et al. 2008), it is now possible to study neuronal ensembles *in vivo* over a period of weeks to months (Tian, et al. 2009).

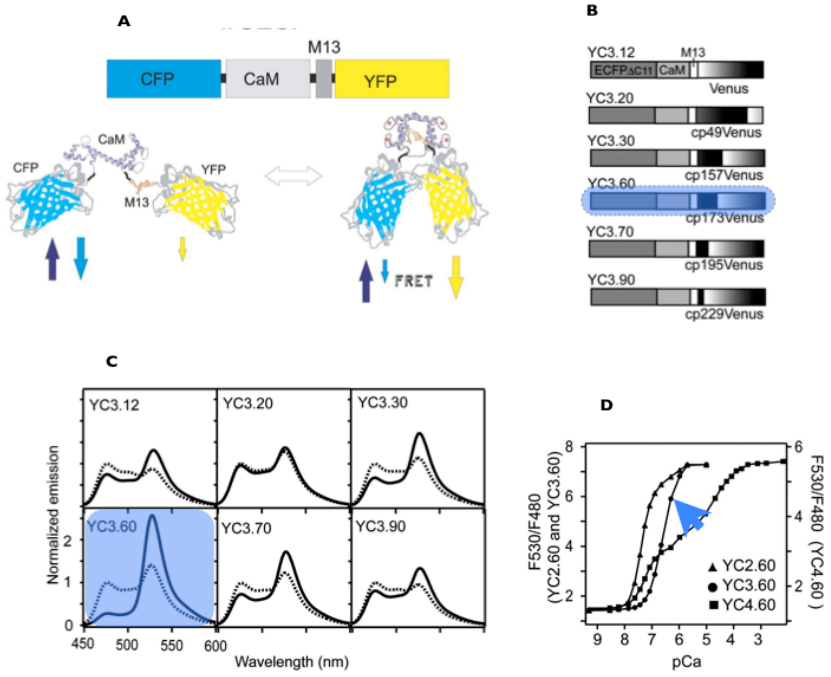

Figure 3.11: YC3.60. (A) Structure of YC3.60 **(B)** construct of the indicator (highlighted in blue), **(C)** excitation emission spectrum of YC3.60 (highlighted in blue), **(D)** response property for physiologic calcium concentration (blue arrow). Images adapted from Kotlikoff 2007, Nagai et al. 2004.

Other indicators apart from YC3.60 which have been used are Camgaroo 1 and 2 in Drosophila model (Yu, et al. 2003), inverse pericam in zebrafish and mouse olfactory bulb (Li, et al. 2005, Yu, et al. 2003), D3cpV in mouse cortex (Wallace, et al. 2008), TN-XL in Drosophila (Mank, et al. 2008), GCaMP2 in mouse olfactory bulb and mouse cerebellum (Diez-Garcia, et al. 2005, Fletcher, et al. 2009), GCaMP3 in mouse cortex, mouse hippocampus, Drosophila and C. elegans (Dombeck, et al. 2010, Seelig, et al. 2010, Tian, et al. 2009). All these studies imaged neuronal network ranging from few days to months. However, there are many disadvantages of GECIs as well; such as poor signal-to-noise ratio, low sensitivity for detecting calcium transients and inability to resolve single action potentials (Liebscher and Meyer-Luehmann 2012). It has also been reported that some of the indicator can cause cell damage (Tian, et al. 2009). Technical developments such as more sensitive cameras, new lasers, improved software, commercial imaging setups are making chronic imaging more realistic (Looger and Griesbeck 2012). Thus, GECIs even though offer great opportunity to study long term functional imaging, is still work under progress.

3.2.3 Rodent barrel cortex

We needed a model system in order to study the effects on neuronal excitability. We chose barrel cortex as the model system because it is a very well developed somatosensory region in rodents. Rodents, being nocturnal animals, must gather information about their surroundings without use of vision. It is this reason that evolution has gifted them with highly sensitive array of facial whiskers (Figure 3.12A). With the use of whiskers, rodents can build spatial representation of their environment, locate objects and perform texture discrimination (Petersen 2007). The whiskers are arranged in a highly organized pattern allowing identification of individual whiskers (Figure 3.12B).

Figure 3.12: Rodent whiskers. (A) Organized array of whiskers **(B)** Pattern and naming of whiskers. The rows are named A-E top to bottom and the arcs 1,2,3… antero-posteriorly **(C)** direction of movement of whiskers. Images adapted from Petersen 2003.

The sensory information from the whiskers is processed in the primary somatosensory cortex (S1) or the so-called 'barrel cortex', where each whisker is represented by a discrete and well-defined structure in layer 4 (Woolsey and Van der Loos 1970). These layer 4 'barrels' are somatotopically arranged in an almost identical fashion to the layout of the whiskers on the snout and the barrels can be easily visualized both in living and stained brain slices (Finnerty, et al. 1999, Petersen and Sakmann 2000). This barrel map, by and large is genetically specified and forms early in development. Deflection of a whisker probably opens mechanogated ion channels in nerve endings of sensory neurons innervating the hair follicle. The resulting depolarization evokes action potential firing in the sensory neurons of the trigeminal nerve, which are relayed in the ventral posterior medial (VPM) nucleus of thalamus and finally projected to the primary somatosensory cortex (Petersen 2007). A stimulus delivered to a layer 4 barrel first causes depolarization within layer 4 barrel, which then in the subsequent milliseconds spreads to depolarize neurons in layer 2/3 in a strictly columnar fashion. 2PM has been able to record single action potentials from evoked calcium transients in layer 2/3 neurons as response to whisker stimulation (Kerr, et al. 2007). It's also known that probability of neuronal response is higher in the barrel than above the septa or neighboring barrel (Kerr, et al. 2007). Thus, the barrel cortex sensory system is an attractive model for investigating active sensory processing and sensorimotor integration.

The well-defined somatotopic map of whiskers allows the use of optical techniques to map the whiskers. In the mouse, highly localized intrinsic signals can be evoked by repetitive deflection of a particular whisker can be imaged through the intact skull (Orbach, et al. 1985). The physical basis of the intrinsic signals are related to changes in blood flow and are therefore similar to those underlying in the blood oxygenation level-dependent (BOLD) signal observed in fMRI. Intrinsic optical imaging has the advantage of being quick and extremely reliable (Petersen 2007).

3.4 Two-Photon Microscopy in AD research

Application of 2PM in AD research is a relatively new approach and the first promising reports are just a decade old. The very first study, which used the technique of 2PM in AD, was Christie, et al 2001. They were able to image beta-amyloid plaques in Tg2576 mice using thioflavine-S and did not see any change in plaque growth over a period of 5 months (Christie, et al. 2001). Since then, the focus has been on *in vivo* imaging of beta-amyloid plaques and the surrounding cellular changes. Structural imaging of neurites in the vicinity of beta-amyloid plaques has shown pathology such as synapse loss (Spires, et al. 2005, Tsai, et al. 2004), neuritic dystrophy and breakage (Spires, et al. 2005, Tsai, et al. 2004). Some models such as APP/PS1 showed ongoing enhanced spine formation and elimination within the pre-plaque region (Tsai, et al. 2004), where as other models such as older Tg2576 mice showed increased spine elimination and decreased formation (Spires-Jones, et al. 2007). Even the triple transgenic mouse model of AD showed apparent hippocampal and frontal cortex spine loss only after plaque deposition (Bittner, et al. 2010). Some studies also observed increase in structural plasticity (Spires-Jones, et al. 2009) and rapid recovery of amyloid-associated neuritic dystrophy (Brendza, et al. 2005).

Numerous studies have reported direct observation of plaque clearance after direct application of anti-Aß antibody on the brain surface (Bacskai, et al. 2001, Prada, et al. 2007). Apart from plaque clearance, 2PM was also used to address the question of growth of plaques over time, a controversial field in itself. A landmark study reported that beta-amyloid plaques appear rapidly in the time frame of 24 hours, and did not change further after appearance (Meyer-Luehmann, et al. 2008). However, recently two more groups reported steady increase in all plaques either independent of plaque size (Hefendehl, et al. 2011) or higher growth rate for newly deposited plaques (Burgold, et al. 2011). 2PM has also been used to study CAA. Longitudinal imaging of AD transgenic mice showed that CAA is a multifactorial event in the form of band-like Aß deposits (Robbins, et al. 2006). It was also shown that passive immunization is able to halt CAA progression and even reduce vascular amyloid in AD transgenic mice (Schroeter, et al. 2008).

Although, much of the research has been plaque and immunotherapy centric, other aspects of the disease are also being addressed. Chronic imaging of microglia revealed the crucial role of microglia in plaque maintenance (Bolmont, et al. 2008). Astrocytes too showed synchronous hyperactivity and intercellular calcium waves (Kuchibhotla, et al. 2009). Aberration in calcium homeostasis causing structural and functional disruption of neuronal networks was seen (Kuchibhotla, et al. 2008). Thus, study of calcium imaging can be employed to understand neuronal activity. Busche, at al. reported cluster of hyperactive neurons near amyloid plaques (with in 60 μm from plaque) in APP/PS1 transgenic mice and decreased number of 'silent' neurons compared to wild type control mice. More recently Grienberger et al. studied spontaneous and visual-evoked response in visual cortex of APP/PS1 mice and reported progressive deterioration of neuronal tuning for orientation of visual stimuli, which occurred in parallel with age-dependent increase of beta-amyloid load. Furthermore, they also showed that this deterioration was seen only in neurons that were hyperactive during spontaneous activity (Grienberger, et al. 2012). It is worth noting that, Busche, et al. and Grienberger, et al. used synthetic calcium indicator OGB-1 for calcium imaging, which are limited to acute experiments and although were recently used for longitudinal imaging by Busche, et al., they have several short comings. The answer lies in the use of genetically encoded calcium indicators. Only chronic imaging can provide us the answers to long-term modulation of neuronal activity. In this dissertation work we performed longitudinal study of neuronal network in an *in vivo* setting, which so far hasn't been done and will help in understanding modulation of neuronal activity in Alzheimer's disease animal models.

The field is fairly young and there are many unresolved questions such as how is the spontaneous activity altered in transgenic mice? how does the neuronal network respond to a sensory stimulation? how does the spatial functional organization of cortical representation change in terms of network activation patterns? how do correlations among neurons within neuronal ensemble changes? what are the effects of systemic application of anti-Abeta immunotherapy on a neuronal network? how is the neuronal activity altered on such an event? etc. One of the challenges is to establish paradigms, which will allow imaging of same animal over time, allowing the study of pre-plaque phase of AD pathology and its alteration upon therapeutic intervention. There have been no longitudinal studies measuring neuronal activity in

AD mice models. Even though genetically encoded calcium indicators have been used (Kuchibhotla, et al. 2008), their application to study neuronal activity have not been completely explored. Also, there have been no studies to measure stimulus-evoked activity at network level. This motivated us to study sensory-evoked activity of barrel cortex neurons chronically, using whisker stimulation as a sensory stimulus in AD mice models with the help of genetically encoded calcium indicators.

3.5 Aim and outline of thesis

The main goal of this thesis work was to apply the techniques of two-photon microscopy and genetically encoded calcium indicators for analysis of neuronal response in transgenic mouse models of brain amyloidosis, There were two main aspects: morphological and functional. The morphological aspect was to image the microglia before and after immunotherapy and the functional aspect was to study neuronal networks with and without sensory stimulus.

Questions we tried to address the following questions:

1. How is the spontaneous activity altered in pre-plaque pathology in animal models of brain amyloidosis? How does the neuronal network respond to a sensory stimulation in these mice compare to wild type mice?
2. What are the effects of systemic application of anti-Abeta immunotherapy on a neuronal network?
3. How is the neuronal activity altered on such an event?

The specific goals were as follows:

1. To establish chronic *in vivo* imaging paradigm in living transgenic mice
2. To image amyloid plaques, microglia, astrocytes, neurons and blood vessels in the brains of living transgenic mice
3. To establish repeated functional imaging from the same neurons over extended periods of time using genetically encoded calcium indicators
4. To investigate spontaneous and whisker-evoked activity for measuring neuronal responses in pre-plaque phase of transgenic mouse model of brain amyloidosis
5. To explore the possibility of the 2PM for evaluating immunotherapy approaches

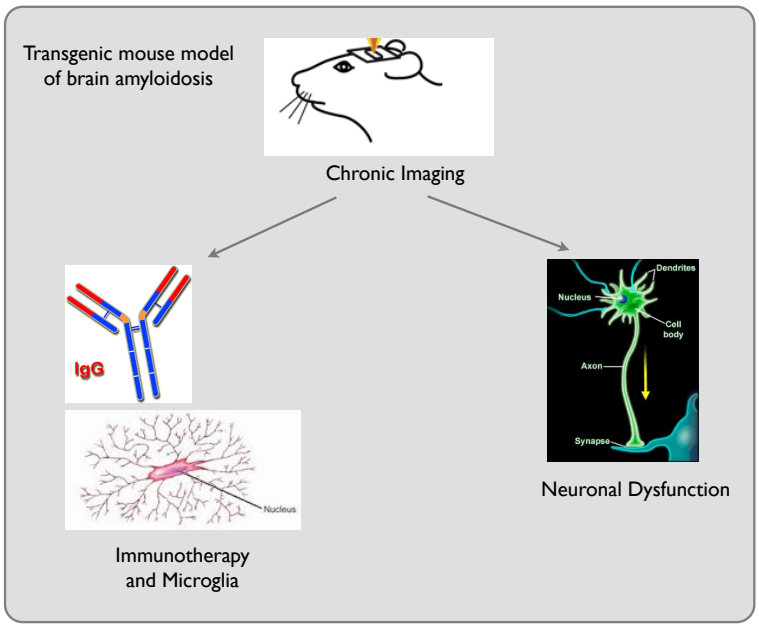

Figure 3.13: Goals of thesis. To use the technique of chronic imaging to image beta-amyloid plaques and other cellular structures in brain of AD mouse models. Images are from internet.

The first step in the project is to establish chronic imaging protocols which includes development of head posts to provide stability during long imaging session and explore novel techniques of cranial window preparations which are optically conducive for longitudinal imaging. The paradigms are standardized by using APPDE9;CX3CR1 heterozygous mice which expressed GFP-positive microglia. These protocols are further tested by applying anti-Aβ antibody topically or by bulk-loading in the vicinity of plaque and performing time-lapse imaging in these mice. The next step then is to inject genetically encoded calcium indicators in barrel cortex of young transgenic mice models of brain amyloidosis, which are in pre-plaque stage. Later, chronic windows are implanted and intrinsic imaging performed to map whisker in the area of viral expression. Although these mice are in pre-plaque stage, Methoxy-X04 is injected prior to each session to observe development of plaques in the imaging area. Baseline imaging sessions are performed and subset of mice receive systemic anti-Aβ antibody. Spontaneous activity and evoked response of same cells over time was measured and comparisons of wild type control, antibody treated and vehicle treated transgenic mice. We further analyze the data for amplitude of

response, response probability between different groups wt control, antibody treated and vehicle treated was also measured. The project overall is technically challenging as most of the protocols had to be standardized.

Chapter 5.1 discusses the standardization of various technical aspects, which were required for chronic imaging. Chapter 5.2 is an ensemble of different techniques, which were used to study plaque-microglia interactions. Chapter 5.3 discusses the use of genetically encoded calcium indicators to study neocortical neuronal network activity in transgenic AD models.

4. Materials and Methods

4.1 Animals

All experimental procedures were performed as per the guidelines of University of Zurich and Swiss veterinary cantonal office (BVET), under the licenses 155/2007 and 210/2010. The transgenic lines used were: APP/PS1dE9, APPsweArc (ArcAbeta), APPswe and CX3CR1. The APPswe, APP/PS1dE9 and CX3CR1 lines were obtained from The Jackson Laboratory. The APPsweArc were generated in house and previously described (Knobloch, et al. 2007b). Both lines were under prion promoter. The APP/PS1dE9 and APPsweArc mice were crossed with CX3CR1 -/- mice to generate APP/PS1dE9;CX3CR1 +/- and APPsweArc;CX3CR1 +/- mice. The genotype of mice was determined by PCR of tail biopsy DNA (Supplementary 1). Non-transgenic littermates were used as controls when specified. All animals were housed in the groups of 2-6 per cage in Type 3 or Type 2 long cages. After the implantation of the chronic cranial window, mice were individually housed. The animals were kept under 12-hour light/dark cycle and had *ad libitum* access to food and water.

4.2 Surgical Procedures

4.2.1 Anesthesia

Isoflurane was used for induction of anesthesia as well as for longer duration anesthesia of maximally 4 hours for most surgeries and experiments. For anesthesia induction, animals were kept inside a chamber with 5% isoflurane (Baxter, Volketswil, Switzerland) and oxygen (800-1000 ml/min) until anesthetized. A nose-mask attached to 1.5-2% isoflurane and 100-300 ml/min carrier gas source was placed over the animal's nose for maintaining anesthesia. Either pure oxygen or air was used as carrier gas. The concentration and rate of the isoflurane flow was continually adjusted to maintain an adequate level of anesthesia. Under these conditions, mice could be under anesthesia for few hours. As an alternative to gas anesthesia, injectable anesthetics were used for viral injection procedures. Specifically, animals were anesthetized with a ketamine/xylazine mixture (ketamine 0.8 mg/kg and xylazine 0.1 mg/kg), intraperitoneal (i.p.) injection. Vitamin A cream (Bausch & Lomb, Switzerland) was applied to prevent dryness of the eyes and damage to cornea. The level of anesthesia was monitored by closely observing the respiratory rate of the

animal and also by testing corneal and foot pinch withdrawal reflexes and absence of whisker movements. A deep anesthesia level was checked and confirmed before starting surgery/experiment and intermittently checked during surgical and experimental procedures. The animals were placed on a heating pad to prevent anesthesia-induced hypothermia. Body temperature was monitored with a rectal probe and regulated to 37°C with the thermostat.

4.2.2 Post-surgery treatment and monitoring

Animals that recovered from a surgical procedure were treated with fluids and analgesics. 200 µl PBS was injected subcutaneously (s.c.) after surgery to maintain the water and electrolyte balance. Analgesic Rimadyl (Carprofen; 5 mg/kg body weight, s.c., effect last for 24 h) was applied directly before the operation, 24 h after the intervention and in a 24 h interval during the first week if required. Following any surgical procedure the animal's health and well-being was evaluated at least twice per day for the first two days. Thereafter, the animals were monitored daily and their condition was documented with the help of a score sheet (see Supplementary 9.2). In the case that the condition of an animal indicated problems (e.g. dehydration, wound infections) or behavioral abnormalities (such as lethargy, overly aggressive, motor deficits), that animal was again monitored at least twice per day and necessary actions were taken (e.g. analgesia, antibiotic treatment) until its condition had improved or a termination criterion was met.

4.2.3 Preparation of thinned-skull and craniotomy

Once anesthetized, animals were placed on an operating plate or a stereotactic apparatus. For preparation of a cranial window, the top of the animal’s head was sterilized with 70% ethanol and shaved. A midline incision of approximately 3 cm was made on the center of scalp, the soft tissue was removed and the skull was cleaned. To access to regions located more laterally (e.g. barrel cortex) muscles were bluntly dissected. For acute (terminal) experiments a thin metal plate was attached to the skull using dental acrylic cement. This metal plate was used for head fixation of anesthetized animals during the experiment and to create a chamber around the craniotomy, to hold the water immersion of the microscope objective. The area for the

cranial window was chosen (1 mm for thinned-skull and 2-4 mm for craniotomy). For thinned-skull the area of interest (somatosensory cortex) was thinned slowly using a high-speed dental drill. Drilling was intermittently stopped and drill bit dipped in normal rat Ringer (NRR) solution (135 mM NaCl, 5.4 mM KCl, 5 mM Hepes, 1.8 mM CaCl2; pH 7.2 with NaOH) to minimize heat-related tissue injury. The drilling was continued until the skull was 20-30 μm thick and the underlying pial vessels were visible through the wet thinned skull. Great care was taken not to put any pressure on the underlying brain the whole time and maximal effort was made to obtain a uniform surface for imaging.

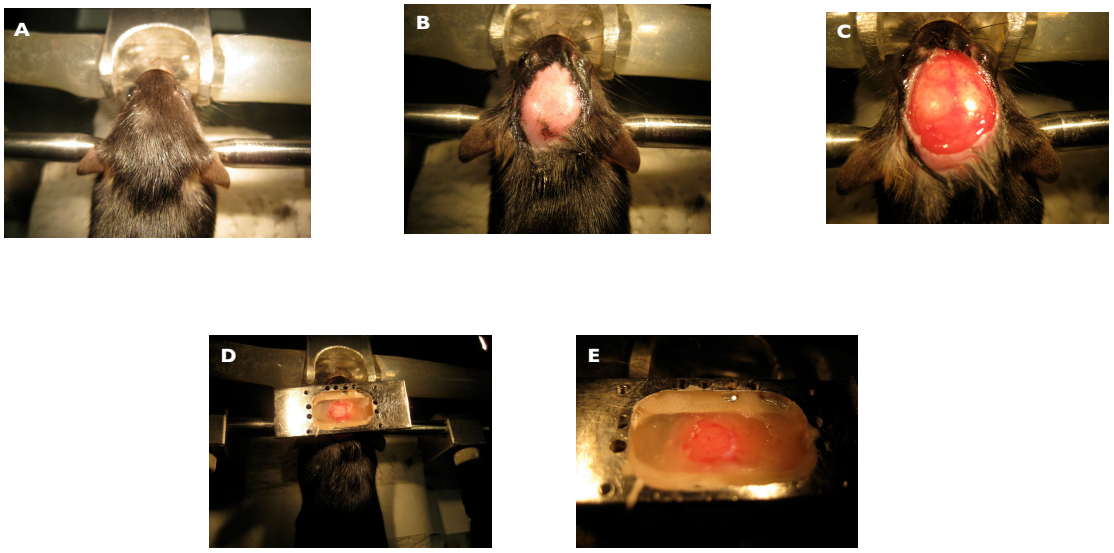

Figure 4.1: Steps of craniotomy. A, fixing the mouse, **B**, incision and cleaning the scalp, **C,** visualizing the landmarks to find the area of interest, **D,** fixing of head plate and marking the edges of craniotomy, **E,** surface vessels on the brain after removal of bone flap

For craniotomy, area of interest (somatosensory cortex or barrel cortex) of 2-4 mm was chosen and margins were drilled with a high-speed drill. The drilling was stopped intermittently and the area washed with normal rat ringer to minimize heat induced tissue injury. The bone flap was carefully removed with fine forceps. Any bleeding usually stopped spontaneously, if not, the surface was washed with normal rat ringer until the bleeding stopped. For acute experiments, the cranial window was filled with agarose (type III-A, Sigma, Buchs, Switzerland; 1% in NRR) and covered with a cover glass to dampen the tissue pulsations induced by heartbeat. For long-term repeated imaging a different head post was implanted and a chronic cranial glass

window was prepared (see below, 4.2.4 and 4.2.5). Following the surgical preparation the animal was transferred to the experimental setup on a holder with heating pad. The anesthesia was continued and the experimental measurements were performed.

4.2.4 Mounting of a head post for head immobilization

This procedure was used in chronic types of experiments, in which the animal after recovery from the initial surgery was further investigated in subsequent experimental sessions. During a short anesthesia period, a small (1.5 cm; <0.5 g) aluminum head post was secured to the skull with super glue and dental cement. In later experiment sessions this head post was clamped to a holder with a screw for fixation of the animal's head (Fig. 4.1). The head post was custom made. Briefly, the skull was cleaned and light-curing dental bonding agent (GLUMA Comfort Bond, Heraeus Kulzer GmbH, Germany) was applied to the damp skull, allowing penetration into the bone. After the bonding agent was cured with blue light, moldable dental cement was applied to the bonding agent, covering the fixable arm of the head post and the entire surface of the exposed skull. The cement was also cured with blue light. This formed a rigid connection between the head post and the skull. Mice with head posts were housed individually. With ad libitum access to food and water, weight and general health status of the mice was maintained on a daily as described in post-surgical procedures section (see 4.2.2). Loosening of the head-post was a criterion for terminating the experiment (see 4.2.6).

4.2.5 Preparation of chronic cranial windows

For repeated imaging of the same volume of brain in mice, chronically implanted glass windows above the cortical region of interest were prepared using standard techniques (Holtmaat, et al. 2009, Tackenberg and Brandt 2009). This type of window preparation permits longitudinal studies of the morphology and function of identical cells in individual animals and thus provides highly valuable longitudinal information over several weeks. Preparation of a chronic window started with a craniotomy as described in 4.2.3. The dura mater was left intact. A manually cut 2-4 mm cover glass with smoothened edges was lowered into the open space, where the skull was previously removed. The cover glass was secured in place with a rim of light-curing

dental cement (Tetric Evoflow, Ivoclar Vivadent, Leichenstein). A final layer of light-curing sealant (OptiGuard, Kerr Italia, Italy) was used to tightly seal the edge of the cover glass. The mice were allowed to recover from anesthesia and post-operative monitoring was performed and documented as described in 4.2.2. To permit stable imaging conditions, a recovery period of at least 10 days after the cranial window implantation was observed (Hofer, et al. 2009). During the recovery period the animals were monitored according to the general post-surgical procedures (see 4.2.2). In addition, the tissue properties and window quality were closely inspected under a stereoscope in the days following the surgery. If tissue or window conditions did not allow high-quality imaging after such a period, the experiment was terminated. In addition, obvious signs of tissue inflammation or deterioration were a criterion for terminating the experiment (see 4.2.6). Previous imaging studies (Hofer, et al., 2009) and our own experience indicated that cranial windows – once they have cleared up and stabilized - remained transparent and stable for prolonged time periods up to 4 months.

4.2.6 Termination criteria for recovery following surgery

If one of the following criteria was met the experiment was terminated and the animal was euthanized by overdose of anesthesia.

1. More than 10% weight loss compared to initial weight
2. More than 50% increased breathing rate compared to normal for more than 24 hours
3. Obvious behavioral abnormalities for more than 24 hours (lethargy, overly aggressive, motor deficits, stereotypic behaviors)
4. Loosening of implanted head-post
5. End of treatment period of 8 weeks
6. Low/No expression of the virus
7. Score less than 15 on the score sheet (Appendix)

Out of 20 animals used for chronic experiments only 2 animals had to be euthanized.

4.2.7 Brain dissection, fixation and histological reconstruction

At the end of an experiment the animal was euthanized with an overdose of Nembutal (6-8 mg/100g body weight, i.p.) or, after deep anesthesia with Nembutal, it was transcardially perfused with 4% paraformaldehyde (PFA) in phosphate buffer for brain fixation. The brains were carefully removed and stored for 0.5-1 d at 4°C in the fixative before transfer to 30% sucrose in phosphate buffer solution. If needed thin fixed tissue sections were cut on a microtome. Standard histological procedures, including immunohistochemistry, were used for microscopy. The brain sections were stored at -20°C in anti-freeze solution (0.5 M phosphate buffer with 30% ethylene glycol and 30% glycerol).

4.2.8 Immunohistochemistry

Paraformaldehyde-fixed and cryoprotected brains were cut in 40 μm thick slices at about -80°C using a microtome (Leica Jung HN40) and kept at -20°C in an anti-freeze solution (phosphate buffer 0.50 M in MilliQ water: ethyleneglycol: glycerol = 1.3:1:1) until stainings were performed. All immunohistochemical stainings were done by using the free-floating method. Washing steps were carried out between all incubations using washing buffer (TBS pH 7.4 containing 0.2%Triton X-100) at RT.
Slices were blocked for 1 hr at RT using blocking buffer (5.0% goat serum 5.0% donkey serum in washing buffer). Blocked slices were incubated overnight at 4°C with slight agitation in primary antibody incubation buffer (2.5% goat serum and 2.5% donkey serum in washing buffer) containing the primary antibody/antibodies (see table 1). Subsequently, secondary antibody incubations were carried out for 2 hours at RT. Slices were washed in washing buffer, mounted on chrom-gelatin-coated microscopy slides (Super-frost-plus, Menzel, Braunschweig, Germany) and glass-covered using Hydromount® (National Diagnostics, Hull, UK).

4.3 *In Vivo* Labeling Procedures

4.3.1 Viral gene transfer of genetically encoded markers and sensors

We induced expression of genetically encoded indicators using viral transfections for labeling cell populations. We used viral constructs coding for fluorescent proteins such as green fluorescent protein (GFP) calcium indicators of the yellow cameleon family. In particular, we used Yellow Cameleon 3.6 construct coupled to Adeno-Associated Virus 2 (AAV2) vector under chicken beta-actin (CAG) or human synapsin (h-syn) (Lutcke, et al. 2010) promoter (Figure 4.2). Our collaborators Hasan and Sebastian Kugler labs prepared the virus as follows. rAAV equipped with YC3.60 under control of a human synapsin or chicken beta actin promoter (Figure 4.2) was co-transfected with pDp1, pDp2 (ratio:3:1) helper plasmids in HEK293 cells (Hasan, et al. 2004, Wallace, et al. 2008). Seventy-two hours after transfection, HEK293 cells were collected and packaged viruses were released by repeated freeze-and-thaw on dry-ice-ethanol bath. Viruses were purified first on the iodixanol gradient and later by pre-casted 1 ml Heparin columns (Amersham) using FPLC (Kügler et al., 2007). Infectious virus titers were determined in primary neuron cultures and was 3 °— 108 transducing units per microliter. Viral injections were performed in a brief (0.5 h) surgical session under isoflurane or ketamine/xylazine anesthesia (Cetin, et al. 2006). Only the virus was prepared by our collaborators, rest of the procedures were done independently. The anesthetized mice were placed in a stereotactic apparatus. A small burr hole was drilled over the region of interest, the barrel cortex (-1mm from Bregma and 3.3 mm lateral). A very thin glass capillary tip was guided to the area of injection and approximately 300 nl of 1 million copies virus-containing solution (with 20% mannitol) was injected through this small hole directly into the brain while maintaining a steady pressure of 50. The pipette was left in place for few minutes before slowly retracting it to reduce the spill over. The burr hole was closed with bone wax and the skin sutured. For long-term imaging experiments, a chronic cranial window was prepared a few days after the virus injection in a separate anesthesia session (see 4.2.5). Sufficient levels of expression were reached within 1-3 weeks following the virus injection.

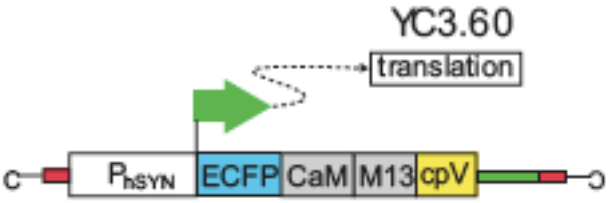

Figure 4.1: Construction of YC3.60. The indicator consists of a circular permuted Venus 173 variant (cpVenus 173) as a yellow fluorescent protein (YFP) FRET partner of cyano fluorescent protein (CFP), which are joined by calmodulin and M13.

We injected 14 mice with CAG promoter and 6 mice with h-syn promoter. Out of 14 mice injected with CAG promoter; 4 mice dropped out of study as they died before imaging started, 6 windows cleared up for imaging and 4 more windows did not. Out of 6 mice injected with h-syn promoter, 4 windows cleared up for imaging and 2 did not. See supplementary for detailed table of injected mice.

4.3.2 Labeling of brain beta-amyloid plaques in vivo

Beta-amyloid plaques in living transgenic mice were labeled with Methoxy-X04, a kind gift from Prof. Klunk, University of Pittsburgh. Methoxy-X04, discovered in 2002 by Prof. Klunk, is a derivative of Congo red and Chrysamine G (Klunk, et al. 2002). Methoxy-X04 (5 mg/kg) was injected i.p. a day before each imaging session. Being highly lipophilic it readily crosses the blood brain barrier and stains both beta-amyloid plaques and cerebrovascular amyloid with good specificity (Klunk, et al. 2002). Two protocols were used for injecting Methoxy-X04.

a) 5 mg/ml Methoxy-X04 in 10% DMSO, 45% propylene glycol and 45% PBS and 5 mg/kg was injected as described in Klunk, et al. 2002.
b) 10 mg of Methoxy-X04 was dissolved in 1 ml DMSO. 10 µl of this solution was dissolved in 20 µl of Cremophor EL and then finally dissolved in 270 µl of PBS, sonicated for 2 min and injected immediately. The amount of Methoxy-X04 injected was about 3 mg/kg. This protocol was obtained by

personal communication with Prof. Bacskai (Massachusetts General Hospital, Boston, MA).

4.3.3 Intravenous injection of fluorescent markers for labeling of blood vessels

For visualization of the vasculature, we injected fluorescent dyes into the tail veins during anesthesia (Kleinfeld, et al. 1998). To avoid rapid dye loss due to clearance in the kidney dextran-conjugated fluorescent dyes including Fluorescein-dextran or Texas Red-dextran (molecular weight 70,000 Da, Invitrogen, Switzerland) were used. Tail veins in anesthetized mice were dilated by heat application (IR lamp or warm solution). The end of the tail was softly clamped and a bolus of dye-containing solution (5% w/v Ringer solution; 0.1 ml) was injected using a 29 G needle attached to a small syringe.

4.3.4 Topical application of fluorescent markers

Various markers are available that stain selected cell populations including astrocytes in a more or less specific manner upon topical application on to the brain surface. This procedure was carried out in anesthetized mice after craniotomy before application of the cover glass. 50 µl of dye-containing solution was applied to the exposed cortical surface. Penetration of the dye into the brain tissue was accelerated by cutting a small slit into the dura with the cutting edge of a needle tip. This type of labeling was for example used for specific staining of astrocytes with the red fluorescent dye sulforhodamine 101 (Nimmerjahn, et al. 2004). Brief application of 5-10 min of 50 µM SR101 was sufficient to obtain bright staining of the astrocytes in red channel (645 nm). Subsequently, the tissue was rinsed with rat ringer solution to remove the excess dye.

4.4 Imaging Procedures

4.4.1 Functional mapping using intrinsic signal imaging

Sensory regions in brain are organized anatomically reflecting the major inputs received from peripheral sensory organs. For example, distinct cortical columns of about 0.4 mm diameter are responsible for the initial cortical processing of

movements by each facial whisker in the primary somatosensory area S1, the 'barrel cortex' (Petersen 2003) (see 3.2.3). Before applying measurements with high-resolution two-photon imaging, we performed functional mapping of the barrel cortex to verify the exact locations where exactly high-resolution measurements are to be performed. For this purpose we used intrinsic signal imaging (ISI; Orbach, et al. 1985, Kerr, et al. 2007). ISI does not require labeling and it was done during anesthesia either through a previously acutely prepared (see 4.2.3) or chronically implanted glass window (see 4.2.4). For functional mapping using ISI the anesthetized animal was placed on a heating pad in a holder under the custom built two-photon microscope (for details see 4.4.2). The cranial window was illuminated with red light and the light reflected from the brain surface was imaged onto a sensitive camera system (Olympus, Tokyo, Japan). Upon whisker stimulation (for details se 4.4.4), the blood flow to the particular area increases, resulting in the absorption of red light and thereby decreasing the signal intensity (Orbach, et al. 1985). By comparing the stimulus-evoked intrinsic signal with a baseline measurement without stimulation, it was possible to delineate individual barrel corresponding to individually stimulated whiskers. The resulting functional map was related to barrel cortex areas using the pattern of large and medium-sized surface blood vessels as landmarks. The individual whisker to be stimulated was chosen by matching up the area of viral expression with the intrinsic signal in the cognate area.

4.4.2 *In vivo* two-photon microscopy

In vivo imaging was performed with a custom-built two-photon-laser-scanning microscope equipped with a Ti:sapphire laser system (MaiTai HP, Spectra-Physics, Santa Clara, USA) tuned to 850 nm wavelength as the light source (about 100 fs output, 1 W power). The laser intensity was adjusted with Pockle's cell (Conoptics, Danburry, USA) such that none of the channels weren saturated. The microscope was equipped with two galvanometric scan mirrors (Model 6210; Cambridge Technologies, Lexington, USA) for scanning the specimen in the *x*–*y* axis, and a piezoelectric focusing element (P-725.4CD PIFOC, Physik Instrumente, Karlsruhe, Germany) for *z*-scanning along the optical axis. The area to be imaged was initially identified by using a 10x air objective (NA 1; Olympus, Tokyo, Japan) and later a 40x water immersion objective (NA 0.8; Olympus, Tokyo, Japan) was mounted onto the

piezo element, focusing the laser beam into the cortical imaging area. Data was acquired by a custom-written software (LabView, National Instruments Corporation, Austin, TX, USA). The fluorescence generated by the two-photon excitation was collected through the same microscope objective and detected in one or more spectral imaging channels corresponding to emission spectra of the fluorophore i.e., 542 nm for green/yellow, 475 nm for blue and 610 nm for red, depending on the specific fluorophore used in the experiment.

4.4.3 Longitudinal imaging using cranial windows over several weeks

We applied chronically implanted cranial windows (see 4.2.5) to repeatedly image identical brain structures by using two-photon microscopy. Longitudinal imaging was started 15-21 days following the window preparation. Mice were re-anesthetized and then re-imaged under the two-photon microscope for up to 8 weeks. The animal was placed under the microscope and imaging was performed as described in 4.4.2. The identical areas in the neocortex and the identical beta-amyloid plaques and cells were identified across sessions based on landmarks provided by the blood vasculature pattern at the brain surface; which had been documented during the initial imaging session. 3-5 imaging locations were chosen for each animal and the identical locations were reimaged during every single imaging session. The integrity of the windows was monitored before starting an imaging session. If needed, additional dental cement or sealant was applied in order to fix the windows. With chronic windows we performed functional imaging of the identical neurons over extended time periods of several weeks or months, as long as imaging conditions permitted optimal microscopy. Long-term imaging over many weeks allowed a significant reduction in the number of experimental animals, because the obtained data were less variable and the same preparation was used for several research questions. At the end of the imaging sessions, the mice were returned to their home cages. Imaging sessions were repeated with intervals of 2-3 days. At later phases of experiment, sessions were repeated about once every week. At the end of the last imaging session, mice were sacrificed and brain tissues processed as described in 4.2.8.

4.4.4 Sensory stimulation and optical recordings

Whisker stimulations were done by wiggling either individual or multiple facial vibrissae on the contralateral side of the craniotomy in various directions using a piezo-electric deflector (Brecht, et al. 2003). Whiskers that were mapped earlier (4.4.1) were stimulated at a frequency of 20 Hz for 0.5 s, repeated every 5 s for 15 times for 5 cycles. Each cycle of evoked-response was preceded by a cycle of spontaneous activity. Thus there were 5 cycles of spontaneous and evoked-response for each location. Approximately 20-30 min were needed for imaging one location and each mouse with 4-5 locations required 2-2.5 hours of imaging time.

4.4.5 Time-lapse imaging of microglia

Time-lapse imaging of microglia was done only in APP/PS1dE9;CX3CR1 and APPsweArc;CX3CR1 transgenic mice. Areas with beta-amyloid plaques were selected and imaged for a period of 6-7 hours. 40-60 μm stacks of the plaque area were acquired every 2 min. Rest of the procedure was same as in 4.4.3.

4.5 Immunotherapy

4.5.1 Intracerebral application of anti-Abeta antibodies

Direct application of the anti-Aß antibody (in-house generated anti-Aβ IgG2a targeted against fibrillar Aβ) into the cortex was done by microinjection with 10-30 μm diameter glass micro-pipettes. This procedure was carried out in anesthetized animals. The micro-pipette was loaded with 5 μl of 1 μg/μl of the antibody. The tip of the micro-pipette was navigated at 45° angle under the visual control to the target area through a cranial window (4.2.3), and antibodies were injected over 4-5 minutes. This type of loading is also known as the multi-cell bolus loading technique (Stosiek, et al. 2003). The micro-pipette was then gently retracted. The craniotomy was then completed as described earlier (4.2.3) or a chronic window was implanted (4.2.5). For some experiments, the antibody was conjugated to a fluorescein or texas red and bulk-loading was done around beta-amyloid plaques.

4.5.2 Systemic passive immunization

Passive immunization of 7-month-old APPsweArc mice was done by i.p. injections of 5 mg/kg anti-Aß antibody injection once a week for 12 weeks period. i.p. injections of anti-Aβ antibody, which was a chimeric monoclonal antibody consisting of human variable domains and mouse IgG2a constant regions. It selectively recognized aggregated forms of Aß1-40 and Aß1-42 with high-affinity (low nM range) (Biscaro, et al. 2009). The control mice received the same amount of vehicle (PBS).

4.6 Data analysis

The initial imaging data processing was done offline with ImageJ software (version 1.42, NIH, USA, http://rsbweb.nih.gov/ij/). For morphological data and time-lapse imaging data, the raw data were converted into stacks and maximal intensity Z projections were created. Subsequently, one plane was chosen and images of the same plane from different stacks were collected and a movie was created with all the images. The X, Y alignment was corrected with a custom written macro by Prof. Helmchen. The intrinsic imaging data was analyzed with a custom written software (LabView, National Instruments Corporation, Austin, TX, USA). The functional data were analyzed with MATLAB R2010b version (Mathworks) using in-house custom written script written by Dr. Lütcke. The ROIs (cell bodies of neurons) were manually drawn using ImageJ. It was made sure that all the spots had exact same number of ROIs. These ROIs were later analyzed for calcium transients. The calcium signals were expressed as $\Delta R/R= (R-R_0)/R_0$ Where R the ratio of background-corrected CFP and YFP fluorescence, i.e. $R=F_{CFP}/F_{YFP}$ and R_0 is the baseline or pre-stimulus ratio value. Identification of spontaneous or evoked events as well as estimation of the number of action potentials underlying observed $\Delta R/R$ calcium signals was done with the peeling algorithm (Grewe, et al. 2010) assuming a reasonable single action potential-evoked calcium signal waveform for YC3.60 (Lütcke, et al. 2010). The neuropil signals were calculated from the whole imaging frames. The spontaneous activity rate was calculated as number of events per second. To measure the evoked activity due to whisker stimulation, the activity 1 second before and after the stimulus were calculated. The difference was the whisker stimulus-evoked activity.

5. Results

The results section is divided in three major parts. In the first part, I present several technical issues regarding the establishment of chronic in vivo imaging in neocortex of mice. In the second section, several experiments exploring the possibilities to further study microglia-plaque interaction are presented. Finally, in the third section, a first study applying genetically-encoded calcium indicators for long term repeated study of neuronal activity in pre-plaque phase of Alzheimer's disease is presented.

5.1 Standardization of chronic imaging protocols

5.1.1 Use of head post reduces movement artifacts

One of the major issues in chronic imaging is minimization of movement artifacts, which are caused by breathing and heartbeat in the anesthetized animal (Helmchen and Denk 2005). Conventionally, the mice placed on a holder with ear bars (Figure 4.1 A). However, this does not provide enough stability and leads to numerous movement artifacts (Figure 5.1). These movement artifacts were observed in 3 out of 3 CX3CR1+/- mice imaged with ear bar fixation. It is very important to have as steady images as possible as movement artifacts interfere with analysis of images. Dynamic and fine structures such as microglia are affected by very small movements (Figure 5.1).

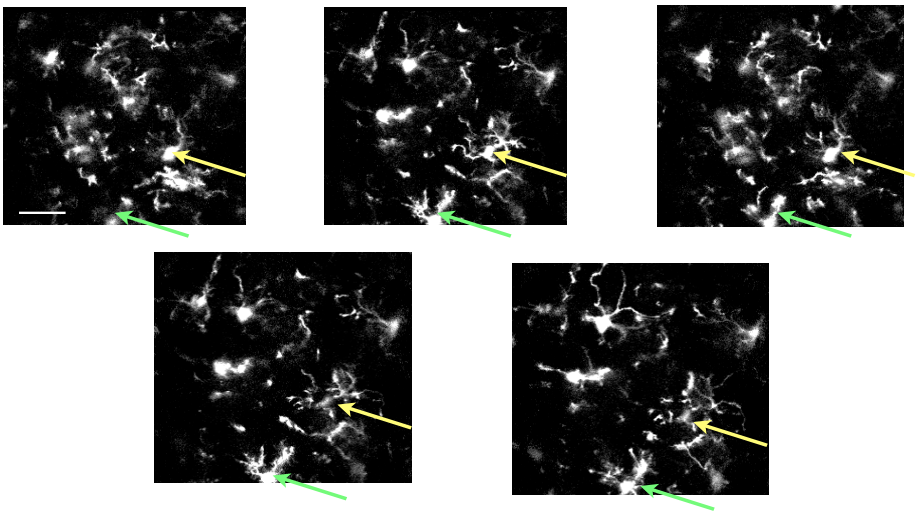

Figure 5.1: Movement artifacts on time-lapse imaging of microglia without head posts. The images are examples of single frame of a time-lapse movie of 20 min in CX3CR1+/- mice. The green and yellow arrows indicate the changes in microglia morphology due to movement artifacts. Large movement artifacts are seen, which make it difficult to localize the microglia. Scale bar=20 µm

These movement artifacts were reduced to an acceptable level with the use of head posts (Figure 5.2). I therefore concluded that head-posts provide improved stability and decided to use head posts for chronic imaging experiments.

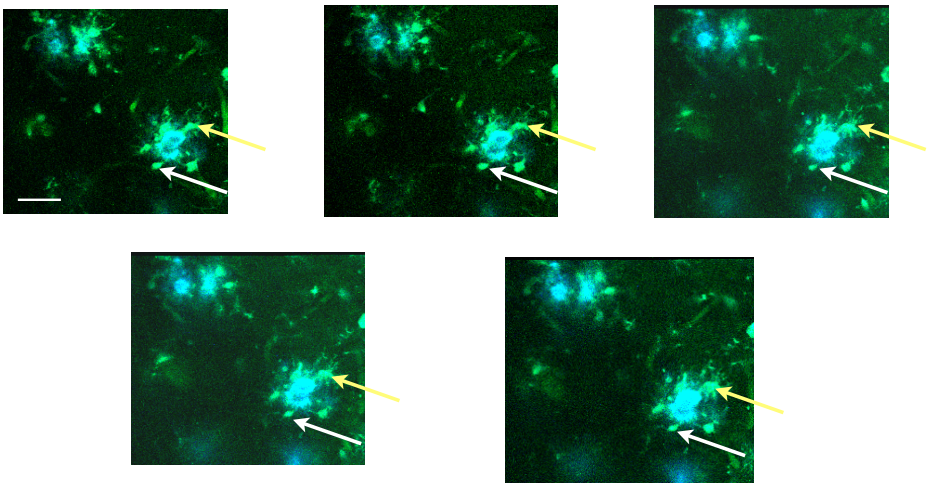

Figure 5.2: Time-lapse imaging of microglia with head posts. The images are examples from single frame of a time-lapse movie of 5 hours in APP/PS1dE9;CX3CR1+/- mouse. The images are stable, the white and yellow arrows indicate no changes in microglia morhphology. Blue: plaques, Green: microglia and Fluorescein dextran labeled blood vessels. Scale bar=50 µm

Custom made head posts were used for all the chronic imaging experiments. The reduction in movement artifacts was uniform and provided good quality images.

5.1.2 Comparison between imaging through thinned-skull and craniotomy in living mice

Technical differences in the cranial window preparation can have a major impact on the imaging quality. We compared thinned-skull and craniotomies for our preparations as it is currently debated if thinned-skull is less invasive than craniotomies (Drew, et al. 2010, Grutzendler and Gan 2006, Xu, et al. 2007). Thinned-skull preparations are shown to cause less microglia and astrocyte reaction in the imaging area and affect dendritic turnover (Drew, et al. 2010, Grutzendler and Gan 2006, Xu, et al. 2007). In the field of Alzheimer's disease both thinned-skull and craniotomies have been used with equal efficacy (Burgold, et al. 2011, Christie, et al. 2001, Hefendehl, et al. 2011, Yan, et al. 2009). Our data show that craniotomies were better for chronic imaging purposes. They were easy to prepare, needed almost no

maintenance and stabilized windows remain transparent for many weeks up to several months. In contrast, thinned-skull preparations require more technical skill, along with re-thinning before each imaging session, which in some cases cause brain injury and lead to termination of the experiment. For imaging finer brain structures including the microglial processes, thinned-skull preparations were inadequate because of poor image quality compared to craniotomies (Figure 5.3). To achieve one goal of one of the experiments, time-lapse imaging of microglia surrounding beta-amyloid plaques, it was very important to visualize microglial processes clearly. Thus, both from a technical perspective as well as for reasons of better image quality, we chose craniotomies for most of the experiments.

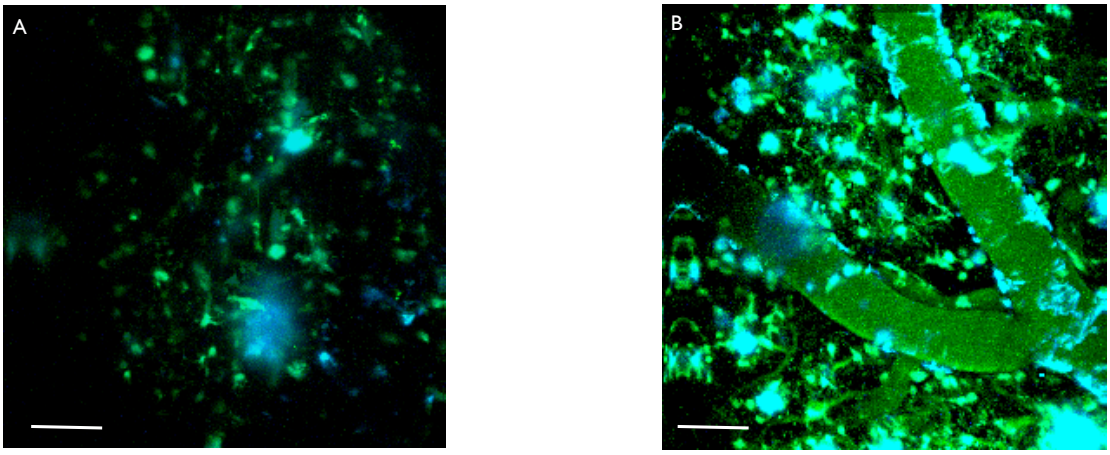

Figure 5.3: Superior imaging quality of craniotomy as compared to thinned-skull preparation. (A): Max. intensity Z-projection (20 μm) image from thinned-skull preparation of a APP/PS1dE9;CX3CR1+/- mouse, showing beta-amyloid plaques in blue and GFP-expressing microglia in green. The cell bodies of microglia are seen clearly but it is difficult to see microglial processes. Scale bar= 20 μm. **(B):** Max. intensity Z-projection (40 μm) image from craniotomy of a APP/PS1dE9;CX3CR1+/- mouse, showing beta-amyloid plaques in blue, GFP-expressing microglia and Fluorescein dextran labeled blood vessels in green. Here both the microglial cell bodies and processes are very easy to identify. Scale bar= 50 μm

5.1.3 Improvements to the chronic craniotomy window imaging technique

For long-term imaging the quality of the chronic cranial window is essential. We therefore tested various modifications in order to optimize window quality. The following procedural modifications turned out to be useful

- special light-curable dental cement, that can be readily molded was used to cure the edges of craniotomy in a step-wise manner
- bonding agent on the wet skull to secure the head post and to make a durable bridge between skull and dental cement

- a sealant to ensure tight fitting of the cover glass around the edges of craniotomy
- manually cut cover glass with smoothened edges to reduce any sort of injury to exposed brain surface

The dental cement, bonding agent and sealant were all light-curable, and a blue light was used for this purpose. Typically the time needed to cure was between 20-60 s. As the dental cement was moldable, the edges of the cranial windows were cured in 2-3 steps, applying different amounts of dental cement each time as needed. This provided flexibility to cover the windows in a systematic manner and eliminated the necessity of covering the whole craniotomy in a single step, and avoided the related complications including bleeding and tissue injury resulting in termination of the experiment thereby.

There was a recovery period of few days up to 2 weeks before imaging sessions were started. During this recovery period the inflammatory reaction following the surgery subsided and the window cleared up for imaging. The cleared up windows stayed transparent for weeks to months (Figure 5.4). Slight bleeding occurring in few cases resolved spontaneously within in few days. In our hands about 50% windows cleared up for imaging purposes, which is slightly above the rates is described in the literature. The 'clean window' was a window without any glial scar tissue formation or without any bleeding and through which the surface blood vessels were clearly visible under stereoscope.

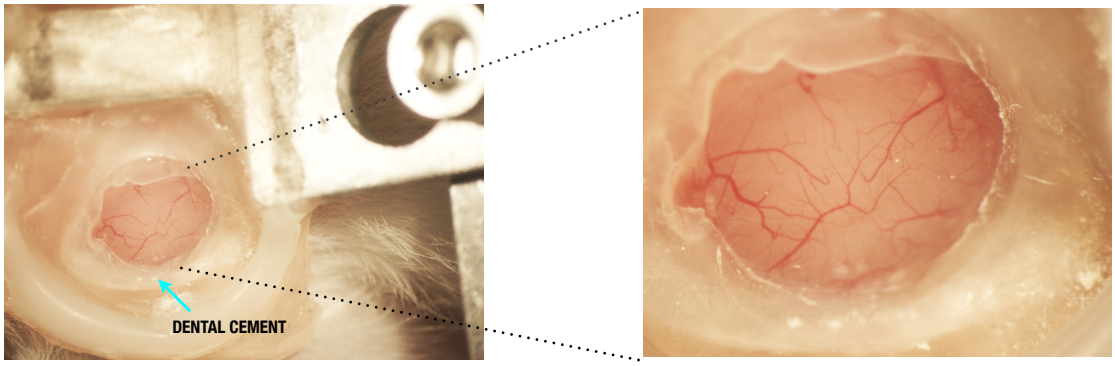

Figure 5.4: Preparation of a chronic cranial imaging window in mouse. *Left*: Anesthetized mouse with a chronic cranial window and head post 60 days after implant. *Right*: Close-up of cortical surface visible through the cranial window.

5.1.4 Labeling of beta-amyloid plaques in living mice

Methoxy-X04 is highly lipophilic and difficult to dissolve in aqueous physiologic buffers. Therefore, different solvents were used for two different protocols (Figure 5.5). With DMSO and propylene glycol protocol, only about 50% of Methoxy-X04 was dissolved and thus, the labeling of plaque was not extensive (Figure 5.6 A). With the Cremophor EL, DMSO protocol, 100% Methoxy-X04 was dissolved and resulted in extensive labeling of beta-amyloid plaques (Figure 5.6 B). Therefore, this protocol was used for all Methoxy-X04 injections.

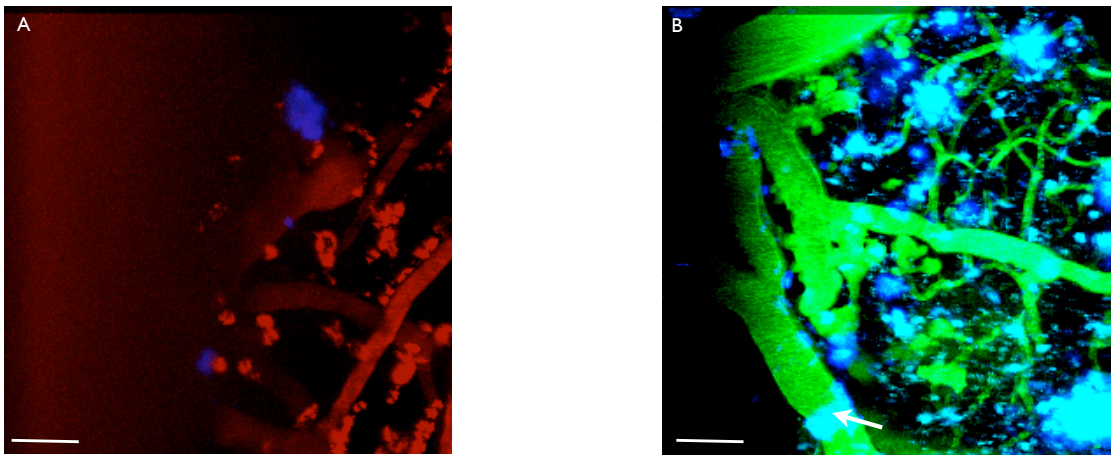

Figure 5.5: Improved beta-amyloid plaque labeling with dissolved in Cremophor EL (A) Protocol with DMSO and propylene glycol shows sparse plaque labeling in 9 month-old APP/PS1dE9 mouse. Blue: plaque, Red: Texas red dextran labeled blood vessels. Scale bar= 30 μm **(B)** Protocol with DMSO and cremophor EL shows extensive plaque labeling in 9 month-old APP/PS1dE9 mouse. Vascular amyloid is also stained (arrow). Blue: plaque, Green: Fluorescein dextran labeled blood vessels and GFP-expressing microglia. Scale bar= 50 μm

Methoxy-X04 is widely used for *in vivo* labeling of beta-amyloid plaques. It needs to be injected intraperitoneally prior to every imaging session (Bacskai and Hyman 2002). However, there are some reports of using it once in a week after a loading dose for first imaging session with satisfactory plaque labeling (Burgold, et al. 2011).

5.2 Various techniques to study microglia-plaque interaction

After establishing the chronic imaging protocols, we tested these protocols for their stability and viability during long imaging sessions, which are vital for obtaining high quality images during longitudinal imaging.

5.2.1 *In vivo* appearance of typical parenchymal and vascular plaque

The parenchymal plaques were seen throughout the imaging volume in all imaged layers of cortex, whereas vascular cerebral amyloid angiopathy (CAA) was seen mainly in the medium-sized arterioles (Figure 5.6 A). Different types of parenchymal plaque morphologies were also seen. APP/PS1dE9 mice showed mainly compact amyloid deposits (Figure 5.6 B) whereas APPsweArc mice showed mainly diffuse amyloid deposits (Figure 5.6 C).

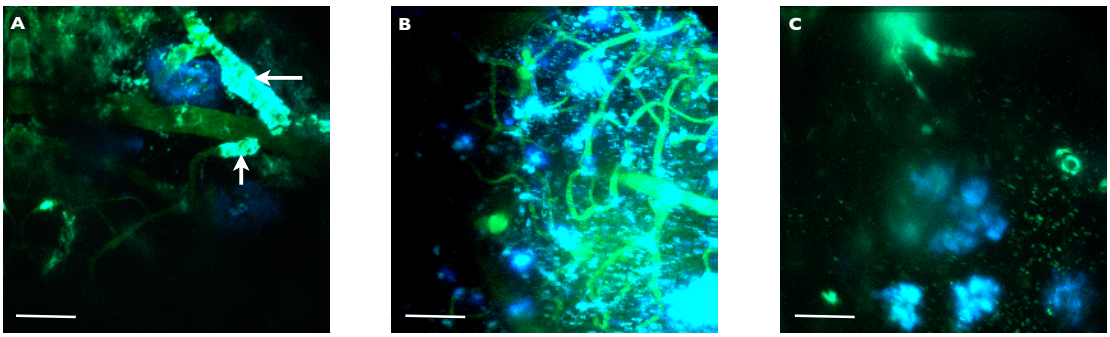

Figure 5.6: Different types of plaques. Blue: plaque, Green: Fluorescein dextran labeled blood vessels. **(A)** Vascular plaque in a 12-month-old APPsweArc mouse (arrows). Max. intensity Z-projection image of 20 µm stack. Scale bar= 50 µm **(B)** Compact plaques in 12-month-old APP/PS1dE9 mouse. Max. intensity Z-projection image of 40 µm stack. Scale bar= 50 µm
(C) Diffuse plaques in 15-month-old APPsweArc mouse. Max. intensity Z-projection of 30 µm stack. Scale bar= 30 µm

In APP/PS1dE9;CX3CR1+/- mice, plaque pathology was characterized by varying plaque size between 20-50 µm in Z-axis and 10-30 µm in X and Y axes (Figure 5.7). There were different tiers of microglia around the plaque. Usually on a single plane 5-8 microglia were seen around a single plaque, which was consistent with earlier reports in APP/PS1;CX3CR1 +/- mice (Bolmont, et al. 2008) (Figure 5.7). Thus, in 3D there would be 20-35 microglia around a typical beta-amyloid plaque.

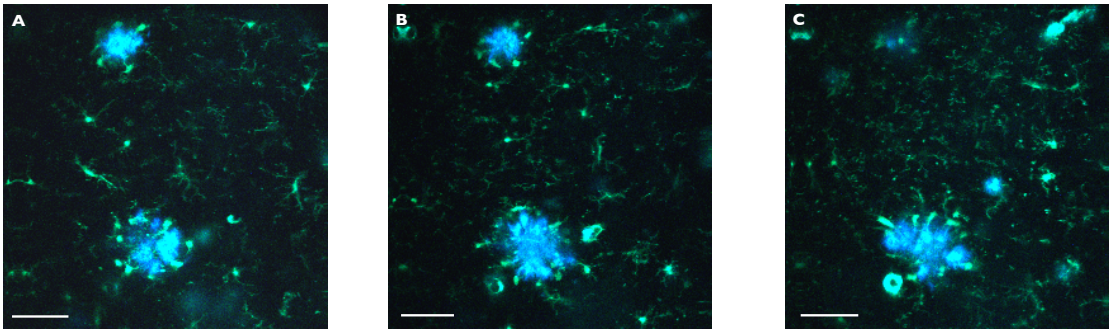

Figure 5.7: Zoomed in plaque. Two plaques zoomed in 15-month-old APPsweArc mouse showing different planes of a plaque. **A, B and C,** are 5, 15 and 30 μm deep in the Z-axis. Many microglia are seen surrounding the plaques at each level. Blue: plaque, Green: microglia and Fluoresecin dextran labeled blood vessels. Scale bar= 30 μm

5.2.2 Plaque targeted antibody application

Any intervention in the brain causes some damage to the tissue and it is important to use techniques, which are as less invasive as possible, and cause as little damage as possible to the tissue. In this experiment we tested if bulk loading of anti-Aß antibody causes any immediate damage to the tissue. The technique of bulk loading was used to inject a small amount of antibody (approx. 1 μg) into the area surrounding a plaque (20-30 μm distance from a plaque). A baseline stack was acquired and stack after the injection was acquired. There was no tissue injury/edema after the injection (Figure 5.8). The dextran is cleared from blood vessels over time (Figure 5.8 B) and there is slight change in imaging plane between A and B.

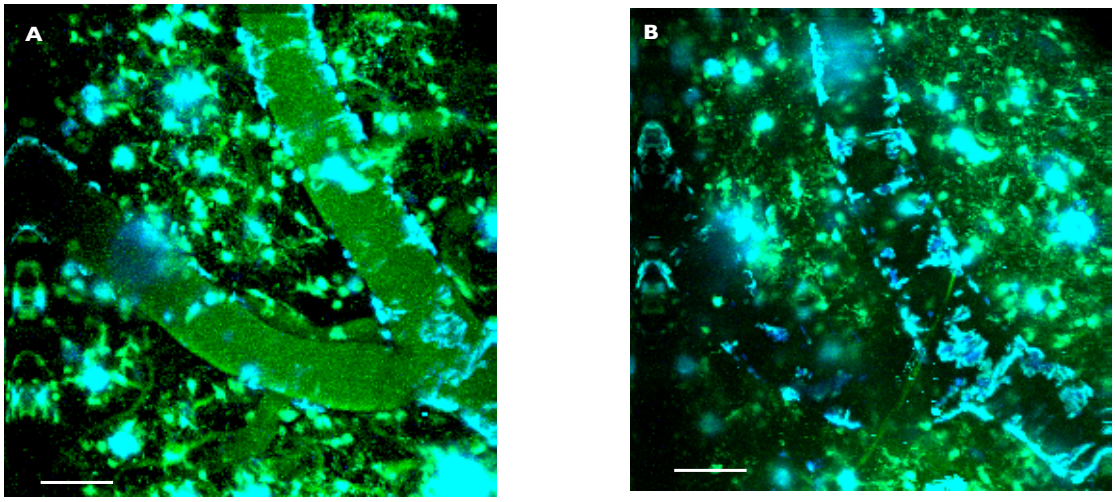

Figure 5.8: Bulk loading of antibody does not cause any tissue injury Blue: plaque, Green: Fluorescein dextran labeled blood vessels and microglia **(A)** Max. intensity Z-projection image from 200 μm baseline stack before the antibody application **(B)** Max. intensity Z-projection image from 200 μm stack acquired after the antibody application. No tissue injury (edema, bleeding) is seen. The dextarn has been cleared from the blood vessel. Both parenchymal and vascular plaques are visible. Scale bars= 50 μm

The same area was imaged for three consecutive days and the size of the same plaque (white arrow) was followed (Figure 5.9). It turned out to be important to use same microscope settings (zoom, laser intensity) each day in order to ensure that these factors did not confound the results. Even when these factors were constant, the morphology of the plaques itself was inconsistent. We compared the size of one plaque (white arrow) with another plaque (yellow arrow). Same plaques were imaged over 3-7 days in 3 APP/PS1dE9;CX3CR1+/- mice. Thus, I successfully established repeated chronic 2-photon imaging of the same plaques over days and I could demonstrate that the combination with antibody application. The preliminary data show that the same plaques can be found in imaging sessions following antibody application, however the data set is too small (and the time duration perhaps too short) to make any statement on affect on plaque size.

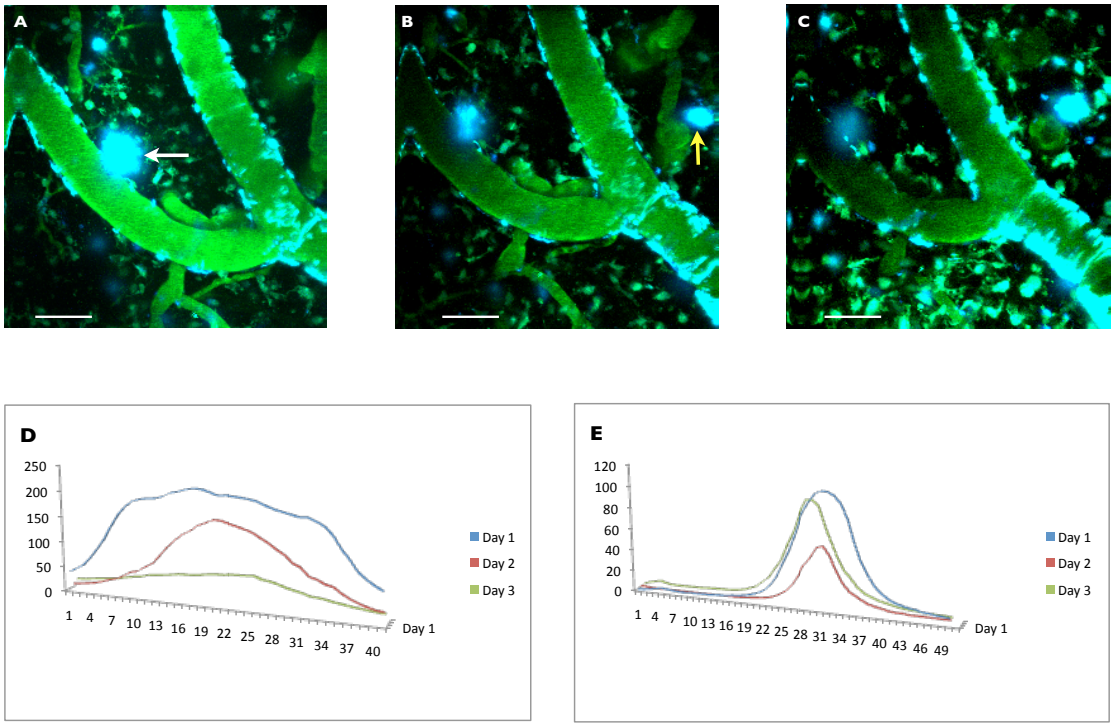

Figure 5.9: Serial imaging of same plaque over days after antibody application. Blue: plaque, Green: Fluorescein dextran labeled blood vessels and microglia. Serial imaging of plaque 1 (white arrow) on Day 1 **(A),** Day 2 **(B)** and Day 3 **(C)** after antibody application shows a reduction in plaque size. Plaque 2 (yellow arrow) was used as a control plaque. Scale bars= 50 μm **(D)** shows changes in the size of plaque 1 measured on a Z-axis and **(E)** shows changes in the size of plaque 2 using same protocol. A reduction of size of plaque 1 is seen whereas size of plaque 2 does not reduce. In both **D** and **E**, X-axis is number of frames and Y-axis is fluorescence units.

5.2.3 Application of fluorescently tagged antibody

Even though it has been almost a decade since immunotherapy was discovered as a therapeutic approach for AD (Bacskai, et al. 2001), the understanding of the essential mechanism underlying its effects is still incomplete (Brody and Holtzman 2008). It is important to visualize the antibody to understand its interaction with the plaque and neighboring cells. Therefore we conjugated the antibody to the fluorescent molecules including Cy-2 (Figure 5.10 A) and Texas red (Figure 5.10 B) and direct intracerebral injection of the conjugated antibody in the periphery of amyloid plaques. These were acute experiments and chronic imaging of these mice was not done.

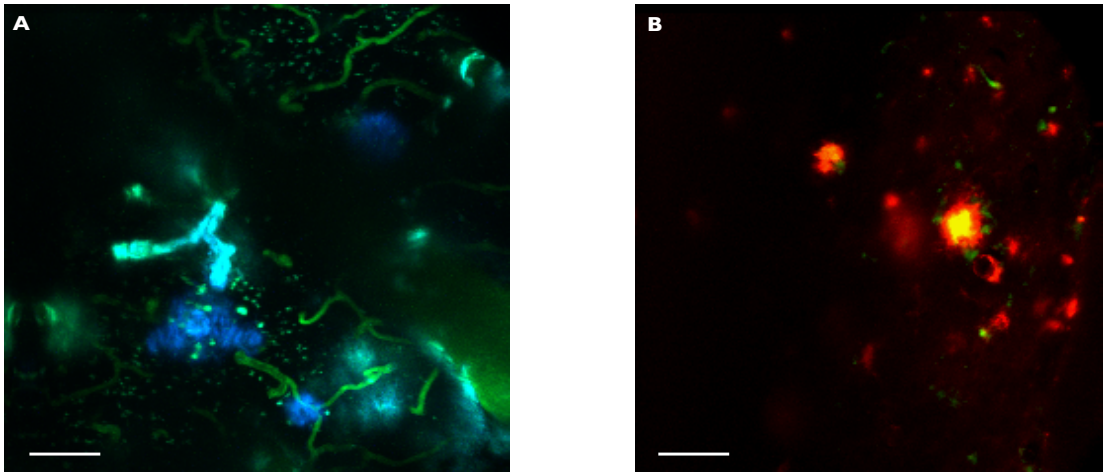

Figure 5.10: Fluorescent tagged antibody. (A) Cy-2 tagged antibody injected intracerebrally in 14-month-old APPsweArc mouse. Blue: plaque, Green: antibody, blood vessels. Scale bar= 30 μm **(B)** Texas red tagged antibody injected intracerebrally in APP/PS1dE9 in 12-month-old mouse. Red: plaque, Green: microglia. Scale bar= 30 μm

As the plaque was imaged in blue channel and microglia in green channel, we chose Texas red tagged antibody, which could be imaged in red channel thus making use of all existing imaging channels. For this reason we did not choose Cy-2 as the green channel was required to image microglia. After the application of Texas red tagged antibody into the cortex of 12-month-old APPsweArc mice (n=2), the same plaque was imaged over hours (Figure 5.11) and later on consecutive days (Figure 5.12). Time-lapse imaging did not show immediate changes in plaque size (Figure 5.11). On chronic imaging it was seen that the antibody bound to plaque started to disappear around day 3. By day 7, almost no antibody was bound to the plaque (Figure 5.12). This could be due to decay of the fluorescent dye itself and clearance of the antibody. However, no change in plaque size was seen (Figure 5.12).

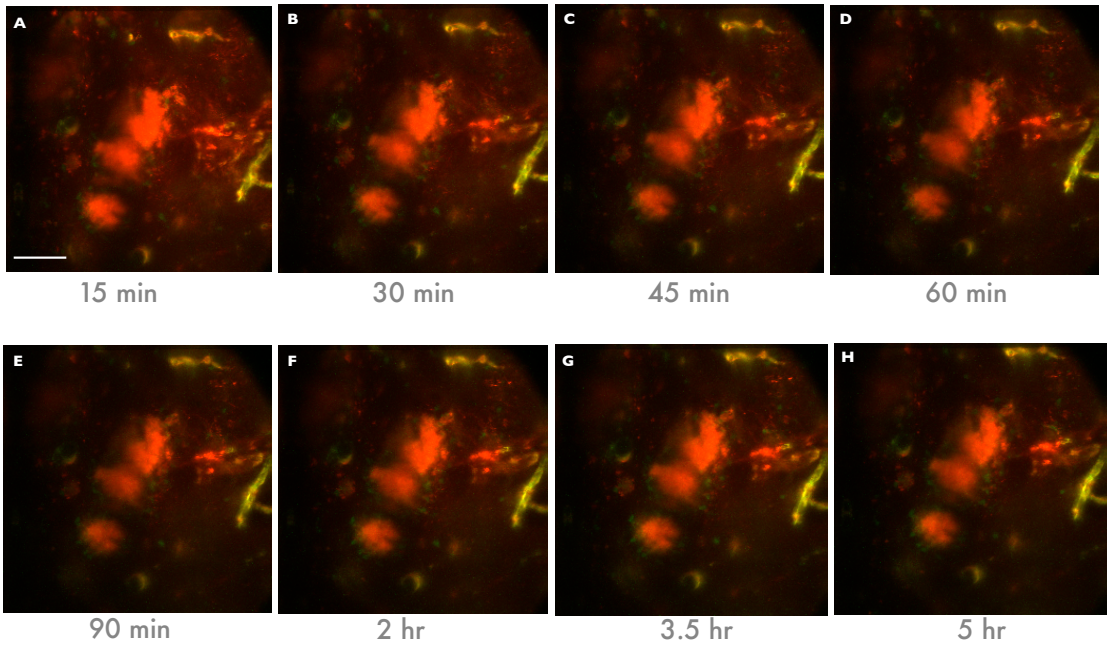

Figure 5.11: Time-lapse imaging after texas red tagged antibody application Images **A-H** show max. intensity Z-projection of 20 µm of 12-month-old APPsweArc mice. Red: plaque, Green: Fluorescein dextran labeld blood vessels and microglia. No change in plaque size was observed in the first 6 hours. Scale bar= 50 µm

5.2.4 Time-lapse imaging of microglia after treatment with tagged and untagged antibody

The next step was to inject Texas red tagged antibody intracerebrally in 12-month-old APPsweArc;CX3CR1 +/- mice (n=3) to study the response of microglia within hours after antibody application (Figure 5.13). We saw the uptake of plaque-antibody complex by microglia around the plaques in one of the mice (Figure 5.13 Panel 2, arrow).

In the next set of experiments, we injected untagged antibody into the brains of 12-month-old APP/PS1dE9;CX3CR1 +/- mice (n=2). Same area was imaged over a period of hours on Day 1 and serially imaged on following days (up to 3 days). Figure 5.14 and 5.15 show recruitment of new microglia in the periphery of plaque where the antibody was injected. The cells reorganized and were seen to be activated microglia after 24 hours. Unfortunately, there was bleeding in the cranial window of mice used for experiment in 5.14 after 24 hours and subsequent imaging could not be done.

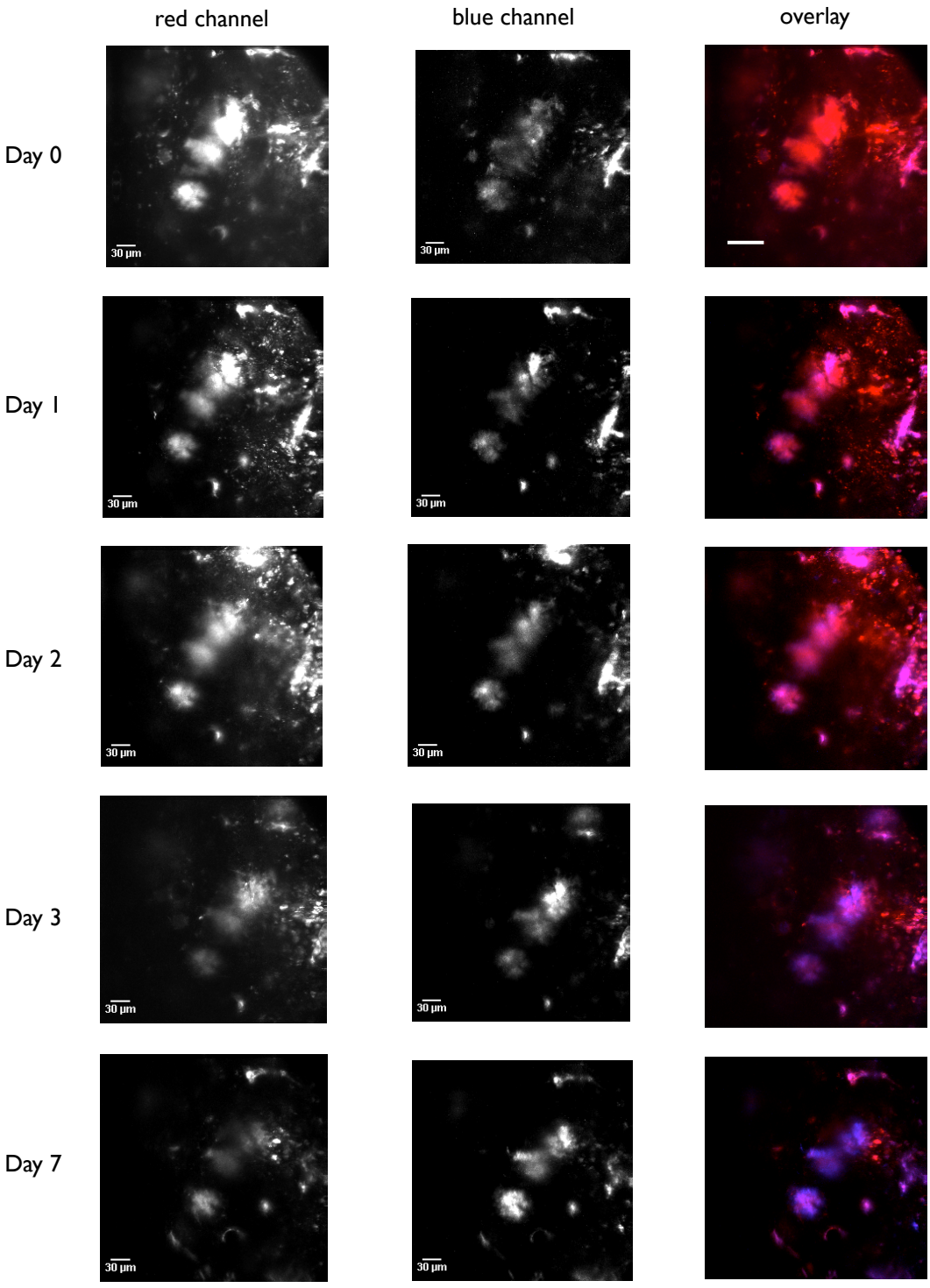

Figure 5.12: Chronic imaging in texas red tagged antibody injected mouse. Images are max. intensity Z-projections of 20 µm of 12-month-old APPsweArc mice. A gradual decrease in the antibody bound to the plaque was observed (red channel), whereas there was no change in the size of plaques was observed (blue channel). Scale bar= 30 µm

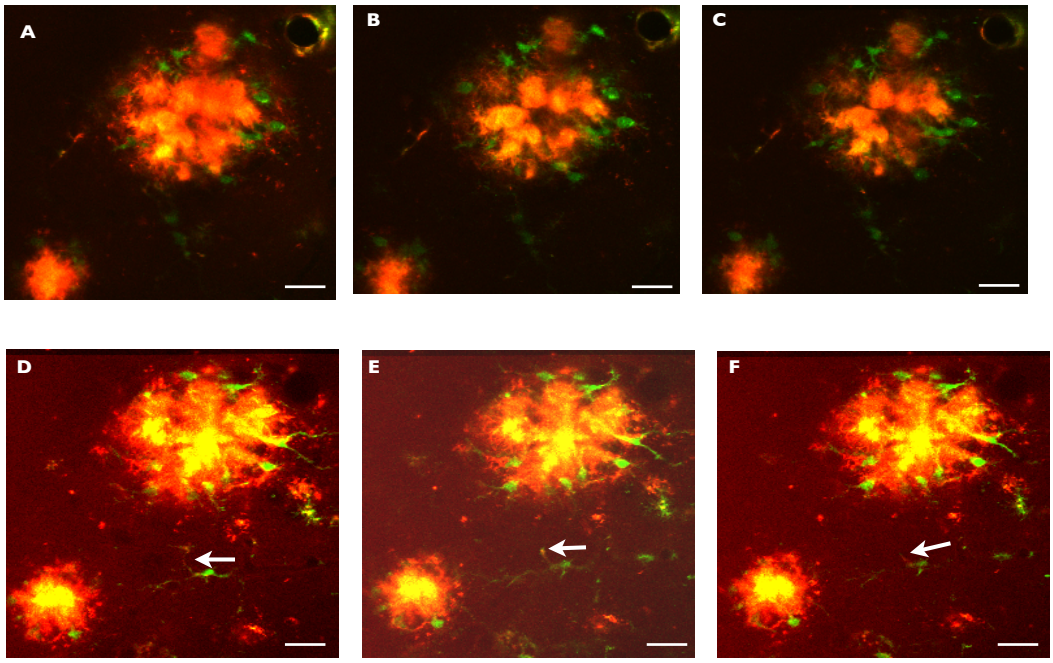

Figure 5.13: Time lapse imaging in APPsweArc;Cx3CR1 +/- mice after Texas red tagged antibody application. Red: plaque, Green: microglia Images **A and D** are 30 min, **B and E** 90 min and **C and F** 4 hours following antibody application. Each image is from a single frame. The arrows show the uptake of plaque-antibody complex by microglia. Scale bar= 30 μm

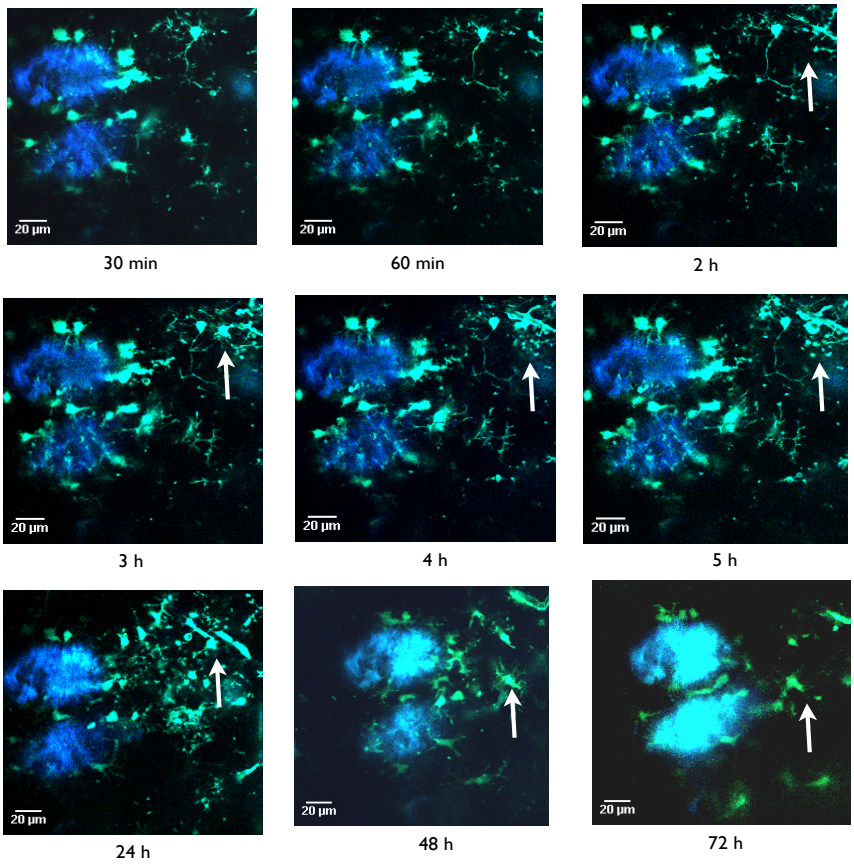

Figure 5.14: Time lapse imaging in APP/PS1dE9;CX3CR 1 +/- mice after untagged antibody application. Blue: plaque, Green: microglia. Images are single frame and time points represent time elapsed after antibody application. Recruitment of new microglia is seen in the periphery of the plaque. The new cells are activated microglia are seen in subsequent days (24, 48 and 72 hours). Scale bar= 20 μm

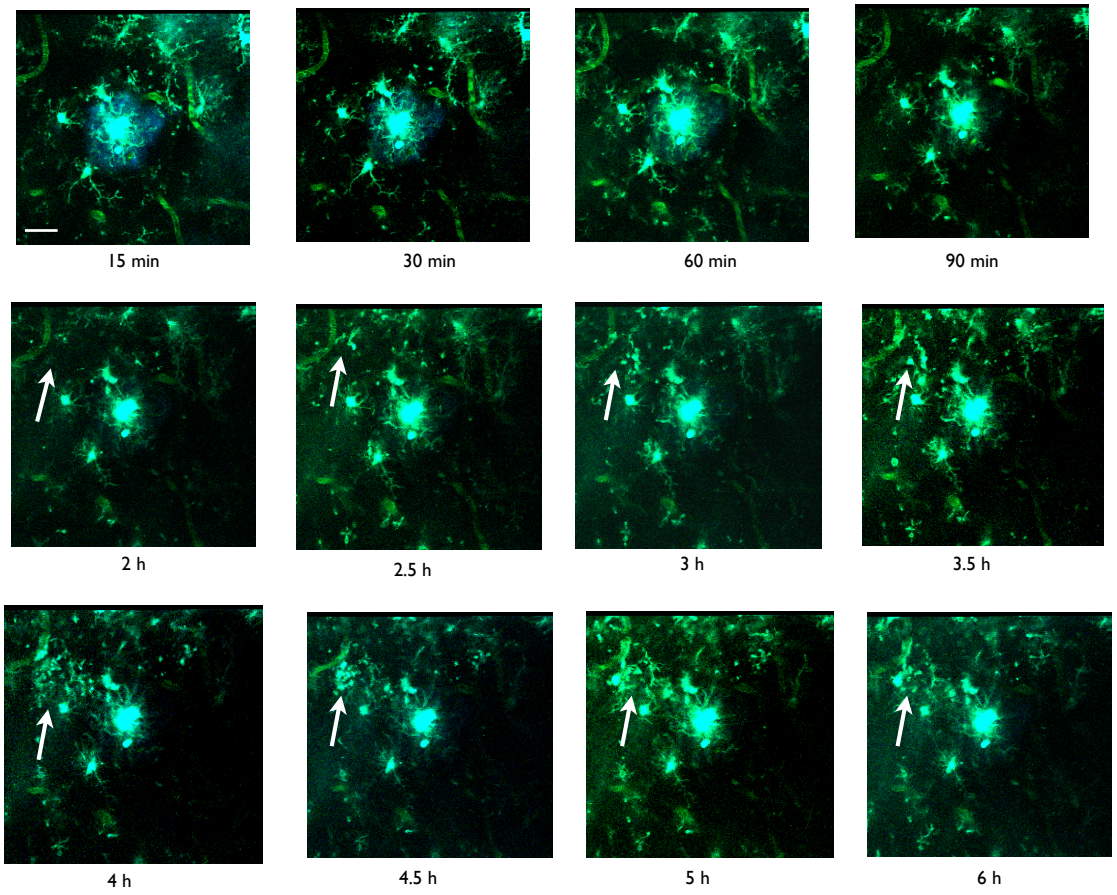

Figure 5.15: Time lapse imaging in APP/PS1dE9;CX3CR1 +/- mice after untagged antibody application. Blue: plaque, Green: Fluorescein dextran labeled blood vessels and microglia. Images are single frame and time points represent time elapsed after antibody application. Recruitment of new microglia in the periphery of the plaque was observed. The new cells are activated microglia are seen within few hours after antibody application. Scale bar= 20 μm

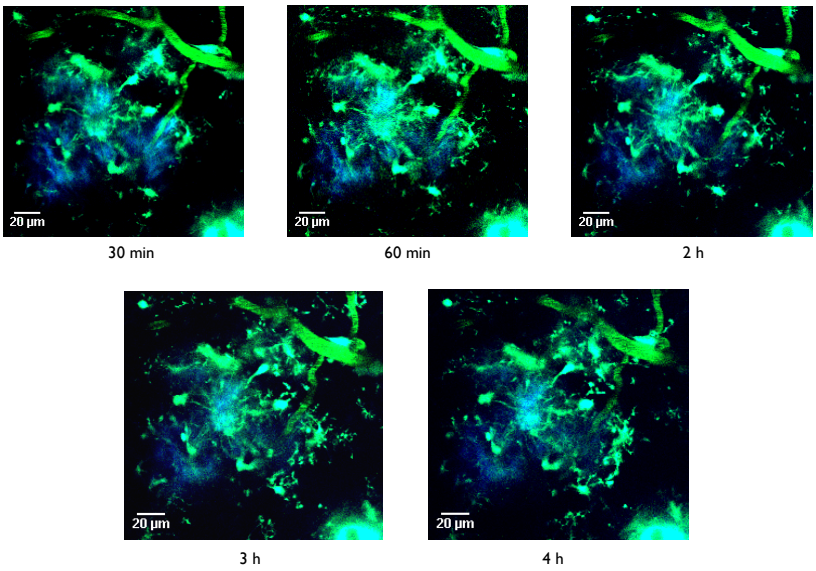

Figure 5.16: Time lapse imaging in APP/PS1dE9;CX3CR1 +/- mice after PBS application. Blue: plaque, Green: microglia. Images are single frame and time points represent time elapsed after PBS application. No changes are seen. Scale bar= 20 μm

PBS injection was used as the control and the imaging protocol was the same. 12-month-old APP/PS1dE9;CX3CR1 +/- mice (n=2) were used. The time-lapse imaging showed less recruitment of microglia in the area surrounding the plaque (Figure 5.16).

Thus, with the techniques of time-lapse and chronic imaging we were able to image microglia and beta-amyloid plaques. Although local anti-Aß antibody application did not show plaque clearance, we observed vigorous recruitment of microglia to plaque periphery after local application of anti-Aß antibody compared to PBS injection. These results although preliminary are promising in the field of plaque-microglia interactions.

5.3 Imaging Cortical Neuronal Activity in Transgenic Models of Brain Amyloidosis

5.3.1 Expression of the genetically encoded calcium indicator: YC3.60

YC3.60 is a genetically encoded calcium indicator (Lutcke, et al. 2010, Nagai, et al. 2004). The indicator cloned in to rAAV was expressed under either one of the two promoters: the chicken ß-actin promoter (CAG) or human synapsin promoter (h-syn). YC3.60 expressed under the CAG promoter labeled about a small percentage of neurons (Figure 5.17 A) while YC3.60 expressed under the h-syn promoter, labeled majority neuronal population (Figure 5.17 B). On the other hand, YC3.60 expressed under the CAG promoter resulted in better labeling of axons as compared to YC expressed under the h-syn promoter.

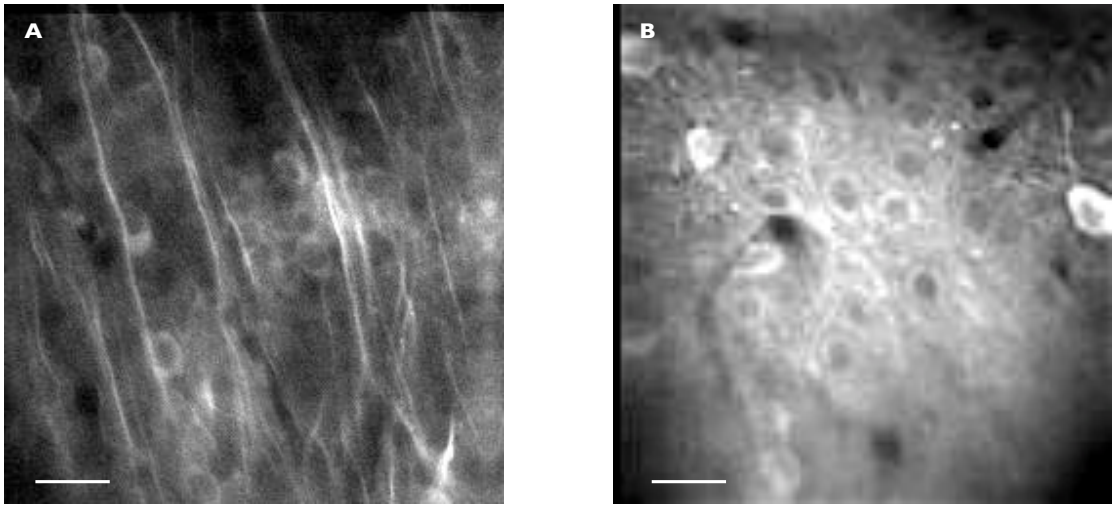

Figure 5.17: Expression of YC3.60 in layer 2/3 of mouse neocortex under CAG **(A)** and h-syn **(B)** promoters after 6 weeks of injections. While the percentage of neuronal labeling is higher in h-syn promoter, axonal labeling is more prominent with CAG promoter. Scale bar= 20 μm

The YC3.60 expression was mainly seen in superficial layers of the cortex up to 350 μm in depth, with some labeling of axons (Figure 5.18 A-C).

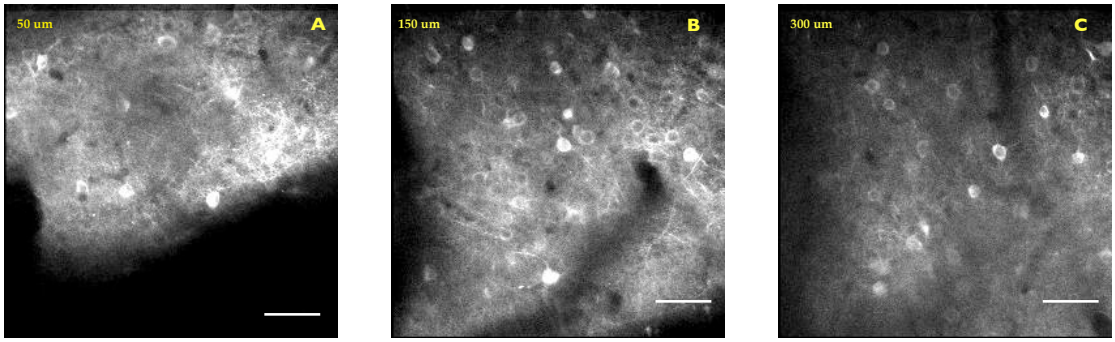

Figure 5.18: Expression of YC3.60 under h-syn promoter in the superficial layers of cortex 6 weeks after virus injection. A, 50 μm, B, 150 μm, and C, 300 μm from the surface. Scale bar= 50 μm

The expression of the indicator was very stable over weeks to months in 9 animals, allowing the identification and imaging of exact same cells over time (Figure 5.19 A-C). In these experiments, the indicator was stable up to 4 months in 2 mice, up to 3 months in 5 mice and up to 9 weeks in 2 mice. Four to five imaging locations were selected for each mouse based on the anatomy of surface vessel patterns. The same locations were identified on each imaging session and aligned in the same X, Y and Z co-ordinates. Optimal laser intensity was ensured between different imaging sessions.

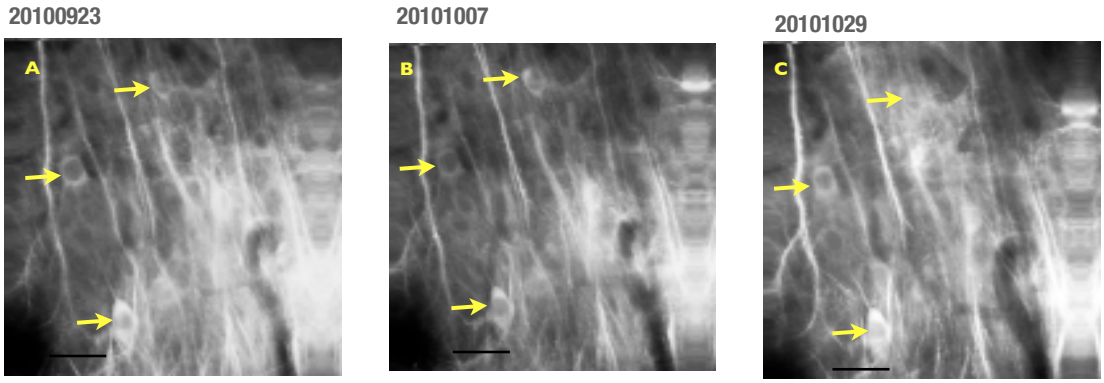

Figure 5.19: Stable expression of YC3.60 indicator. Same cells (arrows) are seen on different imaging days, spanning over a month **(A, B, C).** Similar fluorescence levels were seen. Scale bar= 20 μm

5.3.2 Measuring calcium transients

YC3.60 reports the FRET change caused by conformational changes in the linked CFP-YFP pair, which, in turn is trigged by increase in free intracellular calcium levels. The fluorescence of the acceptor protein YFP, increases while the fluorescence of donor protein CFP, decreases. This percentage change in fluorescence intensities of YFP/CFP ratio, expressed as ΔR/R, was used as measure of neuronal activity because calcium influx in neurons mainly is observed following action potential generation.

Figure 5.20 shows an example of YC3.60 ΔR/R calcium transients, which was calculated by a MATLAB algorithm (see section 4.6). Our goal was to measure calcium signals in pre-plaque phase of Alzheimer's disease and study how it is modulated by therapeutic intervention such as immunotherapy. We thus divided the animals into wt control, antibody treated and vehicle treated groups. We measured spontaneous activity, whisker-evoked response and neuropil activity in these groups.

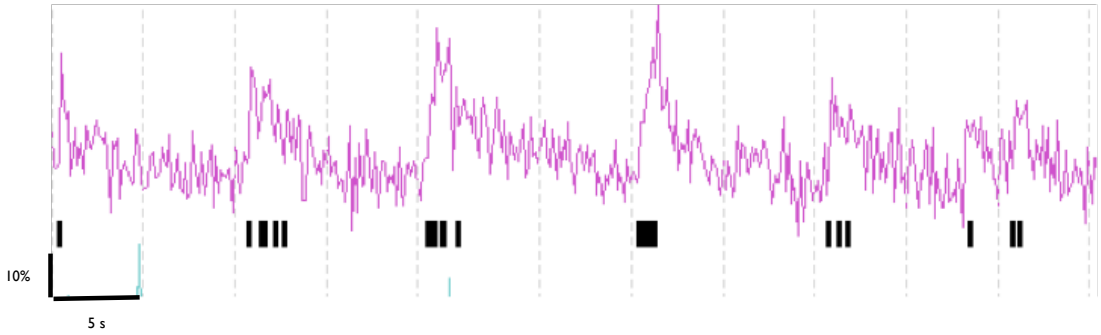

Figure 5.20: Calcium transients reported by YC 3.60. The grey lines in the background indicate the time of whisker stimulation. Each black tick indicates one event as calculated by the algorithm.

5.3.3 Spontaneous Activity

We first assessed spontaneous activity in the barrel cortex of mice in wt control, antibody treated and vehicle treated groups groups. Each measurement trial consisted of frame scan recording of number of events over recording time of 76.8 s duration. We quantified the number of events over this recording period. The value of 0.1 Hz is equivalent to 1 event in 10 seconds. All values are expressed as mean $\pm$ standard deviation. The average rate for antibody treated group (n=177 cells in 3 mice) was 0.14 $\pm$ 0.08 Hz, for vehicle treated group (n=255 cells in 3 mice) was 0.08 $\pm$ 0.06 Hz and for wt control (n=132 cells in 3 mice) was 0.16 $\pm$ 0.11 Hz. Statistical significance ($p<0.05$) was seen between the antibody treated and vehicle treated; between antibody treated and wt control; and between vehicle treated and wt control groups (Figure 5.21). Figure 5.22 shows examples of spontaneous events in a vehicle-treated mouse.

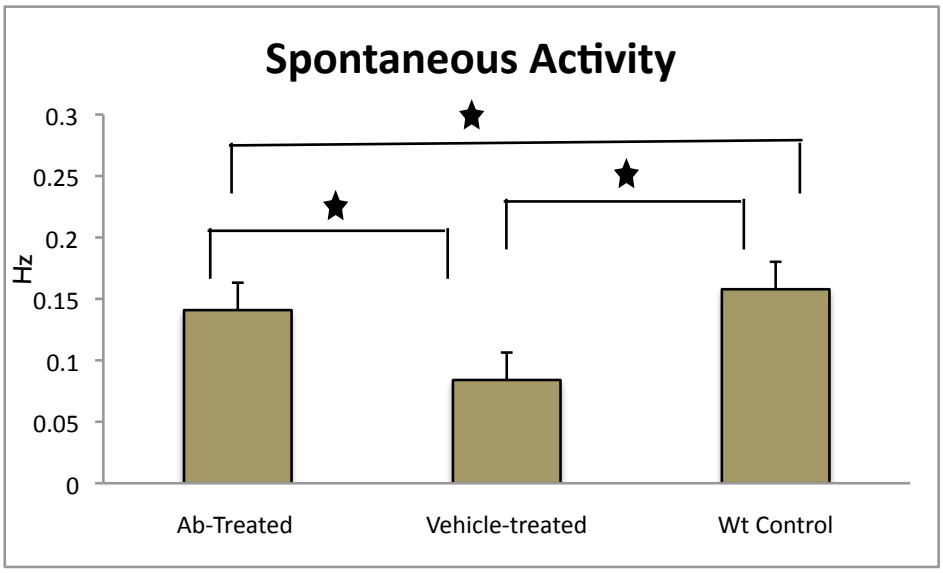

Figure 5.21: Comparison of spontaneous activity in Ab-treated, vehicle-treated and control mice. The values are mean ± SD. The Y-axis represents Hz. Statistical significance ($p<0.05$) was seen between the antibody treated and vehicle treated; between antibody treated and wt control; and between vehicle treated and wt control groups.

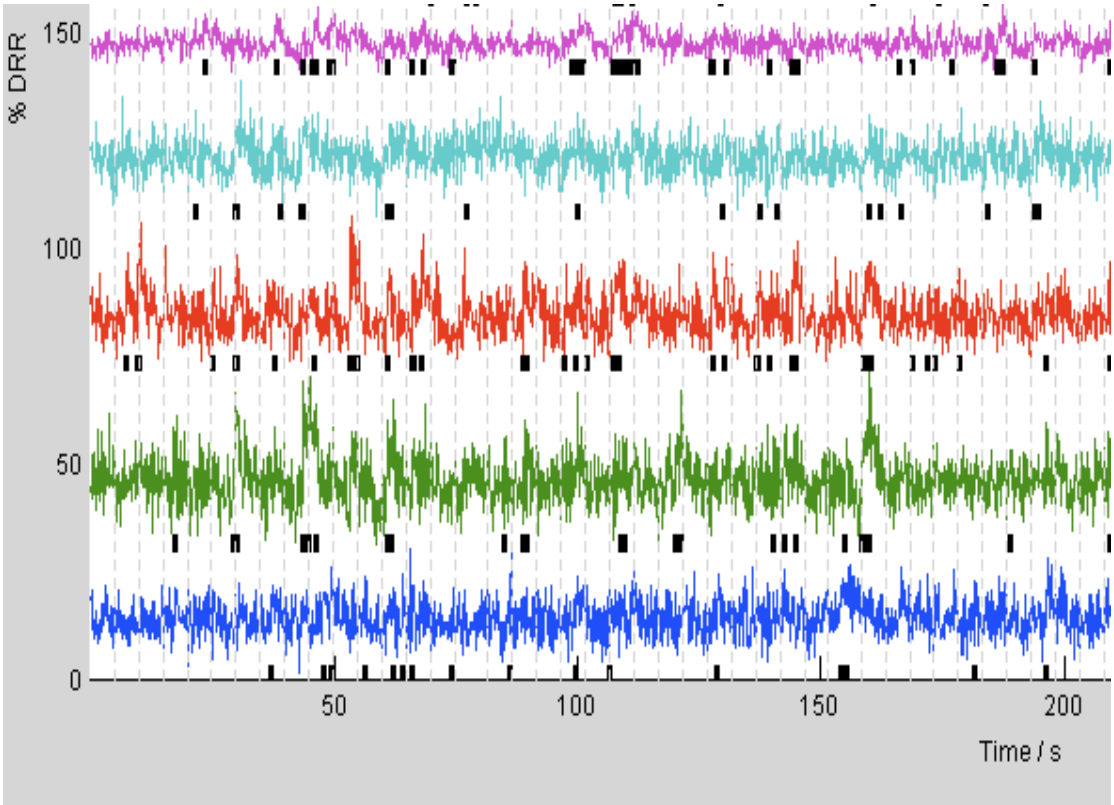

Figure 5.22: Sample Spontaneous Activity. Each trace represents activity of individual cell in a vehicle-treated mouse. There was no whisker stimulation. Each black tick represents a detected event.

Next we analyzed whether we could observe a change in spontaneous activity in the longitudinal imaging sessions. Chronic imaging of the same cells was done and comparisons made over 8 weeks. The first imaging session was considered as baseline value and weekly measurements were made in three groups. The table below shows values for each group. The values are expressed as mean ± SD Hz.

	Ab-treated	**Vehicle-treated**	**Wt control**
Baseline	0.08 ± 0.07	0.14 ± 0.16	0.15 ± 0.15
1 week	0.10± 0.09	0.07± 0.06	0.13 ± 0.13
2 weeks	0.13 ± 0.09	0.11 ± 0.08	0.16 ± 0.15
3 weeks	0.17 ± 0.20	0.13 ± 0.12	0.12 ± 0.08
4 weeks	0.12 ± 0.11	0.12 ± 0.13	0.25 ± 0.13
5 weeks	0.18 ± 0.12	0.12 ± 0.10	0.20 ± 0.10
6 weeks	0.19 ± 0.15	0.08 ± 0.05	
7 weeks	0.17 ± 0.11	0.06 ± 0.04	
8 weeks	0.20 ± 0.11	0.06 ± 0.03	

Table 5.1: Spontaneous event rate of Ab-treated, vehicle-treated and wt control over weeks. The values are given in units of Hz as mean ± SD.

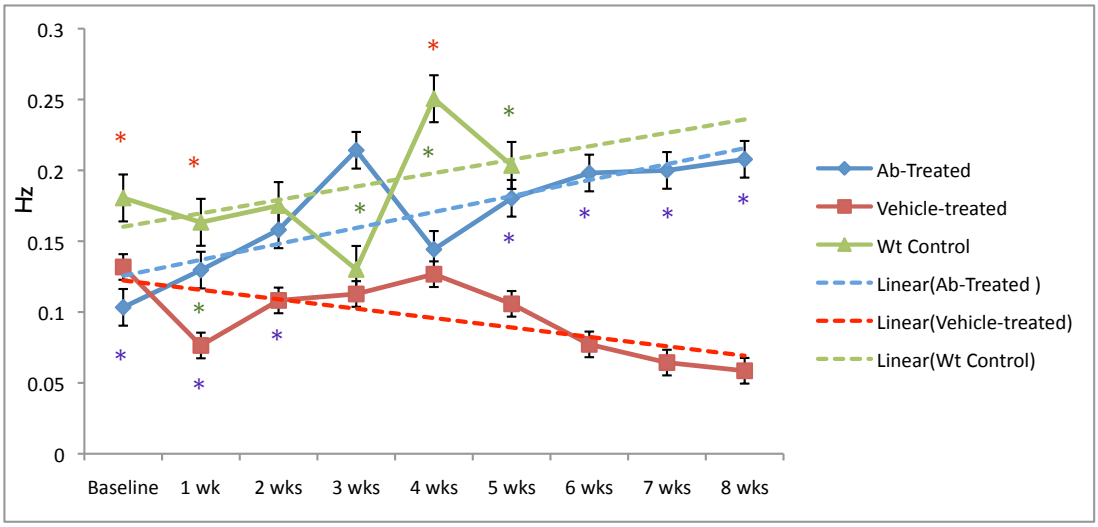

Figure 5.23: Spontaneous activity over weeks. The values are mean ± SD. The Y-axis represents Hz. Statistical significance ($p<0.05$) is seen between the antibody treated and vehicle treated (blue stars) groups at all time points except 3 and 4 weeks; between antibody treated and wt control (red stars) groups at baseline, 1 wk and 4 wks; and between vehicle treated and wt control (green stars) groups at all time points except baseline. The dashed lines represent the linear regression for the time points.

Over the course of weeks, the spontaneous activity of Ab-treated group increased and followed the trend of wt control whereas the response of vehicle-treated group decreased. The linear regression analysis shows that the response of Ab-treated groups at baseline is similar to vehicle-treated group and after antibody treatment it follows the trend line of wt control groups indicating recovery of spontaneous response in antibody-treated groups (Figure 5.23). First of all, the data demonstrate that repeated functional assessment is possible. Secondly, interpretation and statistical analysis is tricky but an interesting trend in Ab-treated versus vehicle-treated is visible. This trend should be further examined in larger animal groups and under even better controlled conditions.

5.3.4 Evoked Activity in AD and wt control mice

Next, we measured calcium transients in response to whisker stimulation in barrel cortex. We first identified the principal whisker corresponding to area of viral expression. Table 5.2 lists the whiskers that were stimulated for each mouse. The evoked activity was measured in all the three groups. We quantified the rate of evoked events before and 1 second after the whisker stimulation. The difference between the two was the measure of evoked activity. The value of 0.1 Hz is equivalent to 1 event in 10 seconds. All values are expressed as mean $\pm$ standard deviation. The average for antibody treated group (n=177 cells in 3 mice) was 0.03 $\pm$ 0.03 Hz, for vehicle treated group (n=255 cells in 3 mice) was 0.02 $\pm$ 0.06 Hz and for wt control (n=132 cells in 3 mice) was 0.30 $\pm$ 0.34 Hz. Statistical significance ($p<0.05$) was seen between the antibody treated and wt control and vehicle treated and wt control groups (Figure 5.24).

Mouse	**Whisker**	**Mouse**	**Whisker**	**Mouse**	**Whisker**
Ab-treated 1	D2	Vehicle-treated 1	C3	Wt control 1	C3
Ab-treated 2	D4	Vehicle-treated 2	C4	Wt control 2	C4
Ab-treated 3	C4	Vehicle-treated 3	C2	Wt control 3	C3

Table 5.2: List of animals and whiskers stimulated

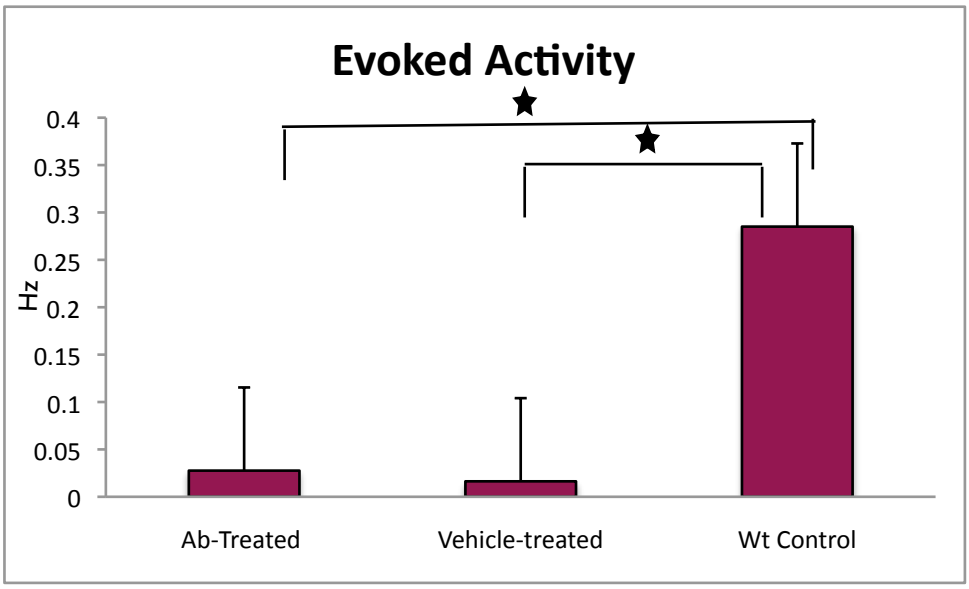

Figure 5.24: Evoked Activity. The values are mean ± SD. The Y-axis represents Hz. The average for antibody treated group (n=177 cells) was 0.0292 ± 0.009, for vehicle treated group (n=255 cells) was 0.0216 ± 0.001 and for wt control (n=132 cells) was 0.2311 ± 0.029. Statistical significance ($p<0.05$) was seen between the antibody treated and wt control and vehicle treated and wt control groups.

A

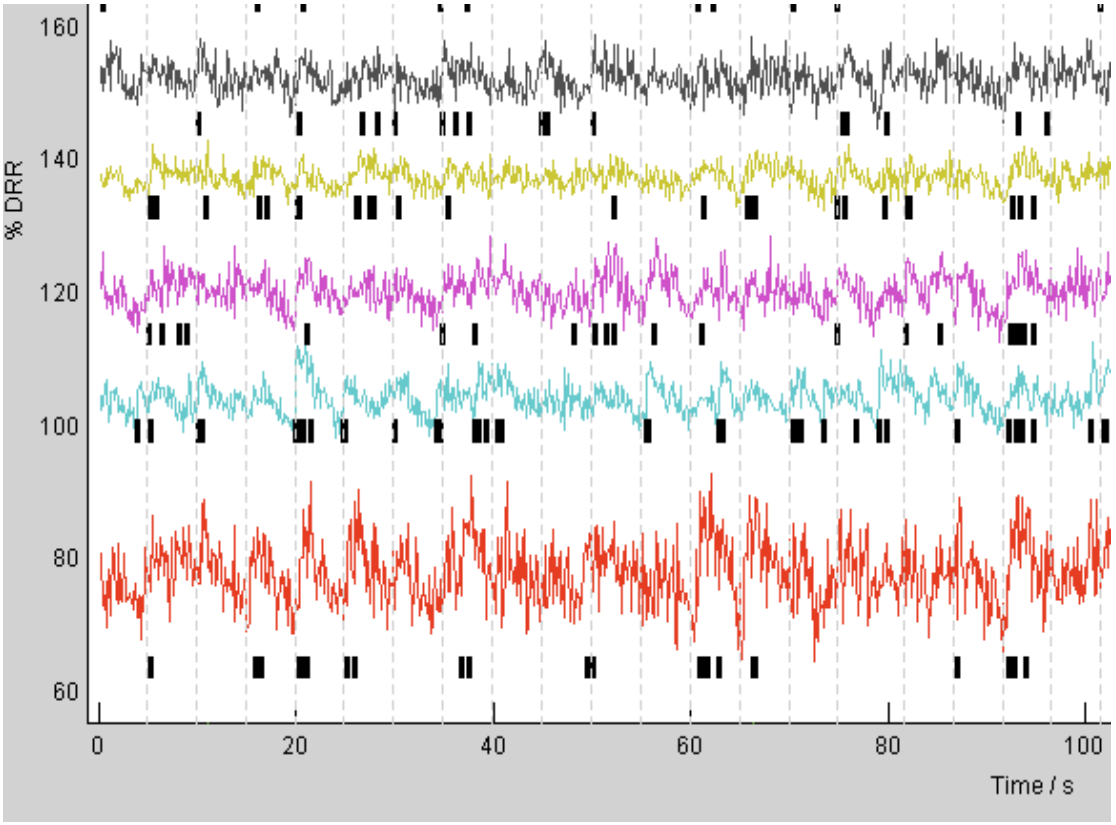

B

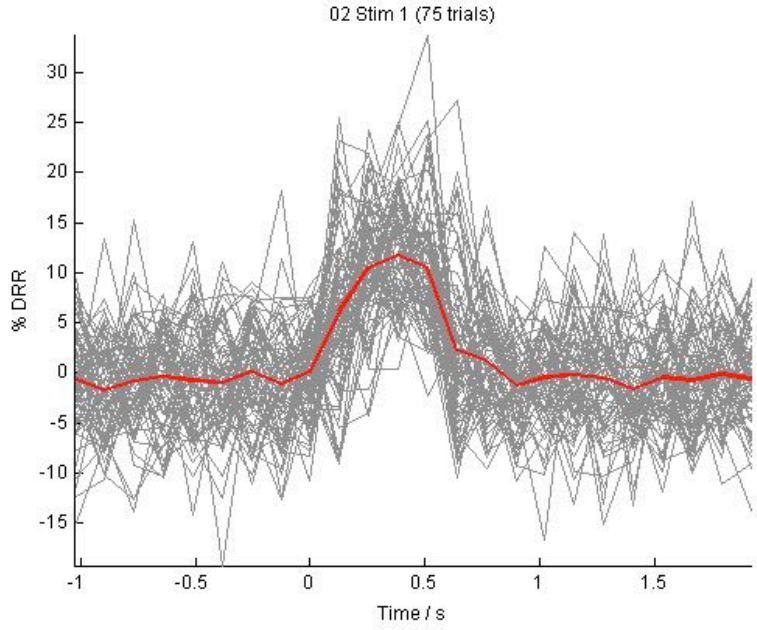

Figure 5.25: Sample Evoked Activity. **A.** Each trace represents activity of individual cells from an Ab-treated mouse. The grey lines indicate whisker stimulation and black tick marks indicate events. Most of the evoked activity is after whisker stimulation. **B.** Whisker stimulated activity of a single cell in an Ab-treated mouse. Time zero indicated the time of whisker stimulation

The chronic imaging of the same cells was done and comparisons made over 8 weeks. The first imaging session was considered as baseline value and weekly measurements were made in three groups. The table 5.3 below shows values for each group. The values are expressed as mean $\pm$ standard deviation. All the mice in wt control died after 5 weeks of imaging.

The wt control animals had higher evoked activity at the baseline and continued to have higher activity than transgenic groups (Ab-treated and vehicle treated). The evoked activity in both transgenic groups followed a similar trend (Figure 5.26). There was significant statistical difference between wt control and transgenic group at all the time points except at 3rd week. However, the statistical significance seen between antibody treated and vehicle treated transgenic groups. The linear regression analysis shows that response of wt control is different to that of Ab-treated and vehicle-treated groups (Figure 5.26). Thus, the data proves that longitudinal imaging

of calcium transients in the same population of cells is feasible. Our data show that the transgenic mice differ from wt control mice with respect to whisker-evoked response. However, our immunotherapy showed only a slight trend of trend in recovery of neuronal activity in response to immunotherapy. This trend should be further examined in larger animal groups and under even better controlled conditions.

	Ab-treated	**Vehicle-treated**	**Wt control**
Baseline	0.03 ± 0.06	0.11 ± 0.24	0.15 ± 0.24
1 week	0.02 ± 0.07	0.02 ± 0.07	0.30 ± 0.53
2 weeks	0.06 ± 0.07	0.03± 0.12	0.28 ± 0.51
3 weeks	0.06 ± 0.10	0.07 ± 0.22	0.22 ± 0.43
4 weeks	0.05 ± 0.08	0.04 ± 0.18	0.17 ± 0.18
5 weeks	0.03 ± 0.08	0.02 ± 0.07	0.20 ± 0.20
6 weeks	0.04 ± 0.07	0.003 ± 0.07	
7 weeks	0.03 ± 0.08	0.01 ± 0.06	
8 weeks	0.014 ± 0.09	0.004 ± 0.05	

Table 5.3: Evoked Response of Ab-treated, vehicle-treated and wt control over weeks. The values are mean ± SD in units of Hz.

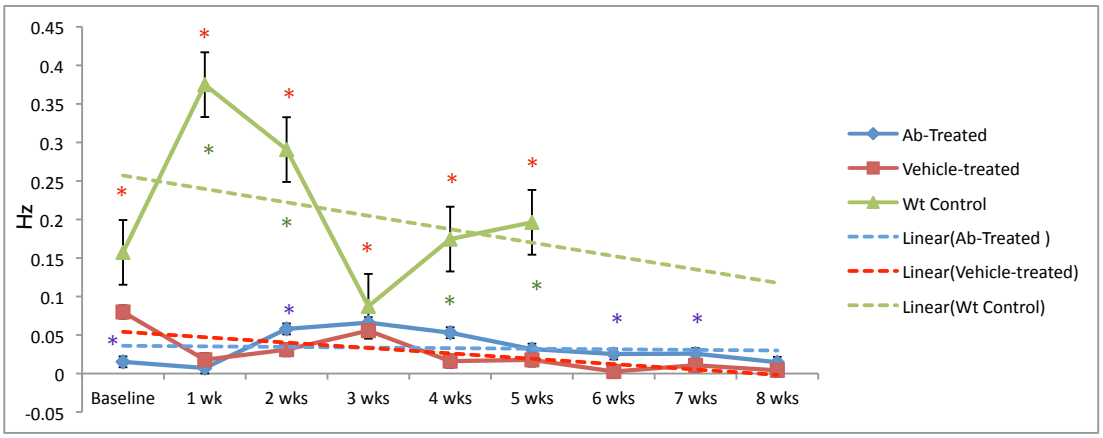

Figure 5.26: Evoked Activity over weeks. The values are mean ± SD. The Y-axis represents Hz. Statistical significance ($p<0.05$) is seen between antibody treated and wt control (red stars) at baseline, 1 wk, 2 wk, 3 wk, 4wk and 5 wk; between vehicle treated and wt control groups (green stars) at 1 wk, 2 wk, 3 wk, 4 wk and 5 wk; between Ab-treated and vehicle treated (blue stars) at baseline, 2 wk, 6 wk and 7 wk. The dashed lines represent the linear regression for the time points.

5.3.5 Neuropil activity

Neuropil is the milieu in which the neuronal networks function. It has been shown that whisker-stimulation elicited clear calcium transients not only in neuronal somata but also in the neuropil (Lutcke, et al. 2010). Therefore, we measure the neuropil activity as well. The neuropil activity was measured in all the three groups and it was similar to evoked activity measurement. We quantified the rate of evoked events before and 1 second after the whisker stimulation. The difference between the two was the measure of evoked activity. The value of 0.1 Hz is equivalent to 1 event in 10 seconds. All values are expressed as mean $\pm$ standard deviation. The average for antibody treated group (n=177 cells) was 0.19 $\pm$ 0.23 Hz, for vehicle treated group (n=255 cells in 3 mice) was 0.06 $\pm$ 0.22 Hz and for wt control (n=132 cells in 3 mice) was 0.13 $\pm$ 0.23 Hz. Statistical significance ($p<0.05$) was seen between the antibody treated and wt control and vehicle treated and wt control groups (Figure 5.27).

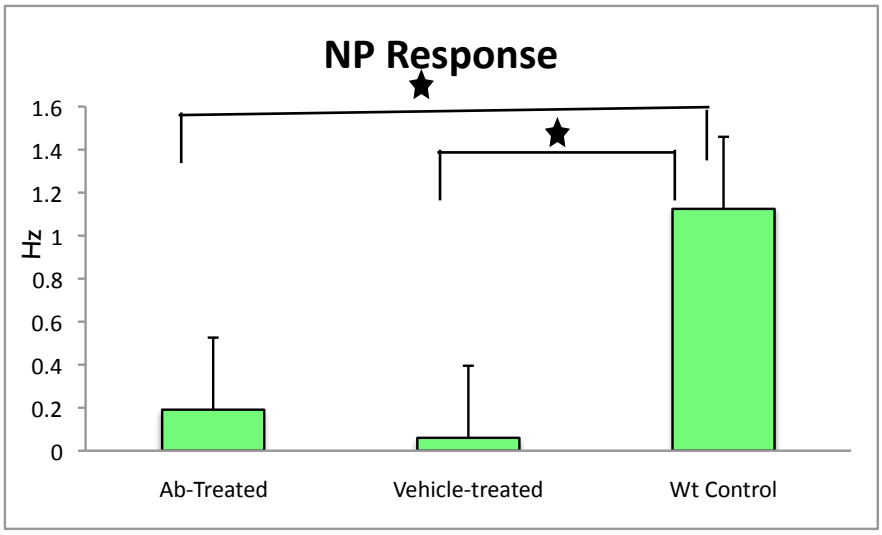

Figure 5.27: Neuropil Activity. The values are mean $\pm$ SD. The Y-axis represents Hz. Statistical significance ($p<0.05$) was seen between antibody treated and wt control; and between vehicle treated and wt control groups.

A

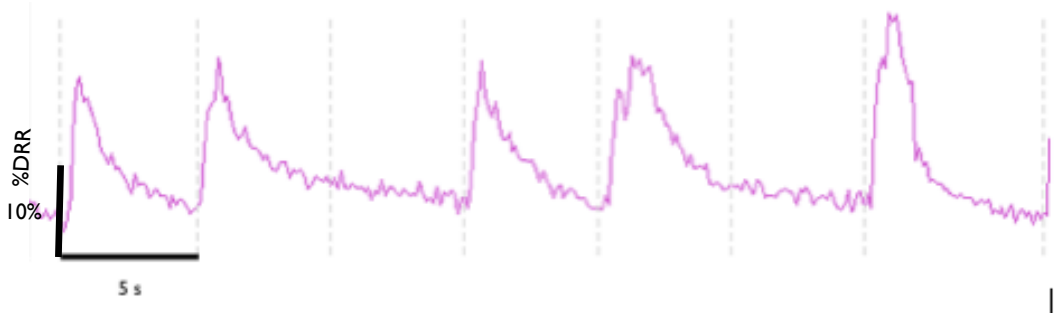

B

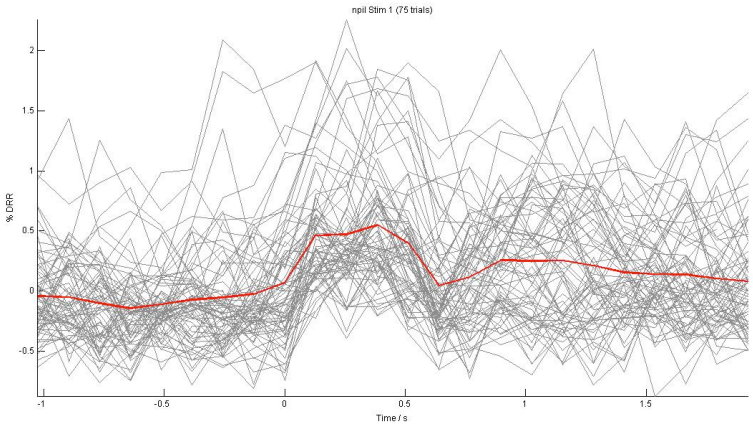

Figure 5.28: Sample Neuropil Activity. **A.** Trace represents neuropil activity of one imaging spot. The grey lines indicate whisker stimulation. Most of the evoked activity is after whisker stimulation. **B.** Whisker stimulated neuropil activity of one imaging spot. Time 0 indicated the time of whisker stimulation

The chronic imaging of the same cells was done and comparisons made over 8 weeks. The first imaging session was considered as baseline value and weekly measurements were made in three groups. The table below shows values for each group. The values are expressed as mean $\pm$ standard deviation.

The neuropil response of cells over weeks shows similar trend as whisker evoked activity. The neuropil activity of wt control decreased over 5 weeks and activity of Ab-treated and vehicle treated follows similar trend (Figure 5.29).

	Ab-treated	Vehicle-treated	Wt control
Baseline	0.18± 0.20	0.29 ± 0.64	0.77 ± 0.81
1 week	0.23 ± 0.40	0.14 ± 0.21	1.37 ± 1.48
2 weeks	0.39 ± 0.36	0.16 ± 0.20	1.41 ± 1.46
3 weeks	0.47 ± 0.34	0.07 ± 0.22	1.06 ± 1.24
4 weeks	0.26 ± 0.28	0.07 ± 0.16	0.22 ± 0.31
5 weeks	-0.03 ± 0.17	-0.03 ± 0.09	0.83 ± 0.35
6 weeks	0.10 ± 0.14	-0.03 ± 0.09	
7 weeks	0.07 ± 0.32	0.01 ± 0.04	
8 weeks	0.003 ± 0.10	0.03 ± 0.10	

Table 5.4: Neuropil activity of Ab-treated, vehicle-treated and wt control over weeks. The values are mean ± SD in units of Hz.

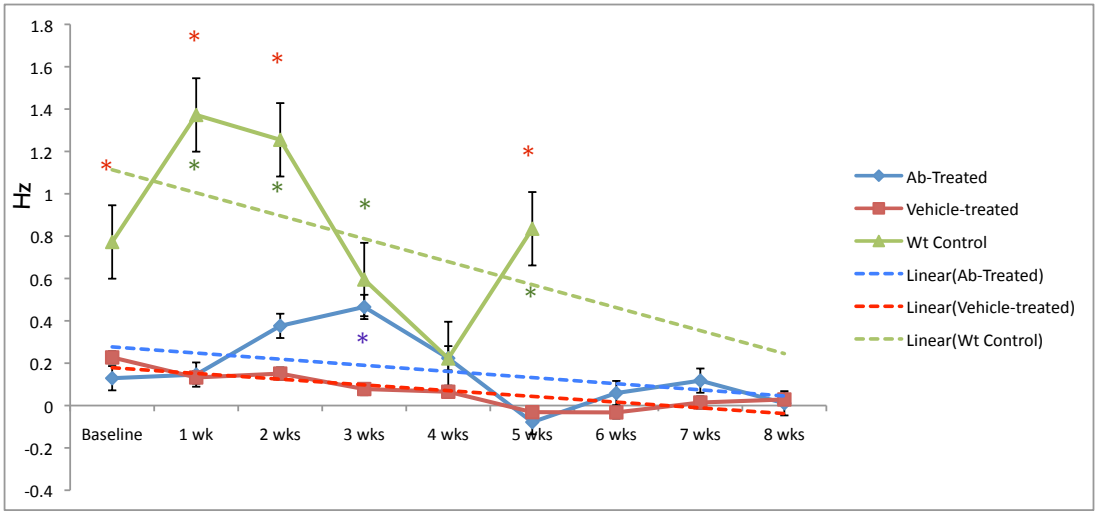

Figure 5.29: Neuropil activity over weeks. The values are mean ± SD. The Y-axis represents Hz. Statistical significance is seen between the antibody treated and vehicle treated; between antibody treated and wt control; and between vehicle treated and wt control groups.

Thus, we successfully used YC3.60 in pre-plaque phase of APPswe mice to measure neuronal activity in the barrel cortex. We measured the spontaneous activity, whisker-evoked response and neuropil response in these mice over period of 8 weeks and noted differences in wt control and transgenic mice.

5.3.6 Immunohistochemistry

After the completion of long term imaging experiments, the mice were sacrificed and brain was sectioned (see section 4.2.8). We wanted to confirm the area of virus injection, confirm neuronal labeling and how these neurons would be different in transgenic mice structurally. We also wanted to examine sections for presence of beta-amyloid plaques.

The floating sections showed viral expression of YC3.60 in the cortex and axonal projections in the white matter (Figure 5.30), which is consistent with published reports (Lutcke, et al. 2010). Beta-amyloid plaques stained by 6E10 are seen in the neocortex of 24-month old APPsweArc mice injected with YC3.60 (Figure 5.30 A) and not in 10-month old APPswe mice (Figure 5.30 B).

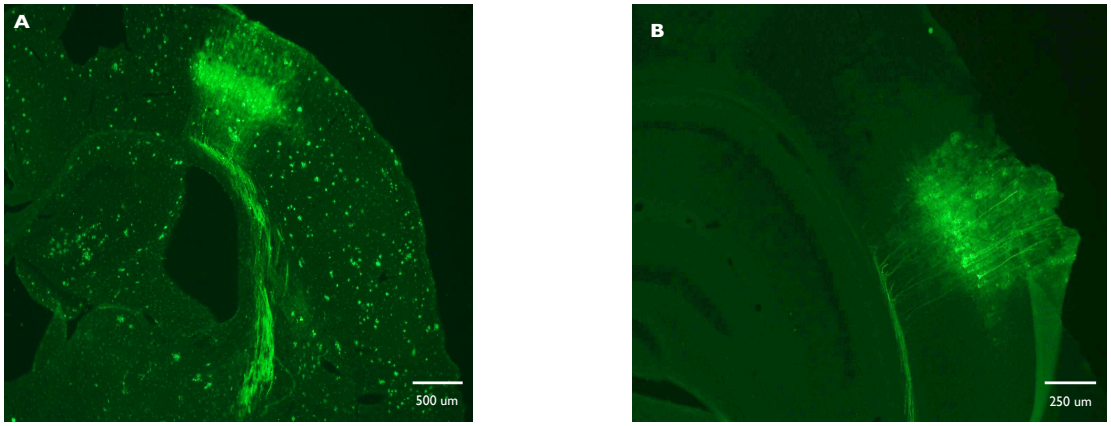

Figure 5.30: Viral Expression in cortex **A.** 24-month old APPsweArc mouse showing YC3.60 expression and beta-amyloid plaques. **B.** 10-month old APPswe mousing showing YC3.60 expression but no beta-amyloid plaques.

The YC3.60 co-localized with NeuN. The YC3.60 labels only a percentage of neuronal population (Figure 5.31).

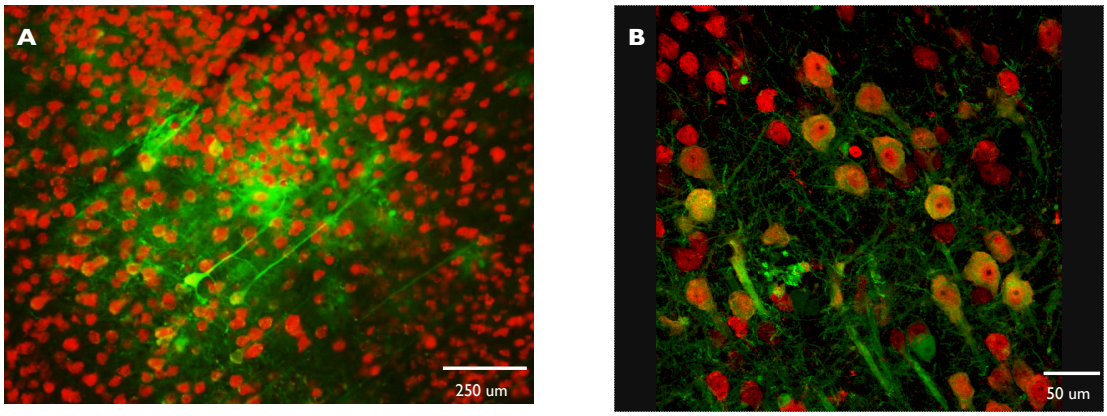

Figure 5.31: YC3.60 and NeuN co-localization **A.** 10-month old APPswe mouse showing co-localization of YC3.60 and NeuN. **B.** 63x magnified confocal image. Red: NeuN, Green: YC3.60

The *in vivo* imaging of transgenic animals over weeks did not reveal development of any plaques in the imaging areas. However, immunohistochemistry showed beta-amyloid plaques in cortex of both Ab-treated and vehicle-treated animals (Figure 5.32). These mice were around 10 month of age at the time of immunohistochemistry. Ab-treated mice had 4-6 beta-amyloid plaques in the cortex whereas vehicle treated mice had 8-10 beta-amyloid plaques. This is the beginning of plaques deposition in APPswe mice (Hsiao, et al. 1996).

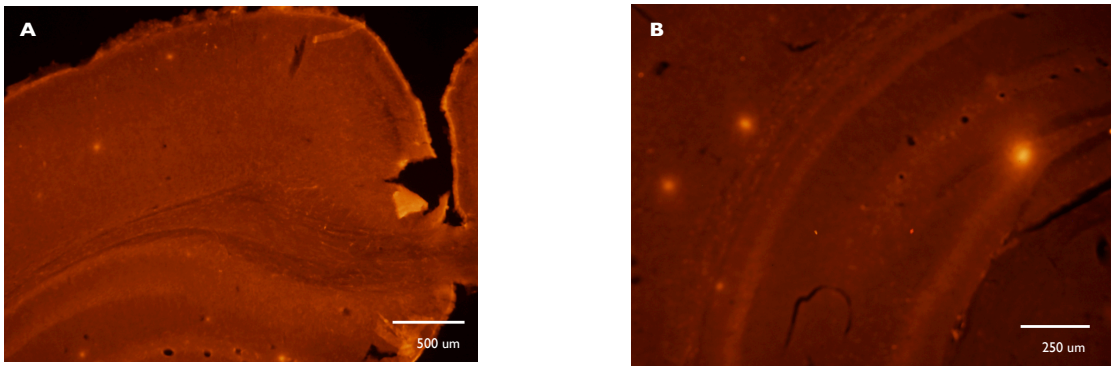

Figure 5.32: Development of amyloid plaques **A.** Ab-treated 10-month old APPswe mouse showing beta-amyloid plaques. **B.** Vehicle-treated 10-month old APPswe mouse showing beta-amyloid plaques.

YC3.60 expression under CAG promoter labeled both neuronal bodies and dendrites (Figure 5.33). The 24-month old APPsweArc mice showed dystrophic neurites (arrows) whereas 10-month old APPswe mice did not show any (Figure 5.34 A and B).

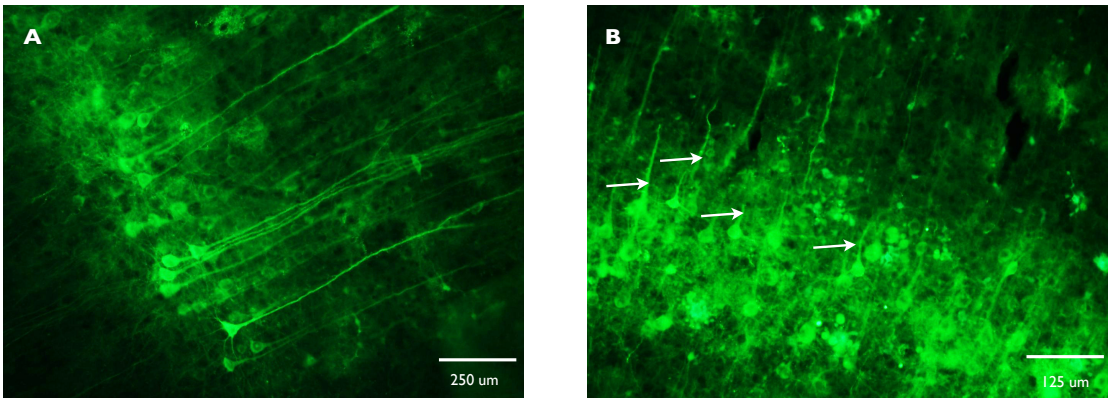

Figure 5.33: Dystrophic neurites **A.** 10-month old APPswe mouse did not show any dystrophic neurites. **B.** 24-month old APPsweArc mouse showing dystrophic neuritis (arrows).

On zooming in the 24-month old APPswe mice showed dystrophic neurites and atrophic neuronal bodies in the periphery of beta-amyloid plaques (Figure 5.34 A and B).

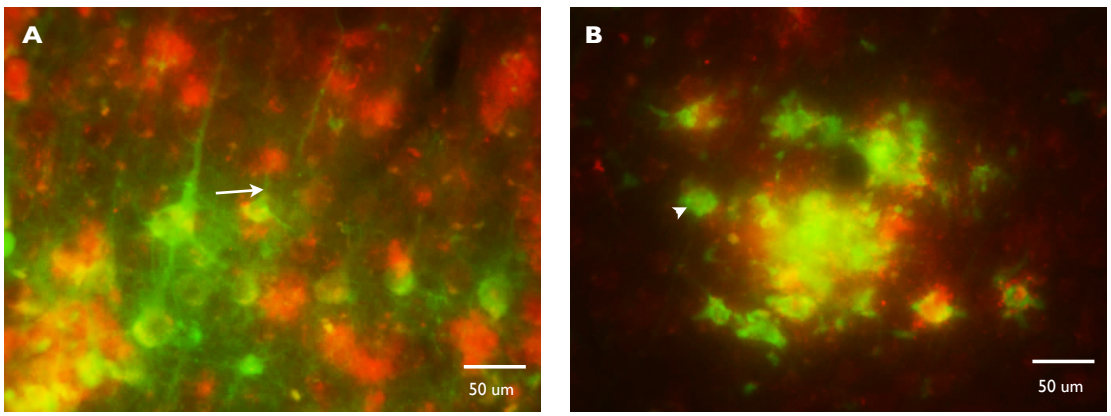

Figure 5.34: Zoomed in dystrophic neurites in 24-month old APPsweArc mouse, shown by arrow and atrophic neuron, shown by arrow head. Red: beta-amyloid plaques, Green: YC3.60

With the technique of immunohistochemistry, we were able to confirm the area of virus injection, confirm neuronal labeling and observe beginning of plaque deposition

in the mice, which were in pre-plaque phase during long-term imaging. Furthermore, we were able to identify dystrophic neurites and atrophic in old APPswe mice injected with YC3.60. These immunohistochemistry results were complementary to the functional imaging data.

6. Discussion

6.1 Standardization of chronic imaging protocols

Chronic observation and manipulation of cells in the cortex is integral part of studies on neurons, glia and microvasculature. The discovery of 2PM was a landmark in the field of chronic imaging (Svoboda, et al. 1997). However, main principles for chronic imaging preparation are stability by reducing motion artifacts, tolerance of the animal, and maintenance of optical quality over weeks, and reproducibility. Without optimizations of these key factors, chronic imaging is not possible.

There have been several reports where head posts were used for chronic imaging (Burgold, et al. 2011, Busche, et al. 2008, Hefendehl, et al. 2011). Custom-made head posts were used in this dissertation work (Figure 5.1), which were very well tolerated for several weeks by the animal. The aluminum used to make these head posts was important key in decreasing the weight. Here, we show that the head posts reduce the motion artifacts to acceptable low levels and provide steady images for time-lapse imaging and calcium imaging (Figure 5.2 and 5.3).

Even as the debate for optimum window for chronic imaging continues, we used craniotomy for the simplicity of technique and wide area available for imaging purposes. Thinned-skull preparations are shown to cause less microglia and astrocyte reaction in the imaging area and affect dendritic turnover (Drew, et al. 2010, Grutzendler and Gan 2006, Xu, et al. 2007). Xu et al. reported that effects of craniotomy on spine dynamics subsided by 2 months. Most of the studies involving imaging of AD animal models have used craniotomy (Bacskai, et al. 2001, Bolmont, et al. 2008, Burgold, et al. 2011, Busche, et al. 2008, Hefendehl, et al. 2011). The optimized procedures used here for preparation of the chronic window had success rate of 60-70% for ‘clearing up’ after 3 weeks and the ‘cleared’ windows remained optically viable for several weeks to months (Figure 5.5).

Another aspect was labeling of beta-amyloid plaques with Methoxy-X04. Several of the published protocols were tried but did not result in satisfactory plaque labeling (Figure 5.6 A). However, the protocol obtained by Prof. Bacskai, produced remarkable labeling of plaques (Figure 5.6 B). We were also able to successfully

inject the genetically encoded calcium indicator, YC3.60 in barrel cortex of APPswe mice and obtain satisfactory labeling of layer 2/3 neocortical neurons (Figure 5.30).

6.2 Various techniques to study microglia-plaque interaction

The second part of the project was the morphological aspect, which was to study microglia-plaque interaction. Most of the papers in the field of immunotherapy in AD and microglia response are done either with topical antibody application and *in vivo* imaging or systemic application with immunohistochemistry. We tried the technique of plaque targeted antibody application, using the principle of bulk-loading of calcium dyes (Garaschuk, et al. 2006). We injected the antibody under microscopic guidance for optimum injection near amyloid plaques. The technique caused minimal tissue damage (Figure 5.8). However, we could not demonstrate plaque removal in APP/PS1dE9 and APPsweArc mice (Figure 5.9 and 5.12). The main drawback of this technique was the limitation of imaging area and this would suggest that the concentration of antibody too low to clear plaques. We also tried the technique of fluorescent antibody application to track the antibody spread and uptake (Figure 5.13). We saw that the antibody was bound to the plaque up to 7 days (Figure 5.12). However, even with this approach no plaque removal was seen (Figure 5.12). We observed similar number of microglia surrounding plaques as reported by Bolmont et al.

The next logic was even if there is no plaque removal, there may be alteration of microglia dynamics. The amyloid plaques had different tiers of microglia surrounding and most plaques had around 5-8 microglia in each plane (Figure 5.7 and Figure 5.13). We performed time-lapse imaging of microglia over 6-8 hours after topical application of anti-Aß antibody (Figure 5.14 and Figure 5.12) and PBS (Figure 16). The preliminary analysis of these data shows vigorous recruitment of microglia to the plaque periphery after topical application of anti-Aß antibody. However, more studies focusing of time-lapse imaging over days is needed to confirm these findings.

We here presented two unique techniques, which can be used to study plaque-microglia reactions.

6.3 Neocortical Neuronal Activity in Alzheimer's Disease Animal Models

Alzheimer's disease is a disorder of neuronal function and biophysically speaking, it can be described as a failure of neuronal circuits. The various neuronal networks involved in cognition, memory and other higher mental functions are affected by neurodegenerative changes. That being said, so far there have not been many *in vivo* studies focusing on dysfunction of neuronal networks in AD. This dissertation work is unique in the sense that we used a genetically encoded calcium indicator to study spontaneous and whisker-evoked activity longitudinally in a mouse model of brain amyloidosis in pre-plaque phase and were able to test therapeutics such as immunotherapy, which so far has been missing in the field of AD.

6.3.1 Expression of YC3.60 and measurement of calcium tranients

The discovery of genetically encoded calcium indicators (Miyawaki, et al. 1997) has led to development of wide repertoire of these indicators (Mank and Griesbeck 2008), and the list is still expanding. Of all the available families of GECIs, GCaMP and Yellow Cameleons are most commonly used. We used calcium indicator Yellow Cameleon 3.60 coupled to AAV for labeling of a population of neurons. Previously it was shown that YC3.60 under human synapsin promoter labeled cortical neurons densely and was observed preferentially in Layer 2/3 and Layer 5 (Lutcke, et al. 2010). We used 2 types of promoters h-synapsin and CAG. One goal was to reproduce the results of Lutcke 2010 and another was to characterize the indicator with CAG promoter and compare it with h-synapsin. We saw expression in L2/3 and L5 (Figure 5.17 and Figure 5.18) and was similar to the published reports (Lutcke, et al. 2010). CAG promoter resulted in extensive axonal labeling than h-synapsin promoter. We also confirmed the labeling by immunohistochemistry (Figure 5.30 and Figure 5.31). We were also able to find the same population of cells in all of the imaging areas in every imaging session in all the animals (Figure 5.19), which was very important part of chronic imaging.

6.3.2 Spontaneous activity in AD transgenic and wt control mice

In vivo calcium imaging of cortical circuits in APP/PS1 AD transgenic mice has revealed that transgenics have a greater proportion of hyperactive and hypoactive neurons than nontransgenic controls (Busche, et al. 2008). This study measured only the spontaneous activity and did not answer the questions regarding long-term modulation of neuronal response to stimuli. The first study which looked at sensory-evoked activity in AD was by Grienberger et al., which reported progressive deterioration of neuronal tuning for orientation of visual stimuli, which occurred in parallel with age-dependent increase of beta-amyloid load in visual cortex of APP/PS1 mice (Busche, et al. 2012). However, both Busche, et al. 2008 and Grienberger, et al. 2012 used OGB-1, which is a synthetic calcium indicator with several short comings when it comes to longitudinal imaging (Mank and Griesbeck 2008).

In this dissertation work, we measured spontaneous response of same population of cells of barrel cortex. We saw statistically significant difference between the antibody treated and vehicle treated; between antibody treated and wt control; and between vehicle treated and wt control groups (Figure 5.21). The linear regression analysis showed that the response of antibody treated animals increased over the period of 8 weeks and follows the trend of wt control, whereas the response of vehicle treated decreased over the same duration (Figure 5.23). This shows a trend towards reversal of the spontaneous activity of in antibody treated transgenics towards activity of nontransgenics. Many different anti-Aß antibodies have been used for immunotherapy in AD transgenics. Passive immunization in PDAPP mice with 3D6 (IgG2b $Aß_{1-15}$) and 10D5 (IgG1 $Aß_{3-7}$) antibodies clears plaques but not 16C11 (IgG1 $Aß_{33-42}$) (Bard, et al. 2000). Many studies used topical application of anti-Aß antibodies in AD transgenics and observed plaque clearance (Bacskai, et al. 2001, Prada, et al. 2007, Spires-Jones, et al. 2009). The antibody we used was in-house generated anti-Aβ IgG2a targeted against fibrillar Aβ, which has shown efficacy in plaque removal (Biscaro, et al. 2009). Unlike Busche et al., we did not find cluster of hyperactive neurons, the baseline spontaneous activity was lower in transgenics compare to nontransgenic controls. This could be attributed to difference in transgenic line (APP/PS1 vs. APPswe), age and difference in AD pathology (plaque vs. pre-plaque

phase). Also, our animal group was small with n=3. Thus, more studies with larger animal groups are warranted.

6.3.3 Evoked Activity in AD transgenic and wt control mice

The recent reports indicate that neuronal activity is affected before development of plaques, which is mainly caused by soluble Aß species (Cheng, et al. 2007, Cleary, et al. 2005, Holcomb, et al. 1998, Klein, et al. 2001, Lesne, et al. 2006, Selkoe 2008, Shankar, et al. 2007, Shankar, et al. 2008, Tomiyama, et al. 2010, Walsh and Selkoe 2007). Most recently, Busche, et al. 2012 looked at neuronal activity in hippocampal CA1 pyramidal cells of APP/PS1 mice in an *in vivo* setting and found selective increase in hyperactive neurons already before the formation of plaques, suggesting that soluble species of Aβ may underlie this impairment. Thus, the emphasis is now shifting towards study of pre-plaque pathology of AD. We selected whisker stimulation as a method to study evoked activity in rodent barrel cortex neuronal networks. The rationale being that it is a well studied system and the whisker stimulation protocol was already standardized in the lab. As far as we know, this is the first study addressing the question of sensory evoked activity in AD animal models using genetically encoded calcium indicators, which looked at the longitudinal measurement of neuronal activity paralleling the progression of AD pathology.

The cumulative analysis of all the cells over 8 weeks did not show significant difference between antibody treated and vehicle treated transgenic groups (Figure 5.24) but there was statistical significance ($p<0.05$) between transgenic and wt control (Figure 5.24), showing the sensitivity of the indicator in detecting changes in calcium transients. However, the linear regression analysis for all the 3 groups showed that the trend of evoked activity decreased over days (Figure 5.26). There are several variables like level of anesthesia, laser intensity, positioning of animal w.r.t. piezo stimulator, inter and intra animal differences, which can change between imaging sessions. We standardized most of the parameters but some inherent biological variable in the animal response could not be avoided. Despite these challenges, the inter-animal variability was low and the response was consistent.

The aim at the beginning of the project was to see if there is any antibody treatment effect on evoked activity in transgenic animals and if it is different from wt control.

We chose APPswe mice for the slow development of pathology, typically starting around 8-10 month (Hsiao, et al. 1996), which we thought would complement the longitudinal measurement of evoked activity. Our results show that the transgenic mice have less evoked activity than wt control mice but there was no significant treatment effect seen between transgenics although there was trend indicating increase in evoked activity in antibody treated mice. The animal group was small in this study and more studies with larger animal groups are warranted. We prove that it is possible to longitudinally image neuronal activity with ongoing AD pathology. This opens the experimental options for further explore AD pathology in real time and correlate disease progression with neuronal dysfunction. It would also be interesting to image awake behaving AD transgenic with these protocols and study neuronal activity during cognitive tasks and further study how therapeutic interventions such as immunotherapy would modify neuronal activity.

6.3.4 Neuropil Activity in AD transgenic and wt control mice

Neuropil is the milieu in which the neuronal networks function. It has been shown that whisker-stimulation elicited clear calcium transients not only in neuronal somata but also in the neuropil (Lutcke, et al. 2010). Thus, whisker-evoked activity correlates to neuropil activity. Hence, we measured neuropil activity in response to whisker stimulation. The analysis was done in the similar fashion to that of whisker-evoked neuronal activity. Linear regression analysis showed that the both transgenic groups had similar trends and differed significantly from wt control group (Figure 5.29). Antibody treatment had no significant effect on neuropil activity of transgenic mice. The neuropil response was similar to whisker-evoked neuronal response. In other words, neuropil activity is an indirect measure of evoked neuronal activity. The further experiments would be in similar lines to study sensory evoked activity.

6.3.5 Immunohistochemistry

After the last imaging session, the animals were perfused and the floating sections were studied for plaques and YC3.60 expression. YC3.60 expression was seen in all the animals injected with the virus (Figure 5.30). We obtained labeling of neurons with h-synapsin promoter and both neurons and axons with CAG promoter. CAG promoter is more suitable for dendritic imaging. Both the promoters had equal success

rate in our hands. All the neurons labeled with YC3.60 colocalized with NeuN staining, proving the fidelity of expression (Figure 5.31).

The animals were 6 months of age when virus was injected and 7 months of age when chronic imaging was started. The deposition of amyloid plaques starts at the age of 8-10 months in APPswe mice and our initial goal was to start imaging in the pre-plaque pathology and visualize appearance of plaques and study response of neurons, which were in the plaque periphery. But, none of the transgenic we imaged developed plaque in the imaging area. However, when the tissue sections were stained with 6E10 plaques were seen in the hippocampus and cortex (Figure 5.32). There was no significant plaque reduction seen after antibody treatment. In other experiment, the 24-month-old APPsweArc mice injected with YC3.60 showed drastic changes in neuronal morphology such as shortened, dystrophic neuritis and shrunken cell bodies compared to 10-month-old APPswe mice (Figure 5.33 and Figure 5.34). This shows that the indicator is sensitive for morphological changes too.

7. Conclusion and Outlook

This dissertation work looked at the functional and morphological aspects of Alzheimer's disease with the technique of two-photon imaging. The first project involved development of different techniques to study microglia-plaque interaction. There were several technical difficulties involved in the project. We were able to show that plaque directed application of antibody could be successfully performed and time-lapse imaging of such animals over hours was possible. Preliminary data also showed recruitment of microglia to the beta-amyloid plaque periphery after topical application of anti-Aß antibody.

The second project looked at the neocortical neuronal activity with the use of genetic ally encoded calcium indicator in APPswe mice who were 6 months of age (pre-plaque phase) at the beginning of experiment. Immunotherapy was combined along with longitudinal imaging of neuronal network of barrel cortex using whisker stimulation as a sensory input. The nontransgenic wt control mice had higher evoked, spontaneous and neuropil activity compared to the transgenic mice. Immunotherapy was effective in improving the spontaneous activity in antibody treated mice but there was no significant increase in evoked and neuropil activity after immunization. The transgenic mice developed plaques in the 8 weeks of imaging and there was no significant difference in antibody treated and vehicle treated mice. These results support the hypothesis that neuronal activity is affected prior to the appearance of plaques. This is a first study in the direction of longitudinal imaging of neuronal network in AD mice. The future experiments would involve another model with faster appearance of plaques and increase the number of animals in each group. We had only 3 animals in each group. Also, there are more options of genetic encoded calcium indicators available (Looger and Griesbeck 2012). Another idea would be to use oligomeric antibodies, which are yet to be completely characterized and study their effect in comparison to anti-Aß antibodies. Further, these techniques could be used to study neuronal activity in awake, behaving mice during cognitive tasks.

Overall, this dissertation was able to establish and use techniques of long term *in vivo* imaging at different stages of Alzheimer's disease pathophysiology. These techniques can be further used to study different aspects ranging from neuronal activity, immunotherapy effects, microglia and astrocyte activities, cognitive tasks, which would help in better understanding of pathophysiology of Alzheimer's disease and

ultimately develop effective therapeutics to help millions suffering from this debilitating illness.

8. References

Aisen, P.S.*, et al.* Effects of rofecoxib or naproxen vs placebo on Alzheimer disease progression: a randomized controlled trial. *JAMA* **289**, 2819-2826 (2003).

Akiyama, H.*, et al.* Inflammation and Alzheimer's disease. *Neurobiol Aging* **21**, 383-421 (2000).

Alzheimer, A., Stelzmann, R.A., Schnitzlein, H.N. & Murtagh, F.R. An English translation of Alzheimer's 1907 paper, "Uber eine eigenartige Erkankung der Hirnrinde". *Clin Anat* **8**, 429-431 (1995).

Bacskai, B.J. & Hyman, B.T. Alzheimer's disease: what multiphoton microscopy teaches us. *Neuroscientist* **8**, 386-390 (2002).

Bacskai, B.J.*, et al.* Imaging of amyloid-beta deposits in brains of living mice permits direct observation of clearance of plaques with immunotherapy. *Nat Med* **7**, 369-372 (2001).

Bacskai, B.J.*, et al.* Non-Fc-mediated mechanisms are involved in clearance of amyloid-beta in vivo by immunotherapy. *J Neurosci* **22**, 7873-7878 (2002).

Bacskai, B.J., Klunk, W.E., Mathis, C.A. & Hyman, B.T. Imaging amyloid-beta deposits in vivo. *J Cereb Blood Flow Metab* **22**, 1035-1041 (2002).

Bard, F.*, et al.* Peripherally administered antibodies against amyloid beta-peptide enter the central nervous system and reduce pathology in a mouse model of Alzheimer disease. *Nat Med* **6**, 916-919 (2000).

Bayer, A.J.*, et al.* Evaluation of the safety and immunogenicity of synthetic Abeta42 (AN1792) in patients with AD. *Neurology* **64**, 94-101 (2005).

Bertram, L., Lill, C.M. & Tanzi, R.E. The genetics of Alzheimer disease: back to the future. *Neuron* **68**, 270-281 (2010).

Bertram, L. & Tanzi, R.E. Genome-wide association studies in Alzheimer's disease. *Hum Mol Genet* **18**, R137-145 (2009).

Biscaro, B., Lindvall, O., Hock, C., Ekdahl, C.T. & Nitsch, R.M. Abeta immunotherapy protects morphology and survival of adult-born neurons in doubly transgenic APP/PS1 mice. *J Neurosci* **29**, 14108-14119 (2009).

Bittner, T.*, et al.* Multiple events lead to dendritic spine loss in triple transgenic Alzheimer's disease mice. *PLoS One* **5**, e15477 (2010).

Blennow, K., de Leon, M.J. & Zetterberg, H. Alzheimer's disease. *Lancet* **368**, 387-403 (2006).

Block, M.L., Zecca, L. & Hong, J.S. Microglia-mediated neurotoxicity: uncovering the molecular mechanisms. *Nat Rev Neurosci* **8**, 57-69 (2007).

Bolmont, T., *et al.* Dynamics of the microglial/amyloid interaction indicate a role in plaque maintenance. *J Neurosci* **28**, 4283-4292 (2008).

Bousso, P. & Robey, E.A. Dynamic behavior of T cells and thymocytes in lymphoid organs as revealed by two-photon microscopy. *Immunity* **21**, 349-355 (2004).

Braak, H. & Braak, E. Development of Alzheimer-related neurofibrillary changes in the neocortex inversely recapitulates cortical myelogenesis. *Acta Neuropathol* **92**, 197-201 (1996).

Brecht, M., Roth, A. & Sakmann, B. Dynamic receptive fields of reconstructed pyramidal cells in layers 3 and 2 of rat somatosensory barrel cortex. *J Physiol* **553**, 243-265 (2003).

Brendza, R.P., *et al.* Anti-Abeta antibody treatment promotes the rapid recovery of amyloid-associated neuritic dystrophy in PDAPP transgenic mice. *J Clin Invest* **115**, 428-433 (2005).

Brody, D.L. & Holtzman, D.M. Active and passive immunotherapy for neurodegenerative disorders. *Annu Rev Neurosci* **31**, 175-193 (2008).

Brookmeyer, R., Johnson, E., Ziegler-Graham, K. & Arrighi, H.M. Forecasting the global burden of Alzheimer's disease. *Alzheimers Dement* **3**, 186-191 (2007).

Bugiani, O. A beta-related cerebral amyloid angiopathy. *Neurol Sci* **25 Suppl 1**, S1-2 (2004).

Burgold, S., *et al.* In vivo multiphoton imaging reveals gradual growth of newborn amyloid plaques over weeks. *Acta Neuropathol* **121**, 327-335 (2011).

Busche, M.A., *et al.* Critical role of soluble amyloid-beta for early hippocampal hyperactivity in a mouse model of Alzheimer's disease. *Proc Natl Acad Sci U S A* (2012).

Busche, M.A., *et al.* Clusters of hyperactive neurons near amyloid plaques in a mouse model of Alzheimer's disease. *Science* **321**, 1686-1689 (2008).

Cagnin, A., *et al.* In-vivo measurement of activated microglia in dementia. *Lancet* **358**, 461-467 (2001).

Cardona, A.E., *et al.* Control of microglial neurotoxicity by the fractalkine receptor. *Nat Neurosci* **9**, 917-924 (2006).

Carter, M.D., Simms, G.A. & Weaver, D.F. The development of new therapeutics for Alzheimer's disease. *Clin Pharmacol Ther* **88**, 475-486 (2010).

Casadesus, G., *et al.* Increases in luteinizing hormone are associated with declines in cognitive performance. *Mol Cell Endocrinol* **269**, 107-111 (2007).

Castellani, R.J., Rolston, R.K. & Smith, M.A. Alzheimer disease. *Dis Mon* **56**, 484-546 (2010).

Cetin, A., Komai, S., Eliava, M., Seeburg, P.H. & Osten, P. Stereotaxic gene delivery in the rodent brain. *Nat Protoc* **1**, 3166-3173 (2006).

Chang, W.P.*, et al.* Amyloid-beta reduction by memapsin 2 (beta-secretase) immunization. *FASEB J* **21**, 3184-3196 (2007).

Cheng, I.H.*, et al.* Accelerating amyloid-beta fibrillization reduces oligomer levels and functional deficits in Alzheimer disease mouse models. *J Biol Chem* **282**, 23818-23828 (2007).

Chin, J. Selecting a mouse model of Alzheimer's disease. *Methods Mol Biol* **670**, 169-189 (2001).

Christie, R.H.*, et al.* Growth arrest of individual senile plaques in a model of Alzheimer's disease observed by in vivo multiphoton microscopy. *J Neurosci* **21**, 858-864 (2001).

Cleary, J.P.*, et al.* Natural oligomers of the amyloid-beta protein specifically disrupt cognitive function. *Nat Neurosci* **8**, 79-84 (2005).

Corder, E.H.*, et al.* Gene dose of apolipoprotein E type 4 allele and the risk of Alzheimer's disease in late onset families. *Science* **261**, 921-923 (1993).

Das, P.*, et al.* Amyloid-beta immunization effectively reduces amyloid deposition in FcRgamma-/- knock-out mice. *J Neurosci* **23**, 8532-8538 (2003).

Davalos, D.*, et al.* ATP mediates rapid microglial response to local brain injury in vivo. *Nat Neurosci* **8**, 752-758 (2005).

De Giorgi, F.*, et al.* Targeting GFP to organelles. *Methods Cell Biol* **58**, 75-85 (1999).

DeMattos, R.B.*, et al.* Peripheral anti-A beta antibody alters CNS and plasma A beta clearance and decreases brain A beta burden in a mouse model of Alzheimer's disease. *Proc Natl Acad Sci U S A* **98**, 8850-8855 (2001).

Denk, W., Strickler, J.H. & Webb, W.W. Two-photon laser scanning fluorescence microscopy. *Science* **248**, 73-76 (1990).

Diez-Garcia, J.*, et al.* Activation of cerebellar parallel fibers monitored in transgenic mice expressing a fluorescent Ca2+ indicator protein. *Eur J Neurosci* **22**, 627-635 (2005).

Dittgen, T.*, et al.* Lentivirus-based genetic manipulations of cortical neurons and their optical and electrophysiological monitoring in vivo. *Proc Natl Acad Sci U S A* **101**, 18206-18211 (2004).

Dombeck, D.A., Harvey, C.D., Tian, L., Looger, L.L. & Tank, D.W. Functional imaging of hippocampal place cells at cellular resolution during virtual navigation. *Nat Neurosci* **13**, 1433-1440 (2010).

Drew, P.J.*, et al.* Chronic optical access through a polished and reinforced thinned skull. *Nat Methods* **7**, 981-984 (2010).

Dubois, B.*, et al.* Research criteria for the diagnosis of Alzheimer's disease: revising the NINCDS-ADRDA criteria. *Lancet Neurol* **6**, 734-746 (2007).

Farrer, L.A.*, et al.* Effects of age, sex, and ethnicity on the association between apolipoprotein E genotype and Alzheimer disease. A m (2010)eta-analysis. APOE and Alzheimer Disease Meta Analysis Consortium. *JAMA* **278**, 1349-1356 (1997).

Fassbender, K.*, et al.* Simvastatin strongly reduces levels of Alzheimer's disease beta -amyloid peptides Abeta 42 and Abeta 40 in vitro and in vivo. *Proc Natl Acad Sci U S A* **98**, 5856-5861 (2001).

Finnerty, G.T., Roberts, L.S. & Connors, B.W. Sensory experience modifies the short-term dynamics of neocortical synapses. *Nature* **400**, 367-371 (1999).

Fletcher, M.L.*, et al.* Optical imaging of postsynaptic odor representation in the glomerular layer of the mouse olfactory bulb. *J Neurophysiol* **102**, 817-830 (2009).

Fox, N.C.*, et al.* Effects of Abeta immunization (AN1792) on MRI measures of cerebral volume in Alzheimer disease. *Neurology* **64**, 1563-1572 (2005).

Fratiglioni, L., De Ronchi, D. & Aguero-Torres, H. Worldwide prevalence and incidence of dementia. *Drugs Aging* **15**, 365-375 (1999).

Fuhrmann, M.*, et al.* Microglial Cx3cr1 knockout prevents neuron loss in a mouse model of Alzheimer's disease. *Nat Neurosci* **13**, 411-413 (2010).

Fuss, B.*, et al.* Purification and analysis of in vivo-differentiated oligodendrocytes expressing the green fluorescent protein. *Dev Biol* **218**, 259-274 (2000).

Garaschuk, O.*, et al.* Optical monitoring of brain function in vivo: from neurons to networks. *Pflugers Arch* **453**, 385-396 (2006).

Garaschuk, O., Milos, R.I. & Konnerth, A. Targeted bulk-loading of fluorescent indicators for two-photon brain imaging in vivo. *Nat Protoc* **1**, 380-386 (2006).

Gatz, M.*, et al.* Role of genes and environments for explaining Alzheimer disease. *Arch Gen Psychiatry* **63**, 168-174 (2006).

Gilman, S.*, et al.* Clinical effects of Abeta immunization (AN1792) in patients with AD in an interrupted trial. *Neurology* **64**, 1553-1562 (2005).

Glabe, C.G. Structural classification of toxic amyloid oligomers. *J Biol Chem* **283**, 29639-29643 (2008).

Gobel, W. & Helmchen, F. In vivo calcium imaging of neural network function. *Physiology (Bethesda)* **22**, 358-365 (2007).

Göppert-Mayer, M. Über Elementarakte mit zwei Quantensprüngen. Annalen der Physik PhD-thesis, University of Göttingen (1931).

Grathwohl, S.A.*, et al.* Formation and maintenance of Alzheimer's disease beta-amyloid plaques in the absence of microglia. *Nat Neurosci* **12**, 1361-1363 (2009).

Grewe, B.F., Langer, D., Kasper, H., Kampa, B.M. & Helmchen, F. High-speed in vivo calcium imaging reveals neuronal network activity with near-millisecond precision. *Nat Methods* **7**, 399-400 (2010).

Grienberger, C.*, et al.* Staged decline of neuronal function in vivo in an animal model of Alzheimer's disease. *Nat Commun* **3**, 774 (2012).

Grutzendler, J. & Gan, W.B. Two-photon imaging of synaptic plasticity and pathology in the living mouse brain. *NeuroRx* **3**, 489-496 (2006).

Hardy, J. & Selkoe, D.J. The amyloid hypothesis of Alzheimer's disease: progress and problems on the road to therapeutics. *Science* **297**, 353-356 (2002).

Hardy, J.A. & Higgins, G.A. Alzheimer's disease: the amyloid cascade hypothesis. *Science* **256**, 184-185 (1992).

Hasan, M.T.*, et al.* Functional fluorescent Ca2+ indicator proteins in transgenic mice under TET control. *PLoS Biol* **2**, e163 (2004).

Hebert, L.E.*, et al.* Age-specific incidence of Alzheimer's disease in a community population. *JAMA* **273**, 1354-1359 (1995).

Hefendehl, J.K.*, et al.* Long-term in vivo imaging of beta-amyloid plaque appearance and growth in a mouse model of cerebral beta-amyloidosis. *J Neurosci* **31**, 624-629 (2011).

Heim, N. & Griesbeck, O. Genetically encoded indicators of cellular calcium dynamics based on troponin C and green fluorescent protein. *J Biol Chem* **279**, 14280-14286 (2004).

Helmchen, F. & Denk, W. Deep tissue two-photon microscopy. *Nat Methods* **2**, 932-940 (2005).

Helmchen, F. & Denk, W. New developments in multiphoton microscopy. *Curr Opin Neurobiol* **12**, 593-601 (2002).

Hirohata, M., Ono, K., Naiki, H. & Yamada, M. Non-steroidal anti-inflammatory drugs have anti-amyloidogenic effects for Alzheimer's beta-amyloid fibrils in vitro. *Neuropharmacology* **49**, 1088-1099 (2005).

Hock, C., *et al.* Generation of antibodies specific for beta-amyloid by vaccination of patients with Alzheimer disease. *Nat Med* **8**, 1270-1275 (2002).

Hock, C., *et al.* Antibodies against beta-amyloid slow cognitive decline in Alzheimer's disease. *Neuron* **38**, 547-554 (2003).

Hofer, S.B., Mrsic-Flogel, T.D., Bonhoeffer, T. & Hubener, M. Experience leaves a lasting structural trace in cortical circuits. *Nature* **457**, 313-317 (2009).

Holcomb, L., *et al.* Accelerated Alzheimer-type phenotype in transgenic mice carrying both mutant amyloid precursor protein and presenilin 1 transgenes. *Nat Med* **4**, 97-100 (1998).

Holtmaat, A., *et al.* Long-term, high-resolution imaging in the mouse neocortex through a chronic cranial window. *Nat Protoc* **4**, 1128-1144 (2009).

Hsiao, K., *et al.* Correlative memory deficits, Abeta elevation, and amyloid plaques in transgenic mice. *Science* **274**, 99-102 (1996).

Hsieh, H., *et al.* AMPAR removal underlies Abeta-induced synaptic depression and dendritic spine loss. *Neuron* **52**, 831-843 (2006).

in t' Veld, B.A., *et al.* Nonsteroidal antiinflammatory drugs and the risk of Alzheimer's disease. *N Engl J Med* **345**, 1515-1521 (2001).

Jama, J.W., *et al.* Dietary antioxidants and cognitive function in a population-based sample of older persons. The Rotterdam Study. *Am J Epidemiol* **144**, 275-280 (1996).

Janus, C., *et al.* A beta peptide immunization reduces behavioural impairment and plaques in a model of Alzheimer's disease. *Nature* **408**, 979-982 (2000).

Jick, H., Zornberg, G.L., Jick, S.S., Seshadri, S. & Drachman, D.A. Statins and the risk of dementia. *Lancet* **356**, 1627-1631 (2000).

Jung, S., *et al.* Analysis of fractalkine receptor CX(3)CR1 function by targeted deletion and green fluorescent protein reporter gene insertion. *Mol Cell Biol* **20**, 4106-4114 (2000).

Kamenetz, F., *et al.* APP processing and synaptic function. *Neuron* **37**, 925-937 (2003).

Kawakami, N., *et al.* Live imaging of effector cell trafficking and autoantigen recognition within the unfolding autoimmune encephalomyelitis lesion. *J Exp Med* **201**, 1805-1814 (2005).

Kerr, J.N., *et al.* Spatial organization of neuronal population responses in layer 2/3 of rat barrel cortex. *J Neurosci* **27**, 13316-13328 (2007).

Kerr, J.N. & Denk, W. Imaging in vivo: watching the brain in action. *Nat Rev Neurosci* **9**, 195-205 (2008).

Kerschensteiner, M., Schwab, M.E., Lichtman, J.W. & Misgeld, T. In vivo imaging of axonal degeneration and regeneration in the injured spinal cord. *Nat Med* **11**, 572-577 (2005).

Kim, J., Basak, J.M. & Holtzman, D.M. The role of apolipoprotein E in Alzheimer's disease. *Neuron* **63**, 287-303 (2009).

Klein, W.L., Krafft, G.A. & Finch, C.E. Targeting small Abeta oligomers: the solution to an Alzheimer's disease conundrum? *Trends Neurosci* **24**, 219-224 (2001).

Kleinfeld, D., Mitra, P.P., Helmchen, F. & Denk, W. Fluctuations and stimulus-induced changes in blood flow observed in individual capillaries in layers 2 through 4 of rat neocortex. *Proc Natl Acad Sci U S A* **95**, 15741-15746 (1998).

Klunk, W.E*., et al.* Imaging Abeta plaques in living transgenic mice with multiphoton microscopy and methoxy-X04, a systemically administered Congo red derivative. *J Neuropathol Exp Neurol* **61**, 797-805 (2002).

Klyubin, I*., et al.* Amyloid beta protein immunotherapy neutralizes Abeta oligomers that disrupt synaptic plasticity in vivo. *Nat Med* **11**, 556-561 (2005).

Knobloch, M., Farinelli, M., Konietzko, U., Nitsch, R.M. & Mansuy, I.M. Abeta oligomer-mediated long-term potentiation impairment involves protein phosphatase 1-dependent mechanisms. *J Neurosci* **27**, 7648-7653 (2007a).

Knobloch, M., Konietzko, U., Krebs, D.C. & Nitsch, R.M. Intracellular Abeta and cognitive deficits precede beta-amyloid deposition in transgenic arcAbeta mice. *Neurobiol Aging* **28**, 1297-1306 (2007b).

Koenigsknecht-Talboo, J*., et al.* Rapid microglial response around amyloid pathology after systemic anti-Abeta antibody administration in PDAPP mice. *J Neurosci* **28**, 14156-14164 (2008).

Kuchibhotla, K.V*., et al.* Abeta plaques lead to aberrant regulation of calcium homeostasis in vivo resulting in structural and functional disruption of neuronal networks. *Neuron* **59**, 214-225 (2008).

Kuchibhotla, K.V., Lattarulo, C.R., Hyman, B.T. & Bacskai, B.J. Synchronous hyperactivity and intercellular calcium waves in astrocytes in Alzheimer mice. *Science* **323**, 1211-1215 (2009).

Laiho, L.H., Pelet, S., Hancewicz, T.M., Kaplan, P.D. & So, P.T. Two-photon 3-D mapping of ex vivo human skin endogenous fluorescence species based on fluorescence emission spectra. *J Biomed Opt* **10**, 024016 (2005).

Lee, W.C*., et al.* Dynamic remodeling of dendritic arbors in GABAergic interneurons of adult visual cortex. *PLoS Biol* **4**, e29 (2006).

Lemere, C.A., *et al.* Sequence of deposition of heterogeneous amyloid beta-peptides and APO E in Down syndrome: implications for initial events in amyloid plaque formation. *Neurobiol Dis* **3**, 16-32 (1996).

Lemere, C.A. & Masliah, E. Can Alzheimer disease be prevented by amyloid-beta immunotherapy? *Nat Rev Neurol* **6**, 108-119 (2010).

Lemere, C.A., *et al.* Evidence for peripheral clearance of cerebral Abeta protein following chronic, active Abeta immunization in PSAPP mice. *Neurobiol Dis* **14**, 10-18 (2003).

Lesne, S., *et al.* A specific amyloid-beta protein assembly in the brain impairs memory. *Nature* **440**, 352-357 (2006).

Li, J., *et al.* Early development of functional spatial maps in the zebrafish olfactory bulb. *J Neurosci* **25**, 5784-5795 (2005).

Li, S., *et al.* Soluble oligomers of amyloid Beta protein facilitate hippocampal long-term depression by disrupting neuronal glutamate uptake. *Neuron* **62**, 788-801 (2009).

Liebscher, S. & Meyer-Luehmann, M. A Peephole into the Brain: Neuropathological Features of Alzheimer's Disease Revealed by in vivo Two-Photon Imaging. *Front Psychiatry* **3**, 26 (2012).

Liu, T., *et al.* Amyloid-beta-induced toxicity of primary neurons is dependent upon differentiation-associated increases in tau and cyclin-dependent kinase 5 expression. *J Neurochem* **88**, 554-563 (2004).

Liu, Z., Condello, C., Schain, A., Harb, R. & Grutzendler, J. CX3CR1 in microglia regulates brain amyloid deposition through selective protofibrillar amyloid-beta phagocytosis. *J Neurosci* **30**, 17091-17101 (2010).

Looger, L.L. & Griesbeck, O. Genetically encoded neural activity indicators. *Curr Opin Neurobiol* **22**, 18-23 (2011).

Lutcke, H., *et al.* Optical recording of neuronal activity with a genetically-encoded calcium indicator in anesthetized and freely moving mice. *Front Neural Circuits* **4**, 9 (2010).

Maat-Schieman, M., Roos, R. & van Duinen, S. Hereditary cerebral hemorrhage with amyloidosis-Dutch type. *Neuropathology* **25**, 288-297 (2005).

Mank, M. & Griesbeck, O. Genetically encoded calcium indicators. *Chem Rev* **108**, 1550-1564 (2008).

Mank, M., *et al.* A FRET-based calcium biosensor with fast signal kinetics and high fluorescence change. *Biophys J* **90**, 1790-1796 (2006).

Mank, M., *et al.* A genetically encoded calcium indicator for chronic in vivo two-photon imaging. *Nat Methods* **5**, 805-811 (2008).

McGeer, P.L., Itagaki, S., Tago, H. & McGeer, E.G. Reactive microglia in patients with senile dementia of the Alzheimer type are positive for the histocompatibility glycoprotein HLA-DR. *Neurosci Lett* **79**, 195-200 (1987).

McKhann, G.*, et al.* Clinical diagnosis of Alzheimer's disease: report of the NINCDS-ADRDA Work Group under the auspices of Department of Health and Human Services Task Force on Alzheimer's Disease. *Neurology* **34**, 939-944 (1984).

Meyer, M.R.*, et al.* APOE genotype predicts when--not whether--one is predisposed to develop Alzheimer disease. *Nat Genet* **19**, 321-322 (1998).

Meyer-Luehmann, M.*, et al.* Rapid appearance and local toxicity of amyloid-beta plaques in a mouse model of Alzheimer's disease. *Nature* **451**, 720-724 (2008).

Minoshima, S., Foster, N.L. & Kuhl, D.E. Posterior cingulate cortex in Alzheimer's disease. *Lancet* **344**, 895 (1994).

Misgeld, T. & Kerschensteiner, M. In vivo imaging of the diseased nervous system. *Nat Rev Neurosci* **7**, 449-463 (2006).

Miyawaki, A.*, et al.* Fluorescent indicators for Ca2+ based on green fluorescent proteins and calmodulin. *Nature* **388**, 882-887 (1997).

Molitoris, B.A. & Sandoval, R.M. Intravital multiphoton microscopy of dynamic renal processes. *Am J Physiol Renal Physiol* **288**, F1084-1089 (2005).

Morgan, D.*, et al.* A beta peptide vaccination prevents memory loss in an animal model of Alzheimer's disease. *Nature* **408**, 982-985 (2000).

Morrison, J.H. & Hof, P.R. Life and death of neurons in the aging brain. *Science* **278**, 412-419 (1997).

Nagai, T., Yamada, S., Tominaga, T., Ichikawa, M. & Miyawaki, A. Expanded dynamic range of fluorescent indicators for Ca(2+) by circularly permuted yellow fluorescent proteins. *Proc Natl Acad Sci U S A* **101**, 10554-10559 (2004).

Nava, R.G.*, et al.* Two-photon microscopy in pulmonary research. *Semin Immunopathol* **32**, 297-304 (2010).

Nicoll, J.A.*, et al.* Neuropathology of human Alzheimer disease after immunization with amyloid-beta peptide: a case report. *Nat Med* **9**, 448-452 (2003).

Nimmerjahn, A., Kirchhoff, F. & Helmchen, F. Resting microglial cells are highly dynamic surveillants of brain parenchyma in vivo. *Science* **308**, 1314-1318 (2005).

Nimmerjahn, A., Kirchhoff, F., Kerr, J.N. & Helmchen, F. Sulforhodamine 101 as a specific marker of astroglia in the neocortex in vivo. *Nat Methods* **1**, 31-37 (2004).

Nitsch, R.*, et al.* Direct impact of T cells on neurons revealed by two-photon microscopy in living brain tissue. *J Neurosci* **24**, 2458-2464 (2004).

Nolte, C.*, et al.* GFAP promoter-controlled EGFP-expressing transgenic mice: a tool to visualize astrocytes and astrogliosis in living brain tissue. *Glia* **33**, 72-86 (2001).

Orbach, H.S., Cohen, L.B. & Grinvald, A. Optical mapping of electrical activity in rat somatosensory and visual cortex. *J Neurosci* **5**, 1886-1895 (1985).

Palmer, A.E., Jin, C., Reed, J.C. & Tsien, R.Y. Bcl-2-mediated alterations in endoplasmic reticulum Ca2+ analyzed with an improved genetically encoded fluorescent sensor. *Proc Natl Acad Sci U S A* **101**, 17404-17409 (2004).

Palop, J.J. & Mucke, L. Amyloid-beta-induced neuronal dysfunction in Alzheimer's disease: from synapses toward neural networks. *Nat Neurosci* **13**, 812-818 (2010).

Perl, D.P. Neuropathology of Alzheimer's disease. *Mt Sinai J Med* **77**, 32-42 (2010).

Petersen, C.C. The barrel cortex--integrating molecular, cellular and systems physiology. *Pflugers Arch* **447**, 126-134 (2003).

Petersen, C.C. The functional organization of the barrel cortex. *Neuron* **56**, 339-355 (2007).

Petersen, C.C. & Sakmann, B. The excitatory neuronal network of rat layer 4 barrel cortex. *J Neurosci* **20**, 7579-7586 (2000).

Portera-Cailliau, C., Weimer, R.M., De Paola, V., Caroni, P. & Svoboda, K. Diverse modes of axon elaboration in the developing neocortex. *PLoS Biol* **3**, e272 (2005).

Prada, C.M.*, et al.* Antibody-mediated clearance of amyloid-beta peptide from cerebral amyloid angiopathy revealed by quantitative in vivo imaging. *J Neurosci* **27**, 1973-1980 (2007).

Prince, M.B., Bryce, R, & Ferri, C. World Alzheimer Report 2011: The benefits of Early Diagnosis and Intervention. London: Institue of Psychiatry, King's College, London (2011)

Raber, J., Huang, Y. & Ashford, J.W. ApoE genotype accounts for the vast majority of AD risk and AD pathology. *Neurobiol Aging* **25**, 641-650 (2004).

Rensink, A.A., de Waal, R.M., Kremer, B. & Verbeek, M.M. Pathogenesis of cerebral amyloid angiopathy. *Brain Res Brain Res Rev* **43**, 207-223 (2003).

Robbins, E.M.*, et al.* Kinetics of cerebral amyloid angiopathy progression in a transgenic mouse model of Alzheimer disease. *J Neurosci* **26**, 365-371 (2006).

Roberson, E.D. & Mucke, L. 100 years and counting: prospects for defeating Alzheimer's disease. *Science* **314**, 781-784 (2006).

Rogers, J. & Lue, L.F. Microglial chemotaxis, activation, and phagocytosis of amyloid beta-peptide as linked phenomena in Alzheimer's disease. *Neurochem Int* **39**, 333-340 (2001).

Rogers, J., Strohmeyer, R., Kovelowski, C.J. & Li, R. Microglia and inflammatory mechanisms in the clearance of amyloid beta peptide. *Glia* **40**, 260-269 (2002).

Roggo, S. Inhibition of BACE, a promising approach to Alzheimer's disease therapy. *Curr Top Med Chem* **2**, 359-370 (2002).

Roses, A.D. Apolipoprotein E alleles as risk factors in Alzheimer's disease. *Annu Rev Med* **47**, 387-400 (1996).

Rubart, M. Two-photon microscopy of cells and tissue. *Circ Res* **95**, 1154-1166 (2004).

Scarmeas, N., Stern, Y., Tang, M.X., Mayeux, R. & Luchsinger, J.A. Mediterranean diet and risk for Alzheimer's disease. *Ann Neurol* **59**, 912-921 (2006).

Schaefer, A.M., Sanes, J.R. & Lichtman, J.W. A compensatory subpopulation of motor neurons in a mouse model of amyotrophic lateral sclerosis. *J Comp Neurol* **490**, 209-219 (2005).

Schenk, D.*, et al.* Immunization with amyloid-beta attenuates Alzheimer-disease-like pathology in the PDAPP mouse. *Nature* **400**, 173-177 (1999).

Schroeter, S.*, et al.* Immunotherapy reduces vascular amyloid-beta in PDAPP mice. *J Neurosci* **28**, 6787-6793 (2008).

Seelig, J.D.*, et al.* Two-photon calcium imaging from head-fixed Drosophila during optomotor walking behavior. *Nat Methods* **7**, 535-540 (2010).

Selkoe, D.J. Soluble oligomers of the amyloid beta-protein impair synaptic plasticity and behavior. *Behav Brain Res* **192**, 106-113 (2008).

Shankar, G.M.*, et al.* Natural oligomers of the Alzheimer amyloid-beta protein induce reversible synapse loss by modulating an NMDA-type glutamate receptor-dependent signaling pathway. *J Neurosci* **27**, 2866-2875 (2007).

Shankar, G.M.*, et al.* Amyloid-beta protein dimers isolated directly from Alzheimer's brains impair synaptic plasticity and memory. *Nat Med* **14**, 837-842 (2008).

Siemers, E.R.*, et al.* Effects of a gamma-secretase inhibitor in a randomized study of patients with Alzheimer disease. *Neurology* **66**, 602-604 (2006).

Small, G.W.*, et al.* Diagnosis and treatment of Alzheimer disease and related disorders. Consensus statement of the American Association for Geriatric Psychiatry, the Alzheimer's Association, and the American Geriatrics Society. *JAMA* **278**, 1363-1371 (1997).

Snyder, E.M.*, et al.* Regulation of NMDA receptor trafficking by amyloid-beta. *Nat Neurosci* **8**, 1051-1058 (2005).

Spires, T.L., *et al.* Dendritic spine abnormalities in amyloid precursor protein transgenic mice demonstrated by gene transfer and intravital multiphoton microscopy. *J Neurosci* **25**, 7278-7287 (2005).

Spires-Jones, T.L., *et al.* Impaired spine stability underlies plaque-related spine loss in an Alzheimer's disease mouse model. *Am J Pathol* **171**, 1304-1311 (2007).

Spires-Jones, T.L., *et al.* Passive immunotherapy rapidly increases structural plasticity in a mouse model of Alzheimer disease. *Neurobiol Dis* **33**, 213-220 (2009).

St George-Hyslop, P.H. & Morris, J.C. Will anti-amyloid therapies work for Alzheimer's disease? *Lancet* **372**, 180-182 (2008).

Stosiek, C., Garaschuk, O., Holthoff, K. & Konnerth, A. In vivo two-photon calcium imaging of neuronal networks. *Proc Natl Acad Sci U S A* **100**, 7319-7324 (2003).

Svoboda, K., Denk, W., Kleinfeld, D. & Tank, D.W. In vivo dendritic calcium dynamics in neocortical pyramidal neurons. *Nature* **385**, 161-165 (1997).

Tackenberg, C. & Brandt, R. Divergent pathways mediate spine alterations and cell death induced by amyloid-beta, wild-type tau, and R406W tau. *J Neurosci* **29**, 14439-14450 (2009).

Tesseur, I., *et al.* Deficiency in neuronal TGF-beta signaling promotes neurodegeneration and Alzheimer's pathology. *J Clin Invest* **116**, 3060-3069 (2006).

Tian, L., *et al.* Imaging neural activity in worms, flies and mice with improved GCaMP calcium indicators. *Nat Methods* **6**, 875-881 (2009).

Tomiyama, T., *et al.* A mouse model of amyloid beta oligomers: their contribution to synaptic alteration, abnormal tau phosphorylation, glial activation, and neuronal loss in vivo. *J Neurosci* **30**, 4845-4856 (2010).

Traynor, B.J. & Singleton, A.B. Nature versus nurture: death of a dogma, and the road ahead. *Neuron* **68**, 196-200 (2010).

Tsai, J., Grutzendler, J., Duff, K. & Gan, W.B. Fibrillar amyloid deposition leads to local synaptic abnormalities and breakage of neuronal branches. *Nat Neurosci* **7**, 1181-1183 (2004).

Tsien, R.Y. A non-disruptive technique for loading calcium buffers and indicators into cells. *Nature* **290**, 527-528 (1981).

Tsien, R.Y. Fluorescent probes of cell signaling. *Annu Rev Neurosci* **12**, 227-253 (1989).

Tsien, R.Y. Intracellular signal transduction in four dimensions: from molecular design to physiology. *Am J Physiol* **263**, C723-728 (1992).

Tuszynski, M.H., *et al.* A phase 1 clinical trial of nerve growth factor gene therapy for Alzheimer disease. *Nat Med* **11**, 551-555 (2005).

Veerhuis, R., *et al.* Cytokines associated with amyloid plaques in Alzheimer's disease brain stimulate human glial and neuronal cell cultures to secrete early complement proteins, but not C1-inhibitor. *Exp Neurol* **160**, 289-299 (1999).

Wallace, D.J., *et al.* Single-spike detection in vitro and in vivo with a genetic Ca2+ sensor. *Nat Methods* **5**, 797-804 (2008).

Walsh, D.M. & Selkoe, D.J. A beta oligomers - a decade of discovery. *J Neurochem* **101**, 1172-1184 (2007).

Wang, Q., Walsh, D.M., Rowan, M.J., Selkoe, D.J. & Anwyl, R. Block of long-term potentiation by naturally secreted and synthetic amyloid beta-peptide in hippocampal slices is mediated via activation of the kinases c-Jun N-terminal kinase, cyclin-dependent kinase 5, and p38 mitogen-activated protein kinase as well as metabotropic glutamate receptor type 5. *J Neurosci* **24**, 3370-3378 (2004).

Watson, D.J., Selkoe, D.J. & Teplow, D.B. Effects of the amyloid precursor protein Glu693-->Gln 'Dutch' mutation on the production and stability of amyloid beta-protein. *Biochem J* **340 (Pt 3)**, 703-709 (1999).

Webber, K.M., *et al.* Estrogen bows to a new master: the role of gonadotropins in Alzheimer pathogenesis. *Ann N Y Acad Sci* **1052**, 201-209 (2005).

Wilcock, D.M., *et al.* Passive amyloid immunotherapy clears amyloid and transiently activates microglia in a transgenic mouse model of amyloid deposition. *J Neurosci* **24**, 6144-6151 (2004a).

Wilcock, D.M., *et al.* Passive immunotherapy against Abeta in aged APP-transgenic mice reverses cognitive deficits and depletes parenchymal amyloid deposits in spite of increased vascular amyloid and microhemorrhage. *J Neuroinflammation* **1**, 24 (2004b).

Woolsey, T.A. & Van der Loos, H. The structural organization of layer IV in the somatosensory region (SI) of mouse cerebral cortex. The description of a cortical field composed of discrete cytoarchitectonic units. *Brain Res* **17**, 205-242 (1970).

Wyss-Coray, T. Tgf-Beta pathway as a potential target in neurodegeneration and Alzheimer's. *Curr Alzheimer Res* **3**, 191-195 (2006).

Xu, H.T., Pan, F., Yang, G. & Gan, W.B. Choice of cranial window type for in vivo imaging affects dendritic spine turnover in the cortex. *Nat Neurosci* **10**, 549-551 (2007).

Yamada, K., *et al.* Abeta immunotherapy: intracerebral sequestration of Abeta by an anti-Abeta monoclonal antibody 266 with high affinity to soluble Abeta. *J Neurosci* **29**, 11393-11398 (2009).

Yan, P., *et al.* Characterizing the appearance and growth of amyloid plaques in APP/PS1 mice. *J Neurosci* **29**, 10706-10714 (2009).

Yu, D., Baird, G.S., Tsien, R.Y. & Davis, R.L. Detection of calcium transients in Drosophila mushroom body neurons with camgaroo reporters. *J Neurosci* **23**, 64-72 (2003).

Zhang, S., Boyd, J., Delaney, K. & Murphy, T.H. Rapid reversible changes in dendritic spine structure in vivo gated by the degree of ischemia. *J Neurosci* **25**, 5333-5338 (2005a).

Zhang, Z.G., *et al.* A model of mini-embolic stroke offers measurements of the neurovascular unit response in the living mouse. *Stroke* **36**, 2701-2704 (2005b).

9. Supplementary

9.1 Genotyping

APP/PS1dE9 and APPsweArc primers:

Prp-sens: 5'- CAGAACTGAACCATTTCAACCGAGC -3'

hAPPdn: 5'- TCAGTGGGTACCTCCAGCGCCCGAG- 3'

Reaction:

2 µl	Tail lysate
2 µl	10x PCR buffer
0.4 µl	dNTPs (10 mM each)
0.4 µl	Primers (20 µM)
1 µl	Redtaq polymerase
13.4 µl	PCR water

Pipetted on ice and following cycling reaction was used.

1. 95°C	2 min
2. 94°C	30 sec
3. 60°C	1 min
4. 72°C	1 min go to step 2, 35 times
5. 72°C	7 min
6. 4°C	hold

Product of PCR: about 180 bp

CX3CR1 primers:

oIMR3945: 5'- TTCACGTTCGGTCTGGTGGG -3'
oIMR3946: 5'- GGTTCCTAGTGGAGCTAGGG- 3'
oIMR3947: 5'- GATCACTCTCGGCATGGACG- 3'

Reaction:

2 µl	Tail lysate
2 µl	10x PCR buffer
0.4 µl	dNTPs (10 mM each)
0.6 µl	oIMR3945 (20 µM)
0.8 µl	oIMR3946 (20 µM)
0.6 µl	oIMR3947 (20 µM)
1 µl	Redtaq polymerase
12.2 µl	PCR water

Pipetted on ice and following cycling reaction was used.

1. 95°C	3 min
2. 94°C	30 sec

3. 60°C 30 sec
4. 72°C 2 min go to step 2, 35 times
5. 72°C 2 min
6. 4°C hold

PCR products: +/+ 970 bp
+/- 1010 and 970 bp
-/- 1010 bp

9.2 Score sheet

SCORE SHEET FOR POST OPERATIVE EVALUATION

Animal # _____ Cage # _____
Date of Operation _____
Pre-operative weight _____(g)
Procedure _____

Date				
Day post-procedure				
Time				
TREATMENTS				
Analgesics (substance/amount)				
EXTERNAL OBSERVATIONS				
Activity 0: lying 1: gets up and moves slowly 2: active movements and exploratory behavior				
Hair coat 0: completely rough 1: rough and shiny in places 2: normal shiny				
Eyes 0: closed 1: open, red 2: Normal				
Eating 0: No 1: Yes				
Drinking 0: No 1: Yes				
Feces 0: No 1: Yes				
Urine 0: No 1: Yes				
PHYSICAL EXAMINATION				
Rate & type of breathing 0: Labored 1: Shallow/Rapid 2: Normal				
Normal gait/paralysis 0: not walking 1: limping/hyperactive 2: normal gait				
Fecal/urine soiling of coat 0: Yes 1: No				
Hydration				

0: severe (no skin turgor, no urine output, dry mouth) 1: moderate (dry mouth) 2: Normally hydrated				
Appearance 0: wasted 1: Normal				
Body weight				
% change from pre-op weight				
SUTURE/STAPLES LINE				
Head post 0: lost 1: loosened 2: present				
Wound edges 0: red 1: slight erythema 2: normal				
Swelling around incision 0: visible swelling 1: slight edema 2: normal				
Swelling under incision 0: visible swelling 1: slight bulge 2: normal				
Sutures 0: missing 1: gaping wound 2: intact sutures				
Exudate from incision 0: Pus/blood 1: serous exudates 2: no exudate				
Sutures/staples removed? **(date)**				
Total Score: **22-32:** Normal, observe next day **15-21:** Observe every 4 h and intervene (analgesics, antibiotics, hydrate, close the wound) **Less than 15:** Terminate				

9.3 List of Animals

Animal No/Tg	Virus	Virus Expression	Window Quality	Outcome	Remarks
1/+	CAG-YC3.60	-	-	Dropout	
2/-	CAG-YC3.60	-	-	Dropout	
3/+	CAG-YC3.60	Good	Clear	Imaged	Immunized
4/+	CAG-YC3.60	-	-	Dropout	
5/+	CAG-YC3.60	-	-	Dropout	
6/+	CAG-YC3.60	Superficial	Clear	Imaged	Immunized
7/-	CAG-YC3.60	Moderate	Some gliosis	Imaged	
8/+	CAG-YC3.60	Good	Clear	Imaged	Non-immunized
9/+	CAG-YC3.60	Good	Clear	Imaged	Non-immunized
10/-	CAG-YC3.60	None	gliosis	Not imaged	
11/-	CAG-YC3.60	Good	Clear	Imaged	Wt Control
12/-	CAG-YC3.60	Faint	Good	Not imaged	Weird behavior
13/-	CAG-YC3.60	Restricted	gliosis	Not imaged	
14/+	CAG-YC3.60	Diffuse	some gliosis	Not imaged	Weird behavior
21/-	h-syn YC3.60	Good	Clear	Imaged	Wt Control
23/+	h-syn YC3.60	Good	Clear	Imaged	Non-immunized
24/-	h-syn YC3.60	Moderate	gliosis	Not imaged	
25/-	h-syn YC3.60	Good	Clear	Imaged	Wt Control
26/+	h-syn YC3.60	Good	Clear	Imaged	Immunized
27/-	h-syn YC3.60	Superficial	Gliosis	Not imaged	

9.4 List of Reagents, buffers, kits and antibodies

Buffer/Reagent	**Composition**
10x PBS	1.4 M NaCl, 27 mM KCl, 100 mM Na2HPO4, 18 mM KH2PO4
10x TBS	0.84 M Tris-HCl, 0.16 M Tris-base, 1.5 M NaCl
TBS-T	1 x TBS, 0.05% Tween20
Ringer solution	135 mM NaCl, 5.4 mM KCl, 5 mM Hepes, 1.8 mM CaCl2; pH 7.2 with NaOH
Anti-freeze solution	0.5 M phosphate buffer with 30% ethylene glycol and 30% glycerol

Kits

1. Dylight 498 antibody labeling kit from Amersham, Switzerland
2. Dylight 588 antibody labeling kit from Amersham, Switzerland

Primary Antibodies

1. Anti 6E10 Signet (SIG-39300)
2. Anti GFAP Advanced ImmunoChemical Inc. (031223)

Secondary Antibodies

1. Anti mouse – Cy5 Jackson Immuno-research #715-176-150
2. Anti mouse – Cy3 Jackson Immuno-research #715-165-151

10. Acknowledgements

This is probably the hardest part of thesis I have to write. Last five years I did not only grow as a researcher but also as an individual. Words may fall short to thank all the people who made this day possible. However, I would like to try!

First and foremost, I want to thank Roger and Fritjof for being two supportive pillars for last five years. I am very much indebted and thankful to Roger for giving me the opportunity to work on this challenging project in such intellectual environment. Roger was always receptive to new ideas and encouraged to materialize the experiments. Thank you for being supportive when I had to move to US for residency and wanted to work on thesis and manuscript from there. I am eternally grateful to Fritjof for such fantastic collaboration. Thanks for all the creative inputs, for helping me solve the problems big or small. Thank you for the warm and sincere support when things were not working out and help me see the light at the end of tunnel. I also want to thank my thesis committee members Prof. Dr. Markus Rudin and Prof. Dr. Stoeckli for their advice and guidance.

Special thanks to Henry, who wrote the MATLAB scripts to analyze the data. I could not have finished this project without his immense assistance and expertise. Note of thanks to Marcel Maier for helping me establish the project and give it a direction.

Working between two labs sure was not easy but people in both labs always made me feel welcome. I will always cherish the time I spent in AFS with Ivana, Mario, Antonella, Michael, Barbara, Zoe, Lisa, Anita, Jordan, Tobias, Garima, Jitin, Saoussen and all the current and former members. Special thanks to Garima and Cornelia for helping me with thesis submission. Back at Irchel, David, Tina, Dominik, Helge helped me with microscope setting and helped me trouble shoot any problems.

These five years would not have been possible without my friends. The time I spent were real ‘stress busters’ and I will always remember them fondly. Last but not the least my family, who have always stood by me and always will. Final thanks to Almighty for keeping me strong and giving me courage to face all adverse situations.

11. Curriculum Vitae

Name: Annapoorna Bhat

Date of birth: 15.10.1980

Nationality: Indian

Education and Practical Experience

2011-present	**Neurology resident at University of Medicine and Dentistry of New Jersey, Newark, NJ, USA**
2007-2012	**University of Zurich, Division of Psychiatry Research, Zurich, Switzerland** PhD research under supervision Prof. Dr. Roger Nitsch 'Chronic Two-photon Imaging of Neuronal Activity in Alzheimer's Disease Animal Models'
2005-2007	**Charité-Universitaetsmedizin, Berlin, Germany** 'Masters in Medical Neurosciences', Master thesis under supervision of Prof. Dr. Gerd Kempermann: 'Role of Rapgef6 and Brdt in adult hippocampal neurogenesis'
2004-2005	**National Center for Biological Sciences, Bangalore, India** Project trainee in the group of Prof. Dr. Obaid Siddiqi: 'Olfactory cross conditioning in *Drosophila melanogaster'*
1998-2004	**Mysore Medical College, Mysore, India** Medical degree
1996-1998	**M.M Arts and Science College, Sirsi, India** Pre-university degree
1993-1996	**Ave Maria High School, Sirsi, India**

Publications and Posters

1. **Annapoorna Bhat**, Henry Lutcke, Roger Nitsch and Fritjof Helmchen**.** Long-term cellular imaging of neuronal activity in a transgenic mouse model of early Alzheimer's disease (in preparation)

2. **A Bhat**, M Maier, F Helmchen, R M Nitsch; 'Microglial Cell Dynamics around Beta-Amyloid Plaques In Vivo'; Annual Meeting of Society for Neuroscience 2009, Chicago, IL, USA (Poster)

3. **A Bhat**, M Maier, F Helmchen, R M Nitsch; 'Characterization of Microglial Cell Dynamic around Beta-amyloid Plaques in Transgenic Mice'; 9th Annual AD/PD Conference 2009, Prague, Czech Republic (Poster)

4. A Bhat, M Maier, F Helmchen, R M Nitsch; 'In vivo Imaging of Beta-amyloid Plaques by two-photon microscopy'; 11th Annual ZNZ Symposium 2008, Zurich, Switzerland (Poster)